# SPEED SENSORLESS VECTOR CONTROL OF INDUCTION MOTOR DRIVE

A THESIS SUBMITTED TO
THE GRADUATE SCHOOL OF NATURAL AND APPLIED SCIENCES
OF
MIDDLE EAST TECHNICAL UNIVERSITY

BY

ERAY ÖZÇELİK

IN PARTIAL FULFILLMENT OF THE REQUIREMENTS
FOR
THE DEGREE OF MASTER OF SCIENCE
IN
ELECTRICAL AND ELECTRONICS ENGINEERING

APRIL 2005

Approval of the Graduate School of Natural and Applied Sciences

_____
Prof. Dr. Canan ÖZGEN
Director

I certify that this thesis satisfies all the requirements as a thesis for the degree of Master of Science.

_____
Prof. Dr. İsmet ERKMEN
Head of Department

This is to certify that we have read this thesis and that in our opinion it is fully adequate, in scope and quality, as a thesis for the degree of Master of Science.

_____
Prof. Dr. Aydın ERSAK
Supervisor

**Examining Committee Members**

Prof. Dr. Muammer ERMİŞ (METU, EE) _____

Prof. Dr. Aydın ERSAK (METU, EE) _____

Prof. Dr. Yıldırım ÜÇTUĞ (METU, EE) _____

Prof. Dr. Işık ÇADIRCI (Hacettepe Unv., EE) _____

Assistant Prof. Dr. Ahmet HAVA (METU, EE) _____

**I hereby declare that all information in this document has been obtained and presented in accordance with academic rules and ethical conduct. I also declare that, as required by these rules and conduct, I have fully cited and referenced all material and results that are not original to this work.**

Name, Last name :

Signature :

# ABSTRACT

## SPEED SENSORLESS VECTOR CONTROL OF INDUCTION MOTOR DRIVE

ÖZÇELİK, Eray
M. Sc. Department of Electrical and Electronics Engineering
Supervisor: Prof. Dr. Aydın Ersak

APRIL 2005, 101 pages

Focus of this work is closed-loop speed control of an induction machine based on direct field-oriented control (DFOC) algorithm, using estimates of speed and flux observers which utilize only stator current and voltage. Theoretical bases of the algorithms are explained in detail and their performances are investigated with simulations and experiments.

Field Orientated Control is based on projections which transform a three phase time and speed dependent system into a two co-ordinate time invariant system. These projections lead to a structure similar to that of a DC machine control. Transformations are done in synchronous frame aligned to d-axis of rotor flux. So rotor flux position must be known accurately to make these transformations. Designed flux observer, in which voltage model is assisted by current model via a closed-loop to compensate voltage model's disadvantages, estimates the position of the rotor flux.

Obtaining adequate torque control via FOC, speed loop is closed using conventional PI regulators. Speed feedback is necessary to complete control loop. Model Reference Adaptive System is studied as a speed estimator. Reactive power scheme is applied to MRAS algorithm to estimate rotor speed.

In this study, the direct (rotor) flux oriented control system with flux and speed estimators is described and tested in real-time with the starter kit named TMS320F2812 eZdsp DSK and the Embedded Target for the TI C2000 DSP tool of Matlab.

Keywords: Sensorless direct field oriented, flux estimation, speed estimation.

# ÖZ

## ENDÜKSİYON MOTOR SÜRÜCÜSÜN HIZ ÖLÇÜMSÜZ VEKTÖR DENETİMİ

ÖZÇELİK, Eray
Yüksek Lisans, Elektrik ve Elektronik Mühendisliği Bölümü
Tez Yöneticisi: Prof. Dr. Aydın Ersak

Nisan 2005, 101 sayfa

Bu çalışmanın odağı, endüksiyon motorunun doğrudan alan yönlendirme yöntemi ile kapalı döngü hız denetiminin yapılmasıdır. Hız ve akı bilgileri sadece stator akım ve gerilimleri ölçülerek kestirilmişlerdir. Çalışma sırasında kullanılan kestirme yöntemlerinin kuramsal içerikleri ayrıntılı olarak anlatılmış ve başarımları benzetim ve denemelerle incelenmiştir.

Alan yönlendirmeli denetim, zamana ve hıza bağlı üç eksenli sistemlerin, hızdan bağımsız iki eksenli sistemlere dönüştürülmesi yöntemine dayanır. Bu dönüşümler ile DC motor denetimine benzer bir denetim yapısı elde edilir. Dönüşümler, senkron hızda dönen rotor akısının d-eksenindeki bileşenine yönlendirme ile gerçekleştirilir. Bunun için rotor akısının yerinin yüksek bir doğrulukla bilinmesi gereklidir. Tasarlanan akı kestiricisi, gerilim modelinin hatalarını, akım modeli yardımıyla ortadan kaldırarak rotor akısının yerini yüksek doğrulukla kestirebilmektedir.

Alan yönlendirmeli denetim yöntemi ile yeterli seviyede kapalı döngü burma denetimi elde edilebilir. Burma denetimini içeriye yerleştirdikten sonra dışarıya da hız denetim döngüsünü yerleştirmek gerekecektir. Dışarıdaki hız kapalı döngüsünü tamamlayabilmek için hız geribeslemesine gereksinim vardır. Hız kestirmesi için modele dayalı uyarlamalı yöntem çalışılmıştır.

Bu çalışmada hız ve akı kestirmeçli, doğrudan rotor akısına yönlendirmeli system anlatılmış ve TMS320F2812 eZdsp DSK başlangıç kartı ve Embedded Target for the TI C2000 DSP yazılımı kullanılarak gerçek zamanlı olarak denenmiştir.

Anahtar Kelimeler: Sensörsüz alan yönlendirmeli denetim, akı kestirme yöntemi, hız kestirme yöntemi

# ACKNOWLEDGEMENTS

I appreciate to Prof. Dr. Aydın ERSAK for his valuable supervision during the development and the improvement stages of this thesis.

I also wish to thank to ASELSAN Inc. for the facilities provided for the completion of this thesis.

Thanks a lot to my friends, Günay ŞİMŞEK, Murat ERTEK, Evrim ARI for their helps during experimental stage of this work.

I appreciate my wife due to her trust, great encouragement and continuous morale support.

# TABLE OF CONTENTS

# LIST OF TABLES

# LIST OF FIGURES

# CHAPTER 1

# INTRODUCTION

Two basic forms of rotor flux field orientation exist. These are the direct field orientation, which relies on direct measurement and estimation of rotor flux magnitude and angle, and the indirect field orientation, which utilizes slip relation. Indirect field orientation is a feedforward approach and is naturally parameter sensitive, especially to the rotor time constant. This has lead to numerous parameter adapting strategies. [**1**]- [**7**]

Direct Field oriented control (DFOC) employs flux angle $\theta_e$ which is classically calculated by sensing the air-gap flux with the flux sensing coils. This adds to the cost and complexity of the drive system. To avoid from using these speed sensors on the induction machine drive systems, many different algorithms are proposed for last three decades to estimate the rotor flux vector and or/ rotor shaft speed. The recent trend in field-oriented control is towards avoiding the use of speed sensors and using algorithms based on the terminal quantities of the machine for the estimation of the fluxes.

One of these above referred flux and speed estimation techniques (algorithms) is saliency based with fundamental or high frequency signal injection. One advantage of the saliency technique is that the saliency is not sensitive to actual motor parameters, but this method fails at low and zero speed level. When applied with high frequency signal injection, the method may cause torque ripples, vibration and audible noise [**8**].

Gabriel avoided the special flux sensors and coils by estimating the rotor flux from the terminal quantities (stator voltages and currents)[**9**]. This technique requires the knowledge of the stator resistance along with the stator-leakage, and rotor-leakage inductances and the magnetizing inductance. This method is commonly known as the Voltage Model Flux Observer (VMFO)

Voltage model utilizes the measured stator voltage and current, but not the velocity. These types of estimators require a pure integration without feedback. So it is difficult to implement them for low excitation frequencies due to the offset and initial condition problems. Due to the lack of feedback which is necessary for convergence, low pass filter is often used to provide stability in practice. Accuracy of voltage model based observer is completely insensitive to rotor resistance but is most sensitive to stator resistance at low velocities. At high velocities the stator resistance IR drop is less significant relative to the speed voltage. This reduces sensitivity to stator resistance. The study of parameter sensitivity shows that the leakage inductance can significantly affect the system performance regarding to stability, dynamic response and utilization of the machine and the inverter.

The Current Model Flux Observer (CMFO) is an alternative approach to overcome the problems caused by the changes in leakage inductance and stator resistance at low speed.

Current model based observers use the measured stator currents and rotor velocity. The velocity dependency of the current model is a drawback since this means that even though using the estimated flux eliminates the flux sensor, position sensor is still required. Furthermore, at zero or low speed operation rotor flux magnitude response is sensitive primarily to the rotor resistance, although the phase angle is insensitive to all parameters. Near rated slip, both of them are sensitive to the rotor resistance and magnetizing inductance. In whole speed range accuracy is unaffected by the rotor leakage inductance.

In addition there is an estimator based on cancellation methods. In these methods approximate differentiation of signals is used to cancel the effects of integration. This approach is known as pole/zero cancellation in linear systems. Due to differentiation, such approaches are intensive to measurement and quantization

noise. A full order open-loop observer on the other hand can be formed using only the measured stator voltage and rotor velocity as inputs where the stator current appears as an estimated quantity. Because of its dependency on the stator current estimation, the full order observer will not exhibit better performance than the current model. Furthermore, parameter sensitivity and observer gain are the problems to be tuned in a full order observer design [**10**].

These observer structures are all open-loop schemes, based on the induction machine model and they do not employ any feedback. Therefore they are quite sensitive to parameter variations.

A prior approach to provide a smooth transition between current and voltage models was developed by Takahashi and Noguchi. They combined two stator flux models via a first order lag-summing network[**11**].

Closed-loop observer approach proposed in [**12**] [**13**] [**14**] combines the best accuracy attributes of current and voltage models by smooth and deterministic transition between flux estimates produced by these models. Closed loop observer proposed in (11) is formed from two open-loop observers which are referred as current and voltage models. Inputs of the current model are measured stator currents and rotor position. The current model is implemented in rotor flux frame because, implementation in stationary frame requires measured rotor velocity. Transformation to the rotor flux frame permits the use of rotor position instead of velocity. Voltage model utilizes measured stator voltages and currents. The smooth transition between current and voltage models flux estimates is governed by rotor flux regulator. A rotor-flux-regulated and –oriented system is sensitive to leakage inductance under high slip operation. Both a stator-flux-regulated and –oriented system and stator-flux-regulated, rotor-flux-oriented system have reduced parameter sensitivity.

In [**15**] stator-flux-regulated, rotor-flux-oriented closed-loop observer is used for direct torque control (DTC) algorithm. This estimator is able to generate accurate flux estimation for whole speed range.

DTC algorithm handles torque control problem but to achieve good speed response, rotor speed also must be known. Verghese have approached speed estimation problem from a parameter identification point of view [**16**] [**17**] [**18**]. The

idea is to consider the speed as an unknown constant parameter, and to find the estimated speed that best fits the measured or calculated data to the dynamic equations of the motor. But parameter variations have significant impact on performance of the estimator. Possible stator resistance variation due to ohmic heating results in deterioration in performance [**19**].

Yoo and Ha [**20**] [**21**] studied on non-linear method. Method they proposed estimates the speed without assuming that the speed is slowly varying compared to electrical variables. Their approach uses polar coordinate model of the fluxes rather than the cartesian coordinates. They constructed two estimators; main flux estimator and complementary flux estimator. Main flux estimator could not quarantie convergence for all operating conditions. In this operating conditions such as start up complementary estimator is used. Significant sensitivity to parameter uncertainty is observed with this method.

Speed estimator based on MRAS studied in [**22**] [**23**]. In MRAS, in general a comparison is made between the outputs of two estimators. The estimator which does not contain the quantity to be estimated can be considered as a reference model of the induction machine. The other one, which contains the estimated quantity, is considered as an adjustable model. The error between these two estimators is used as an input to an adaptation mechanism. For sensorless control algorithms most of the times the quantity which differ the reference model from the adjustable model is the rotor speed. When the estimated rotor speed in the adjustable model is changed in such a way that the difference between two estimators converges to zero asymptotically, the estimated rotor speed will be equal to actual rotor speed. In [**24**],[**25**],[**26**] voltage model is assumed as reference model, current model is assumed as the adjustable model and estimated rotor flux is assumed as the reference parameter to be compared. In [**23**] similar speed estimators are proposed based on the MRAS and a secondary variable is introduced as the reference quantity by putting the rotor flux through a first-order delay instead of a pure integration to nullify the offset. However their algorithm produces inaccurate estimated speed if the excitation frequency goes below certain level. In addition these algorithms suffer from the machine parameter uncertainties because of the reference model since the parameter

variation in the reference model cannot be corrected. [**22**] suggests an alternative MRAS based on the electromotive force rather than rotor flux as reference quantity for speed estimation where the integration problem has been overcome. Further in [**22**], another new auxiliary variable is introduced which represents the instantaneous reactive power for maintaining the magnetizing current. In this MRAS algorithm stator resistance disappear from the equations making the algorithm robust to that parameter.

This work is mainly focused on closed loop speed control of induction machine. Speed is estimated using MRAS algorithm which assumes reactive power as a reference parameter. Rotor flux estimated from stator currents and voltages- using closed-loop flux observer - is employed in DFOC to achieve adequate level torque control. It is shown that the rotor flux and speed estimation performance of these schemes is quite satisfactory in both simulations and experimental results.

# CHAPTER 2

# INDUCTION MACHINE MODELING, SVPWM and FOC

In this chapter, state equations of induction machine, which are necessary to develop current and voltage observers explained in the next chapters, will be introduced. For this, let us now proceed to calculate the state equations of idealized three phase induction machine.

## 2.1. System Equations in the Stationary a,b,c Reference Frame

In particular we will asume the winding configuration shown in the Figure 2-1. In this case the winding placement is only conseptually shown with the center line of equivalent inductors directed along the magnetic axes of the windings. An elementary two pole machine is considered. Balanced 3ph windings are assumed for both stator and rotor. That is all 3 stator windingds designated as the as,bs and cs windings are assumed to have the same number of effective turns, Ns, and the bs and cs windings are symetricaly displaced from the as winding by $\pm 120^{o}$. The subscript 's' is used to denote that these windings are stator or stationary windings. The rotor windings are similarly arranged but have Nr turns. These windings are designated by ar,br and cr in which second subscript reminds us that these three windings are rotor or rotating windings.

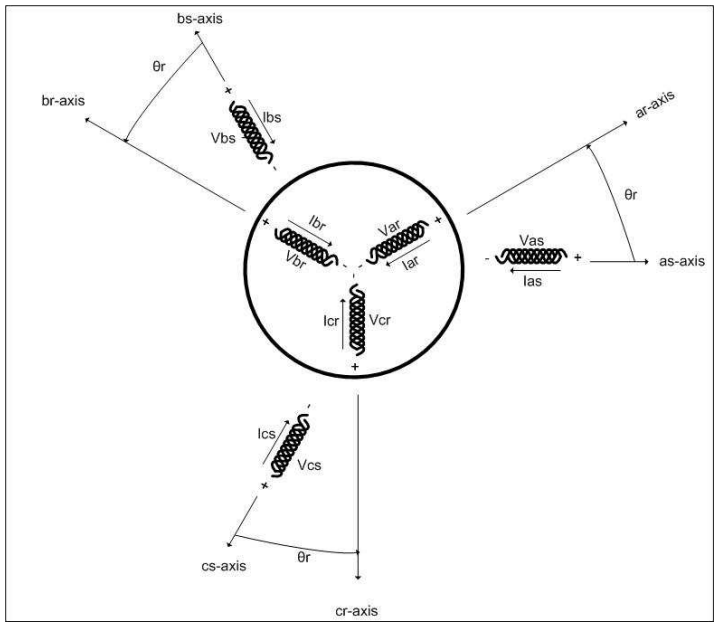


Figure 2-1 Magnetic axes of three phase induction machine

The voltage equations describing the stator and rotor circuits can be written conveniently in the matrix form as

$$\begin{aligned} v_{abcs} &= r_s i_{abcs} + p\psi_{abcs} \\ v_{abcr} &= r_r i_{abcr} + p\psi_{abcr} \end{aligned} \tag{2-1}$$

Where p is derivative operator and $v_{abcs}$, $i_{abcs}$ and $\psi_{abcs}$ are 3x1 vectors defined by

$$v_{abcs} = \begin{bmatrix} v_{as} \\ v_{bs} \\ v_{cs} \end{bmatrix}; \quad i_{abcs} = \begin{bmatrix} i_{as} \\ i_{bs} \\ i_{cs} \end{bmatrix}; \quad \psi_{abcs} = \begin{bmatrix} \psi_{as} \\ \psi_{bs} \\ \psi_{cs} \end{bmatrix} \tag{2-2}$$

Similar definitions apply for the rotor variables $v_{abcr}$, $i_{abcr}$ and $\psi_{abcr}$.

In general coupling clearly exists between all of the stator and rotor phases. The flux linkages are therefore related to the machine currents by the following matrix eqn.

$$\psi_{abcs} = \psi_{abcs(s)} + \psi_{abcs(r)}$$
$$\psi_{abcr} = \psi_{abcr(s)} + \psi_{abcr(r)} \tag{2-3}$$

where

$$\psi_{abcs(s)} = \begin{bmatrix} L_{as} & L_{abs} & L_{acs} \\ L_{abs} & L_{bs} & L_{bcs} \\ L_{acs} & L_{bcs} & L_{cs} \end{bmatrix} i_{abcs} \tag{2-4}$$

$$\psi_{abcs(r)} = \begin{bmatrix} L_{as,ar} & L_{as,br} & L_{as,cr} \\ L_{bs,ar} & L_{bs,br} & L_{bs,cr} \\ L_{cs,ar} & L_{cs,br} & L_{cs,cr} \end{bmatrix} i_{abcr} \tag{2-5}$$

$$\psi_{abcr(r)} = \begin{bmatrix} L_{ar} & L_{abr} & L_{acr} \\ L_{abr} & L_{br} & L_{bcr} \\ L_{acr} & L_{bcr} & L_{cr} \end{bmatrix} i_{abcr} \tag{2-6}$$

$$\psi_{abcr(s)} = \begin{bmatrix} L_{ar,as} & L_{ar,bs} & L_{ar,cs} \\ L_{br,as} & L_{br,bs} & L_{br,cs} \\ L_{cr,as} & L_{cr,bs} & L_{cr,cs} \end{bmatrix} i_{abcs} \tag{2-7}$$

Note that as a result of reciprocity, the inductance matrix in the third flux linkage equation, (2-6), above is simply transpose of the inductance matrix in the second equation, (2-5).

### 2.1.1. Determination of Induction Machine Inductances

While the number of inductances defined is large, Task of solving for all of these inductances is staightforward.

The mutual inductance between winding x and winding y is calculated according to equation

$$L_{xy} = \mu_0 N_x N_y \left(\frac{rl}{g}\right)\left(\frac{\pi}{4}\right)\cos\alpha \tag{2-8}$$

Where r is radious, l is lenght of the motor and g is the lenght of airgap. $N_x$ is the number of effective turns of the winding x and $N_y$ is the number of effective turns of the winding y. Notice that alpha is the angle between magnetic axes of the phases x and y.

The self inductance of stator phase as is obtained by simply setting α=0, and by setting $N_x$ and $N_y$ in (2-8) to $N_s$. Whereby,

$$L_{am} = \mu_0 N_s^2 \left(\frac{rl}{g}\right)\left(\frac{\pi}{4}\right) \tag{2-9}$$

The subscript m is again used to denote the fact that this inductance is magnetizing inductance. That is, it is associated with flux lines which cross the air gap and link rotor as well as stator windings. In general, it is necessary to add a relatively small, but important, leakage term to (2-9) to account for leakage flux. This term accounts for flux lines which do not cross the gap but instead close with the stator slot itself (slot leakage), in the air gap (belt and harmonic leakage) and at the ends of the machine (end winding leakage). Hence, the total self inductance of phase as can be expressed.

$$L_{as} = L_{ls} + L_{am} \tag{2-10}$$

where $L_{ls}$ represents the leakage term. Since the windings of the bs and the cs phases are identical to phase as, it is clear that the magnetizing inductances of these windings are the same as phase as so that, also

$$\begin{aligned} L_{bs} &= L_{ls} + L_{bm} \\ L_{cs} &= L_{ls} + L_{cm} \end{aligned} \tag{2-11}$$

It is apparent that $L_{am}$, $L_{bm}$, $L_{cm}$ are equal making the self inductances also equal. It is therefore useful to define stator magnetizing inductance

$$L_{ms} = \mu_0 N_s^2 \left(\frac{rl}{g}\right)\left(\frac{\pi}{4}\right) \tag{2-12}$$

so that

$$L_{as} = L_{bs} = L_{cs} = L_{ls} + L_{ms} \tag{2-13}$$

The mutual inductance between phases as and bs, bs and cs, and cs and as are derived by simply setting $\alpha=2\pi/3$ and $N_x=N_y=N_s$ in (2-8). The result is

$$L_{abs} = L_{bcs} = L_{cas} = -\mu_0 N_s^2 \left(\frac{rl}{g}\right)\left(\frac{\pi}{8}\right) \tag{2-14}$$

or, in terms of (2-12),

$$L_{abs} = L_{bcs} = L_{cas} = -\frac{L_{ms}}{2} \tag{2-15}$$

The flux linkages of phases as, bs and cs resulting from currents flowing in the stator windings can now be expressed in matrix form as

$$\psi_{abcs(s)} = \begin{bmatrix} L_{ls}+L_{ms} & -\frac{L_{ms}}{2} & -\frac{L_{ms}}{2} \\ -\frac{L_{ms}}{2} & L_{ls}+L_{ms} & -\frac{L_{ms}}{2} \\ -\frac{L_{ms}}{2} & -\frac{L_{ms}}{2} & L_{ls}+L_{ms} \end{bmatrix} i_{abcs} \tag{2-16}$$

Let us now turn our attention to the mutual coupling between the stator and rotor windings. Referring to Figure 2-1, we can see that the rotor phase ar is displaces by stator phase as by the electrical angle $\theta_r$ where $\theta_r$ in this case is a variable. Similarly the rotor phases br and cr are displaced from stator phases bs and cs respectively by $\theta_r$. Hence, the corresponding mutual inductances can be obtained by setting $N_x=N_s$, $N_y=N_r$,and $\alpha=\theta_r$ in (2-8).

$$\begin{aligned} L_{as,ar} = L_{bs,br} = L_{cs,cr} &= \mu_0 N_s N_r \left(\frac{rl}{g}\right)\cos\theta_r \\ &= \frac{N_r}{N_s} L_{ms}\cos\theta_r \end{aligned} \tag{2-17}$$

The angle between the as and br phases is $\theta_r$+2π/3, so that

$$L_{as,br} = L_{bs,cr} = L_{cs,ar} = \frac{N_r}{N_s} L_{ms} \cos\left(\theta_r + 2\pi/3\right) \tag{2-18}$$

Finally, the stator phase as is displaced from the rotor cr phase by angle $\theta_r - 2\pi/3$. Therefore,

$$L_{as,cr} = L_{bs,ar} = L_{cs,br} = \frac{N_r}{N_s} L_{ms} \cos\left(\theta_r - 2\pi/3\right) \tag{2-19}$$

The above inductances can now be used to establish the flux linking the stator phases due to currents in the rotor circuits. In matrix form,

$$\psi_{abcs(r)} = \frac{N_r}{N_s} L_{ms} \begin{bmatrix} \cos\theta_r & \cos\left(\theta_r + 2\pi/3\right) & \cos\left(\theta_r - 2\pi/3\right) \\ \cos\left(\theta_r - 2\pi/3\right) & \cos\theta_r & \cos\left(\theta_r + 2\pi/3\right) \\ \cos\left(\theta_r + 2\pi/3\right) & \cos\left(\theta_r - 2\pi/3\right) & \cos\theta_r \end{bmatrix} i_{abcr} \tag{2-20}$$

The total flux linking the stator windings is clearly the sum of the contributions from the stator and the rotor circuits, (2-16) and (2-20),

$$\psi_{abcs} = \psi_{abcs(s)} + \psi_{abcs(r)} \tag{2-21}$$

It is not difficult to continue the process to determine the rotor flux linkages. In terms of previously defined quantities, the flux linking the rotor circuit due to rotor currents is

$$\psi_{abcr(r)} = \begin{bmatrix} L_{lr} + \left(\frac{N_r}{N_s}\right)^2 L_{ms} & -\frac{1}{2}\left(\frac{N_r}{N_s}\right)^2 L_{ms} & -\frac{1}{2}\left(\frac{N_r}{N_s}\right)^2 L_{ms} \\ -\frac{1}{2}\left(\frac{N_r}{N_s}\right)^2 L_{ms} & L_{lr} + \left(\frac{N_r}{N_s}\right)^2 L_{ms} & -\frac{1}{2}\left(\frac{N_r}{N_s}\right)^2 L_{ms} \\ -\frac{1}{2}\left(\frac{N_r}{N_s}\right)^2 L_{ms} & -\frac{1}{2}\left(\frac{N_r}{N_s}\right)^2 L_{ms} & L_{lr} + \left(\frac{N_r}{N_s}\right)^2 L_{ms} \end{bmatrix} i_{abcr} \tag{2-22}$$

where $L_{lr}$ is the rotor leakage inductance. The flux linking the rotor windings due to currents in the stator circuit is

$$\psi_{abcr(s)} = \frac{N_r}{N_s} L_{ms} \begin{bmatrix} \cos\theta_r & \cos(\theta_r - 2\pi/3) & \cos(\theta_r + 2\pi/3) \\ \cos(\theta_r + 2\pi/3) & \cos\theta_r & \cos(\theta_r - 2\pi/3) \\ \cos(\theta_r - 2\pi/3) & \cos(\theta_r + 2\pi/3) & \cos\theta_r \end{bmatrix} i_{abcs} \qquad (2\text{-}23)$$

Note that the matrix of (2-23) is the transpose of (2-20).

The total flux linkages of the rotor windings are again the sum of the two components defined by (2-22) and (2-23), that is

$$\psi_{abcr} = \psi_{abcr(r)} + \psi_{abcr(s)} \qquad (2\text{-}24)$$

### 2.1.2. Three-Phase to Two-Phase Transformation

It is apparent that extensive amount of coupling between the six circuits makes the analysis of this machine a rather formidable task. However we are now in position to determine if there is any simplification that can be expected between these coupled equations.

In the study of generalized machine theory, mathematical transformations are often used to decouple variables, to facilitate the solutions of difficult equations with time varying coefficients, or to refer all variables to a common reference frame. For this purpose, the method of symmetrical components uses a complex transformation to decouple the abc phase variables:

$$[f_{012}] = [T_{012}][f_{abc}] \qquad (2\text{-}25)$$

The variable, $f_{abc}$ in (2-1) may be the three-phase ac currents, voltages or fluxes. The subscripts a,b and c indicate three distinct phases of three phase systems. The transformation is given by:

$$[T_{012}] = \frac{1}{3} \begin{bmatrix} 1 & 1 & 1 \\ 1 & a & a^2 \\ 1 & a^2 & a \end{bmatrix} \qquad (2\text{-}26)$$

Where $a = e^{j\frac{2\pi}{3}}$. Its inverse is given by:

$$[T_{012}]^{-1} = \frac{1}{3}\begin{bmatrix} 1 & 1 & 1 \\ 1 & a^2 & a \\ 1 & a & a^2 \end{bmatrix} \tag{2-27}$$

The symmetrical component transformation is applicable to steady-state vectors or instantaneous quantities equally.

#### 2.1.2.1. Park Transformation

The Park's transformation is a well known three-phase to two-phase transformation. The transformation transforms three-phase quantities $f_{abc}$ into two-phase quantities developed on a rotating dq0 axes system, whose speed is $w$ as shown in the Figure 2-2.

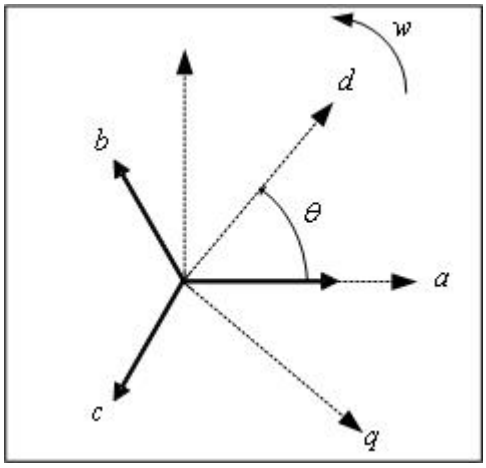


Figure 2-2 Relationship between the dq and the abc quantities

$$[f_{dq0}] = [T_{dq0}(\theta)][f_{abc}] \tag{2-28}$$

where the dq0 transformation matrix is defined as:

$$[T_{dq0}(\theta)] = \frac{2}{3}\begin{bmatrix} \cos\theta & \cos\left(\theta - \frac{2\pi}{3}\right) & \cos\left(\theta + \frac{2\pi}{3}\right) \\ -\sin\theta & -\sin\left(\theta - \frac{2\pi}{3}\right) & -\sin\left(\theta + \frac{2\pi}{3}\right) \\ \frac{1}{2} & \frac{1}{2} & \frac{1}{2} \end{bmatrix} \quad (2\text{-}29)$$

and the inverse is given by:

$$[T_{dq0}(\theta)]^{-1} = \begin{bmatrix} \cos\theta & -\sin\theta & 1 \\ \cos\left(\theta - \frac{2\pi}{3}\right) & -\sin\left(\theta - \frac{2\pi}{3}\right) & 1 \\ \cos\left(\theta + \frac{2\pi}{3}\right) & -\sin\left(\theta + \frac{2\pi}{3}\right) & 1 \end{bmatrix} \quad (2\text{-}30)$$

where $\theta$ is the angle between the phases a and d. Notice that, $\theta$ is time integral of $w$, which is the rotation speed of the dq reference frame and it is chosen arbitrarily for the sake of generality.

### 2.1.3. Circuit Equations in Arbitrary dq0 Reference Frame

The dq0 reference frames are usually selected on the basis of conveniences or computational reduction. The two common reference frames used in the analysis of induction machine are the stationary frame (i.e. $w = 0$), with a frame notation $d^sq^s$, and synchronously rotating frame (i.e. $w = w_s$, synchronous speed), with a frame notation $d^eq^e$. Each has an advantage for some purpose. In the stationary rotating reference frame, the $d^sq^s$ variables of the machine are in the same frame as those normally used for the supply network. In the synchronously rotating frame, the $d^eq^e$ variables are dc in steady state. First of all, the equations of the induction machine in the arbitrary reference frame, which is rotating at a speed $w$, in the direction of the rotor rotation, will be derived. When the induction machine runs in the stationary frame, these equations of the induction machine, can then be obtained by setting $w = 0$. These equations can also be obtained in the synchronously rotating frame by setting $w = w_e$.

### 2.1.3.1. qd0 Voltage Equations

In matrix notation, the stator winding abc voltage equations can be expressed as:

$$v_{abcs} = r_s i_{abcs} + p\psi_{abcs} \tag{2-31}$$

Applying the transformations given in (2-29) and (2-30), to the voltage, current and flux linkages, (2-31) becomes

$$v_{dq0s} = \left[T_{qd0}(\theta)\right] p\left(\left[T_{qd0}(\theta)\right]^{-1}\left[\psi_{dq0s}\right]\right) + \left[T_{qd0}(\theta)\right] r_s \left(\left[T_{qd0}(\theta)\right]^{-1}\left[i_{dq0s}\right]\right) \tag{2-32}$$

applying the chain rule in (2-32)

$$\begin{aligned} v_{dq0s} &= \left[T_{qd0}(\theta)\right]\left\{\left(p\left[T_{qd0}(\theta)\right]^{-1}\right)\left[\psi_{dq0s}\right] + \left[T_{qd0}(\theta)\right]^{-1}\left(p\left[\psi_{dq0s}\right]\right)\right\} \\ &+ r_s\left[T_{qd0}(\theta)\right]\left[T_{qd0}(\theta)\right]^{-1}\left[i_{dq0s}\right] \end{aligned} \tag{2-33}$$

which is equal to

$$\begin{aligned} v_{dq0s} &= \left[T_{qd0}(\theta)\right]\left(p\left[T_{qd0}(\theta)\right]^{-1}\right)\left[\psi_{dq0s}\right] + \left[T_{qd0}(\theta)\right]\left[T_{qd0}(\theta)\right]^{-1}\left(p\left[\psi_{dq0s}\right]\right) \\ &+ r_s\left[T_{qd0}(\theta)\right]\left[T_{qd0}(\theta)\right]^{-1}\left[i_{dq0s}\right] \end{aligned} \tag{2-34}$$

Note that

$$\left[T_{dq0}\right]\left(p\left[T_{dq0}\right]^{-1}\right) = \frac{d\theta}{dt}\begin{bmatrix} 0 & 1 & 0 \\ -1 & 0 & 0 \\ 0 & 0 & 0 \end{bmatrix} \tag{2-35}$$

Then (2-34) becomes:

$$v_{dq0s} = w\begin{bmatrix} 0 & 1 & 0 \\ -1 & 0 & 0 \\ 0 & 0 & 0 \end{bmatrix}\psi_{dq0s} + p\psi_{dq0s} + r_{dq0s} i_{dq0s} \tag{2-36}$$

where

$$w = \frac{d\theta}{dt} \qquad and \qquad r_{dq0s} = r_s \begin{bmatrix} 1 & 0 & 0 \\ 0 & 1 & 0 \\ 0 & 0 & 1 \end{bmatrix} \tag{2-37}$$

Likewise, the rotor voltage equation becomes:

$$v_{dq0r} = (w - w_r) \begin{bmatrix} 0 & 1 & 0 \\ -1 & 0 & 0 \\ 0 & 0 & 0 \end{bmatrix} \psi_{dq0r} + p\psi_{dq0r} + r_{dq0r} i_{dq0r} \tag{2-38}$$

### 2.1.3.2. qd0 Flux Linkage Relation

The stator qd0 flux linkages are obtained by applying $[T_{qd0}(\theta)]$ to the stator abc flux linkages equation.

$$\psi_{dq0s} = [T_{qd0}(\theta)]\psi_{abcs} \tag{2-39}$$

referring (2-21), (2-39) is written as

$$\psi_{dq0s} = [T_{qd0}(\theta)]\left(\psi_{abcs(s)} + \psi_{abcs(r)}\right) \tag{2-40}$$

putting (2-22) and (2-23) into (2-40);

$$\begin{aligned} \psi_{dq0s} = \left[T_{dq0}(\theta)\right] & \begin{bmatrix} L_{ls} + L_{ms} & -\frac{L_{ms}}{2} & -\frac{L_{ms}}{2} \\ -\frac{L_{ms}}{2} & L_{ls} + L_{ms} & -\frac{L_{ms}}{2} \\ -\frac{L_{ms}}{2} & -\frac{L_{ms}}{2} & L_{ls} + L_{ms} \end{bmatrix} i_{abcs} \\ + \left[T_{dq0}(\theta)\right] \frac{N_r}{N_s} L_{ms} & \begin{bmatrix} \cos\theta_r & \cos(\theta_r + 2\pi/3) & \cos(\theta_r - 2\pi/3) \\ \cos(\theta_r - 2\pi/3) & \cos\theta_r & \cos(\theta_r + 2\pi/3) \\ \cos(\theta_r + 2\pi/3) & \cos(\theta_r - 2\pi/3) & \cos\theta_r \end{bmatrix} i_{abcr} \end{aligned} \tag{2-41}$$

skipping the transformation steps the stator and the rotor flux linkage relationships can be expressed compactly:

$$\begin{bmatrix} \psi_{qs} \\ \psi_{ds} \\ \psi_{0s} \\ \psi_{qr} \\ \psi_{dr} \\ \psi_{0r} \end{bmatrix} = \begin{bmatrix} L_s & 0 & 0 & L_m & 0 & 0 \\ 0 & L_s & 0 & 0 & L_m & 0 \\ 0 & 0 & L_{ls} & 0 & 0 & 0 \\ L_m & 0 & 0 & L_r & 0 & 0 \\ 0 & L_m & 0 & 0 & L_r & 0 \\ 0 & 0 & 0 & 0 & 0 & L_m \end{bmatrix} \begin{bmatrix} i_{qs} \\ i_{ds} \\ i_{0s} \\ i_{qr} \\ i_{dr} \\ i_{0r} \end{bmatrix} \tag{2-42}$$

where

$$\begin{aligned} L_s &= L_{ls} + L_m \\ L_r &= L_{lr} + L_m \end{aligned} \tag{2-43}$$

and

$$L_m = \frac{3}{2} L_{ms} = \frac{3}{2} N_s^2 \left( \mu_0 \frac{rl}{g} \right) \frac{\pi}{4} \tag{2-44}$$

### 2.1.3.3. qd0 Torque Equations

The sum of the instantaneous input power to all six windings of the stator and rotor is given by:

$$p_{in} = v_{as} i_{as} + v_{bs} i_{bs} + v_{cs} i_{cs} + v_{ar} i_{ar} + v_{br} i_{br} + v_{cr} i_{cr} \quad W \tag{2-45}$$

in terms of dq quantities

$$p_{in} = \frac{3}{2} (v_{qs} i_{qs} + v_{ds} i_{ds} + 2 v_{0s} i_{0s} + v_{qr} i_{qr} + v_{dr} i_{dr} + 2 v_{0r} i_{0r}) W \tag{2-46}$$

Using stator and rotor voltages to substitute for the voltages on the right hand side of (2-46), we obtain three kinds of terms: $i^2 r, i p\psi, and\ w\psi i$. $i^2 r$ terms are the cupper losses. The $i p\psi$ terms represent the rate of exchange of magnetic field energy between windings. The electromechanical torque developed by the machine is given by the sum of the $w\psi i$ terms divided by mechanical speed, that is:

$$T_{em} = \frac{3}{2}\frac{p}{2w_r}\left[w(\psi_{ds}i_{qs} - \psi_{qs}i_{ds}) + (w - w_r)(\psi_{dr}i_{qr} - \psi_{qr}i_{dr})\right] \quad Nm \qquad (2\text{-}47)$$

using the flux linkage relationships, $T_{em}$ can also be expressed as follows:

$$T_{em} = \frac{3}{2}\frac{P}{2w_r}\left[w(\psi_{ds}i_{qs} - \psi_{qs}i_{ds}) + (w - w_r)(\psi_{dr}i_{qr} - \psi_{qr}i_{dr})\right] \quad Nm \qquad (2\text{-}48)$$

Using the flux linkage relationships, one can show that

$$T_{em} = \frac{3}{2}\frac{P}{2}(\psi_{qr}i_{dr} - \psi_{dr}i_{qr}) \quad Nm$$

$$= \frac{3}{2}\frac{P}{2}(\psi_{ds}i_{qs} - \psi_{qs}i_{ds}) \quad Nm \qquad (2\text{-}49)$$

$$= \frac{3}{2}\frac{P}{2}L_m(i_{dr}i_{qs} - i_{qr}i_{ds}) \quad Nm$$

### 2.1.4. qd0 Stationary and Synchronous Reference Frames

There is seldom a need to simulate an induction machine in the arbitrary rotating reference frame. But it is useful to convert a unified model to other frames. The most commonly used ones are, two marginal cases of the arbitrary rotating frame, stationary reference frame and synchronously rotating frame. For transient studies of adjustable speed drives, it is usually more convenient to simulate an induction machine and its converter on a stationary reference frame. Moreover, calculations with stationary reference frame are less complex due to zero frame speed (some terms cancelled). For small signal stability analysis about some operating condition, a synchronously rotating frame which yields dc values of steady-state voltages and currents under balanced conditions is used.

Since we have derived the circuit equations of induction machine for the general case that is in the arbitrary rotating reference frame, the circuit equations of the machine in the stationary reference frame (denoted as $d^sq^s$) and synchronously rotating reference frame (denoted as $d^eq^e$) can be obtained by simply setting $w$ to zero

and $w_e$, respectively. To distinguish these two frames from each other, an additional superscript will be used, s for stationary frame variables and e for synchronously rotating frame variables.

Stator $q^s d^s$ voltage equations:

$$v^s_{qs} = p\psi^s_{qs} + r_s i^s_{qs}$$
$$v^s_{ds} = p\psi^s_{ds} + r_s i^s_{ds} \tag{2-50}$$

Rotor $q^s d^s$ voltage equations:

$$v^s_{qr} = p\psi^s_{qr} + (-w_r)\psi^s_{dr} + r_r i^s_{qr}$$
$$v^s_{dr} = p\psi^s_{dr} + (w_r)\psi^s_{qr} + r_r i^s_{dr} \tag{2-51}$$

where

$$\begin{bmatrix} \psi^s_{qs} \\ \psi^s_{ds} \\ \psi^s_{qr} \\ \psi^s_{dr} \end{bmatrix} = \begin{bmatrix} L_s & 0 & L_m & 0 \\ 0 & L_s & 0 & L_m \\ L_m & 0 & L_r & 0 \\ 0 & L_m & 0 & L_r \end{bmatrix} \begin{bmatrix} i^s_{qs} \\ i^s_{ds} \\ i^s_{qr} \\ i^s_{dr} \end{bmatrix} \tag{2-52}$$

Torque Equations:

$$T_{em} = \frac{3}{2}\frac{P}{2}(\psi^s_{qr} i^s_{dr} - \psi^s_{dr} i^s_{qr}) \ Nm$$
$$= \frac{3}{2}\frac{P}{2}(\psi^s_{ds} i^s_{qs} - \psi^s_{qs} i^s_{ds}) \quad Nm \tag{2-53}$$
$$= \frac{3}{2}\frac{P}{2} L_m (i^s_{dr} i^s_{qs} - i^s_{qr} i^s_{ds}) \ Nm$$

Stator $q^e d^e$ voltage equations:

$$v^e_{qs} = p\psi^e_{qs} + w_e\psi^e_{ds} + r_s i^e_{qs}$$
$$v^e_{ds} = p\psi^e_{ds} - w_e\psi^e_{qs} + r_s i^e_{ds} \tag{2-54}$$

Rotor $q^e d^e$ voltage equations:

$$v^e_{qr} = p\psi^e_{qr} + (w_e - w_r)\psi^e_{dr} + r_r i^e_{qr}$$
$$v^e_{dr} = p\psi^e_{dr} - (w_e - w_r)\psi^e_{qr} + r_r i^e_{dr} \quad (2\text{-}55)$$

where

$$\begin{bmatrix} \psi^e_{qs} \\ \psi^e_{ds} \\ \psi^e_{qr} \\ \psi^e_{dr} \end{bmatrix} = \begin{bmatrix} L_s & 0 & L_m & 0 \\ 0 & L_s & 0 & L_m \\ L_m & 0 & L_r & 0 \\ 0 & L_m & 0 & L_r \end{bmatrix} \begin{bmatrix} i^e_{qs} \\ i^e_{ds} \\ i^e_{qr} \\ i^e_{dr} \end{bmatrix} \quad (2\text{-}56)$$

Torque Equations:

$$T_{em} = \frac{3}{2}\frac{P}{2}(\psi'^e_{qr} i'^e_{dr} - \psi'^e_{dr} i'^e_{qr}) \qquad Nm$$
$$= \frac{3}{2}\frac{P}{2}(\psi^e_{ds} i^e_{qs} - \psi^e_{qs} i^e_{ds}) \qquad Nm \quad (2\text{-}57)$$

## 2.2. Space Vector Pulse Width Modulation (SVPWM)

### 2.2.1. Voltage Fed Inverter (VSI)

A diagram of the power circuit of a three phase VSI is shown in the Figure 2-3. The circuit has bridge topology with three branches (phases), each consisting of two power switches and two freewheeling diodes. The inverter here is supplied from an uncontrolled, diode-based rectifier, via d.c. link which contains an LC filter in the inverted configuration. It allows the power flow from the supply to the load only. Power flow cannot be reversed, if the load is to feed the power back to the supply due to the diode rectifier structure at the input side of the dc link. Therefore, in drive systems where the VSI-fed motor may not operate as a generator, a more complex supply system must be used. These involve either a braking resistance connected across the d.c. link or replacement of the uncontrolled rectifier by a dual converter. The inverter may be supported with braking resistance connected across the d.c. link

via a free wheeling diode and a transistor. When the power flow is reversed it is dissipated in the braking resistor putting the system into dynamic braking mode of operation.

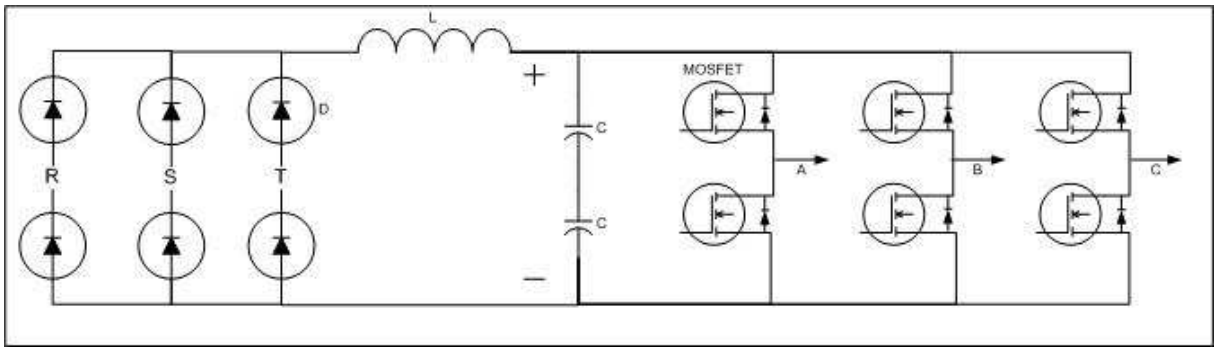


Figure 2-3 Circuit diagram of VSI

Because of the constraint that the input lines must never be shorted and the output current must be continuous a voltage fed inverter can assume in operation only eight distinct topologies. They are shown in Figure 2-4. Six out of these eight topologies produce a non-zero output voltage and are known as non-zero switching states and the remaining two topologies produce zero output and are known as zero switching state.

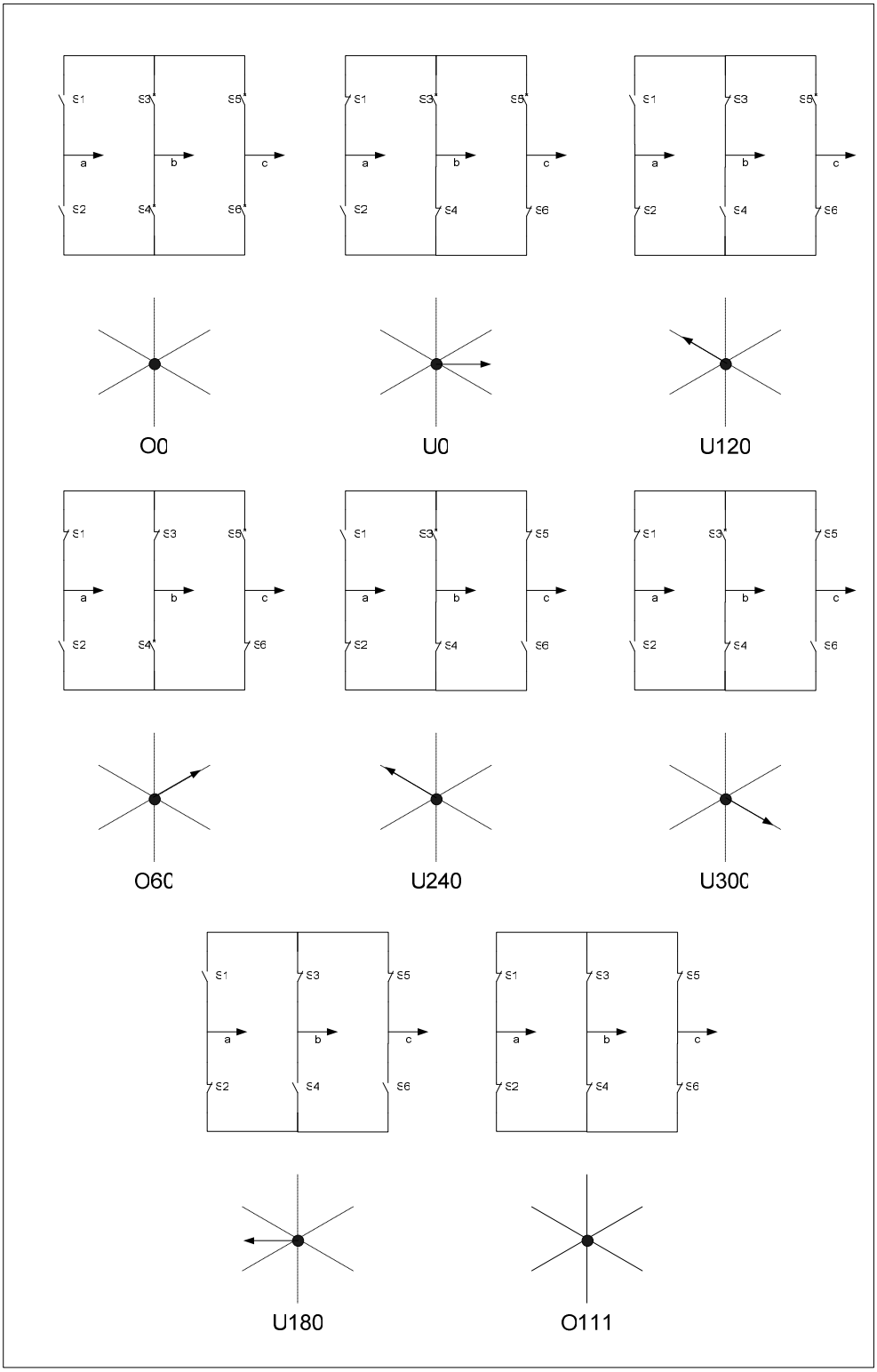


Figure 2-4 Eight switching state topologies of a voltage source inverter

### 2.2.2. Voltage Space Vectors

Space vector modulation for three leg VFI is based on the representation of the three phase quantities as vectors in two-dimensional ($d^s$-$q^s$) plane. Considering the first switching state in Figure 2-5, line-to-line voltages are given by:

$$Vab = Vs$$

$$Vbc = 0$$

$$Vca = -Vs$$

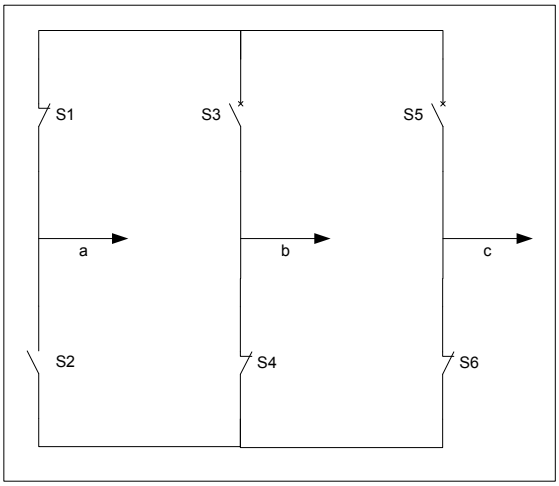


Figure 2-5 First switching state –V1

This can be represented in ($d^s$-$q^s$) plane as shown in Figure 2-6 where Vab, Vbc and Vca are the three line voltage vectors displaced 120° in space. The effective voltage vector generated by this topology is represented as V1 (pnn) in Figure 2-6. Here (pnn) refers to the three leg /phases a, b, c being either connected to the positive dc rail (p) or to the negative dc rail (n). For the first switching state V1, phase a connected to positive dc rail and phases b and c are connected to negative dc rail. Similar to the V1, six non-zero voltage vectors can be shown as in Figure 2-7. The

tips of these vectors form a regular hexagon. We define the area enclosed by two adjacent vectors, within the hexagon, as a sector.

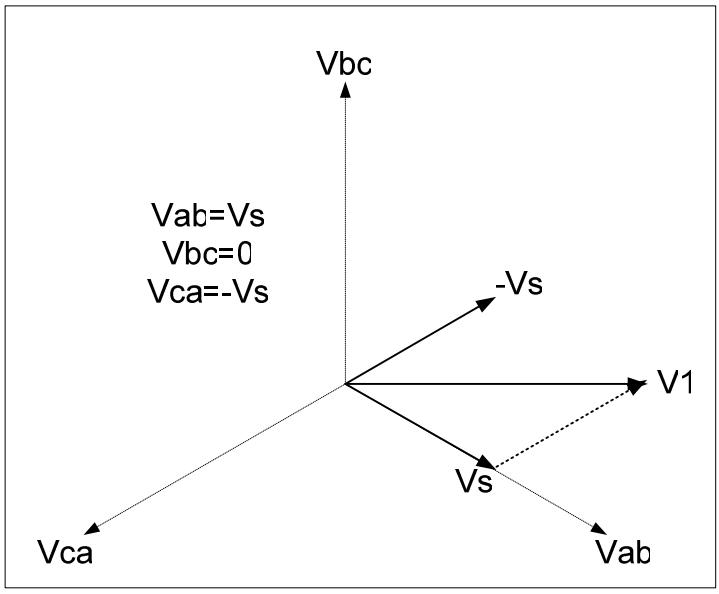

Figure 2-6 Representation of topology 1 in ($d^s$-$q^s$) plane

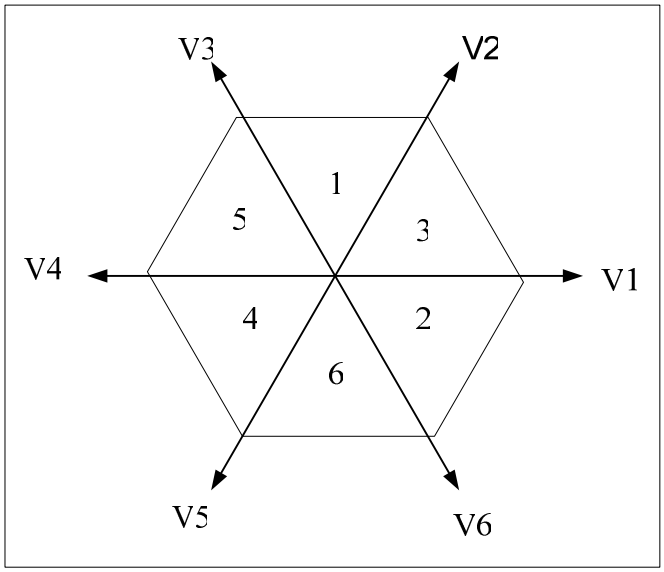

Figure 2-7 Non-zero voltage vectors in ($d^s$-$q^s$) plane

The first and the last two topologies of Figure 2-4 are zero state vectors. The output line voltages in these topologies are zero.

$$Vab = 0$$

$$Vbc = 0$$

$$Vca = 0$$

These are represented as vectors which have zero magnitude and hence are referred as zero switching state vectors. They are represented with dot at the origin instead of vectors as shown in Figure 2-8.

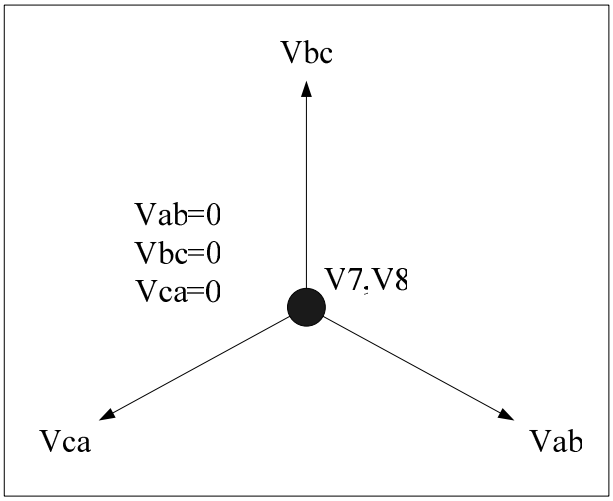


Figure 2-8 Representation of the zero voltage vectors in ($d^s$-$q^s$) plane

### 2.2.3. SVPWM Application to the Static Power Bridge

In the case of AC drive applications, sinusoidal voltage sources are not used. Instead, they are replaced by 6 power IGBTs which act as on/off switches to the rectified DC bus voltage. The aim is to create sinusoidal current in the windings to generate rotating field. Owing to the inductive nature of the phases, a pseudo

sinusoidal current is created by modulating the duty-cycle of the power switches. The switches (IGBT) shown in the Figure 2-9 are activated by signals (a, b, c) and their complement values. Eight different combinations are available with this three phase VFI including two zero states. It is possible to express each phase to neutral voltages, for each switching combination of IGBT's as listed in Table.

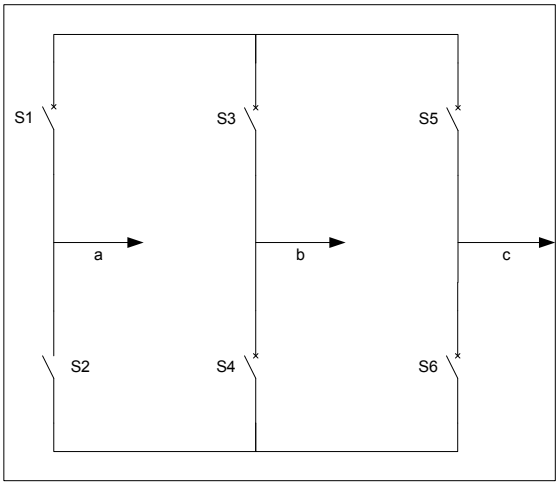

Figure 2-9 Three phase inverter with switching states

Table 2-1 Power Bridge Output Voltages (VAN, VBN, VCN)

| Switch Positions | | | Phase Voltages | | |
|---|---|---|---|---|---|
| S1 | S2 | S3 | VAN | VBN | VCN |
| 0 | 0 | 0 | 0 | 0 | 0 |
| 0 | 0 | 1 | -Vdc/3 | -Vdc/3 | 2Vdc/3 |
| 0 | 1 | 0 | -Vdc/3 | 2Vdc/3 | -Vdc/3 |
| 0 | 1 | 1 | -2Vdc/3 | Vdc/3 | Vdc/3 |
| 1 | 0 | 0 | 2Vdc/3 | -Vdc/3 | -Vdc/3 |
| 1 | 0 | 1 | Vdc/3 | -2Vdc/3 | Vdc/3 |
| 1 | 1 | 0 | Vdc/3 | Vdc/3 | -2Vdc/3 |
| 1 | 1 | 1 | 0 | 0 | 0 |

In field oriented control algorithm, the control variables are expressed in rotating frame. The current vector $I_{sref}$ that directly controls the torque is transformed in a voltage vector by the inverse Park transform. This voltage reference is expressed in the ($d^s$-$q^s$) frame. Using this transformation three phase voltages (VAN, VBN,

VCN) and the reference voltage vector are projected in the ($d^s$-$q^s$) frame. The expression of the three phase voltages in the ($d^s$-$q^s$) frame are given by general Clarke transformation:

$$\begin{bmatrix} V_{sd}^{s} \\ V_{sq}^{s} \end{bmatrix} = \frac{2}{3}\begin{bmatrix} 1 & -\frac{1}{2} & -\frac{1}{2} \\ 0 & \frac{\sqrt{3}}{2} & -\frac{\sqrt{3}}{2} \end{bmatrix}\begin{bmatrix} V_{AN} \\ V_{BN} \\ V_{CN} \end{bmatrix} \tag{2-58}$$

Since only 8 combinations are possible for the power switches, $V^s_{ds}$, $V^s_{qs}$ can also take finite number of values in the ($d^s$-$q^s$) frame Table 2-2 according to the IGBT command signals (a, b, c).

Table 2-2 Stator Voltages in ($d^s$-$q^s$) frame and related Voltage Vector

| Switch Positions | | | ($d^s$-$q^s$) frame Voltages | | |
|---|---|---|---|---|---|
| S1 | S2 | S3 | $V^s_{ds}$ | $V^s_{qs}$ | Vectors |
| 0 | 0 | 0 | 0 | 0 | V0 |
| 0 | 0 | 1 | -Vdc/3 | -Vdc/√3 | V1 |
| 0 | 1 | 0 | -Vdc/3 | Vdc/√3 | V2 |
| 0 | 1 | 1 | -2Vdc/3 | 0 | V3 |
| 1 | 0 | 0 | 2Vdc/3 | 0 | V4 |
| 1 | 0 | 1 | Vdc/3 | -Vdc/√3 | V5 |
| 1 | 1 | 0 | Vdc/3 | Vdc/√3 | V6 |
| 1 | 1 | 1 | 0 | 0 | V7 |

The eight voltage vectors re-defined by the combination of the switches are represented in Figure 2-10.

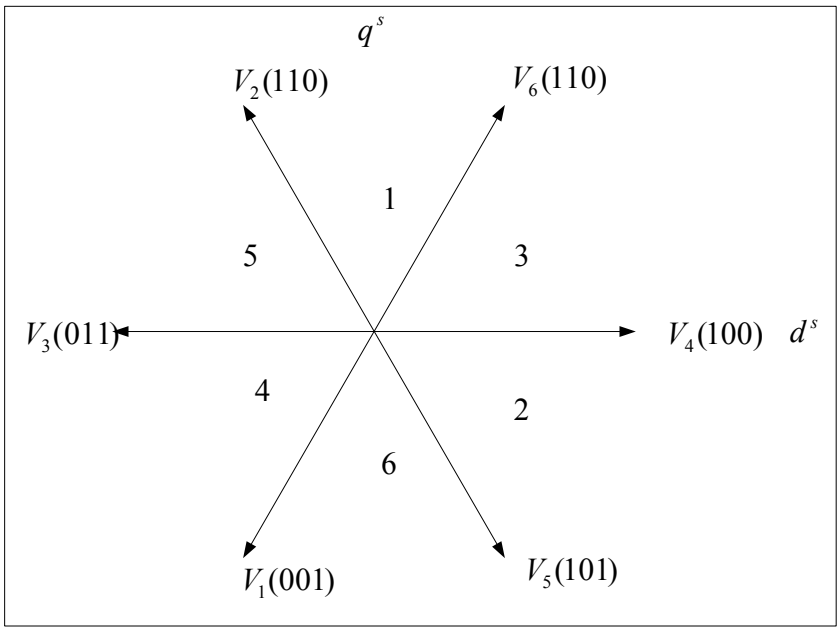

Figure 2-10 Voltage vectors

Given a reference voltage (coming from the inv. Park transform), the following step is used to approximate this reference voltage by the above defined eight vectors. The method used to approximate the desired stator reference voltage with only eight possible states of switches combines adjacent vectors of the reference voltage and modulates the time of application of each adjacent vector. In Figure 2-11 the reference voltage $V_{sref}$ is in the third sector and the application time of each adjacent vector is given by:

$$T = T_4 + T_6 + T_0$$

$$V_{sref} = \frac{T_4}{T}\vec{V}_4 + \frac{T_6}{T}\vec{V}_6 \qquad (2\text{-}59)$$

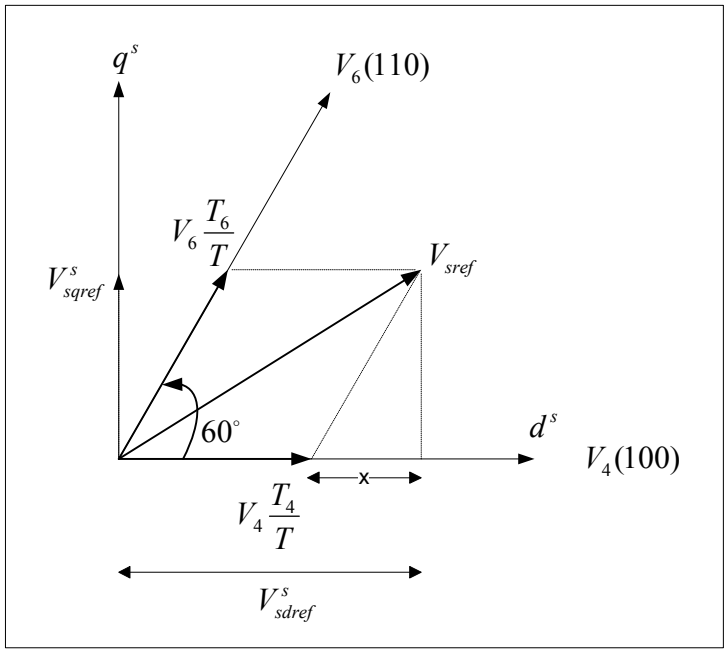

Figure 2-11 Projection of the reference voltage vector

The determination of the amount of times $T_4$ and $T_6$ is given by simple projections:

$$V^s_{sq} = \frac{T_6}{T}\left\|\vec{V}_6\right\|\cos(30^0)$$

$$V^s_{sd} = \frac{T_4}{T}\left\|\vec{V}_4\right\| + x \qquad (2\text{-}60)$$

$$x = \frac{V^s_{sq}}{tg(60^0)}$$

Finally, with the ($d^s$-$q^s$) component values of the vectors given in Table 2-2, the duration periods of application of each adjacent vector is:

$$T_4 = \frac{T}{2V_{dc}}(3V^s_{sd} - \sqrt{3}V^s_{sq}) \qquad (2\text{-}61)$$

$$T_6 = \frac{T}{V_{dc}} \sqrt{3} V_{sq}^s \tag{2-62}$$

The rest of the period spent in applying the null vector ($T_0$=T-$T_6$-$T_4$). For every sector, commutation duration is calculated. The amount of times of vector application can all be related to the following variables:

$$X = \sqrt{3} V_{sq}^s$$

$$Y = \frac{\sqrt{3}}{2} V_{sq}^s + \frac{3}{2} V_{sd}^s \tag{2-63}$$

$$Z = \frac{\sqrt{3}}{2} V_{sq}^s - \frac{3}{2} V_{sd}^s$$

In the previous example for sector 3, $T_4$ = -Z and $T_6$ = X. Extending this logic, one can easily calculate the sector number belonging to the related reference voltage vector. The following basic algorithm helps to determine the sector systematically.

If X > 0 then A=1 else A=0
If Y > 0 then B=1 else B=0
If Z > 0 then C=1 else C=0
Sector = A+2B+4C

The duration of the sector boundary vectors application can be determined as follows:

sector
1: t1= Z t2= Y
2: t1= Y t2=-X
3: t1=-Z t2= X
4: t1=-X t2= Z
5: t1= X t2=-Y

6: t1=-Y t2=-Z

Saturations

If (t1+ t2) > PWMPRD then

t1sat = (t1/ t1+t2)*PWMPRD

t2sat = (t2/ t1+t2)*PWMPRD

The third step is to compute the three necessary duty-cycles. This is shown below:

$$t_{aon} = \frac{PWMPRD - t_1 - t_2}{2}$$

$$t_{bon} = t_{aon} + t_1$$

$$t_{con} = t_{bon} + t_2$$

The last step is to assign the right duty-cycle (txon) to the right motor phase (in other words, to the right CMPRx) according to the sector. Table 2-3 below depicts this determination.

Table 2-3 Assigned duty cycles to the PWM outputs

| | 1 | 2 | 3 | 4 | 5 | 6 |
|---|---|---|---|---|---|---|
| CMPR1 | tbon | taon | taon | tcon | tbon | tcon |
| CMPR2 | taon | tcon | tbon | tbon | tcon | taon |
| CMPR3 | tcon | tbon | tcon | taon | taon | tbon |

## 2.3. Field Oriented Control (FOC)

The concept of field orientation control is used to accomplish a decoupled control of flux and torque. and has three requirements [27]:

- an independently controlled armature current to overcome the effects of armature winding resistance, leakage inductance and induced voltage
- an independently controlled constant value of flux
- An independently controlled orthogonal spatial angle between the flux axis and magneto motive force (MMF) axis to avoid interaction of MMF and flux.

If all of these three requirements are met at every instant of time, the torque will follow the current, allowing an immediate torque control and decoupled flux and torque regulation.

Next a two phase d-q model of an induction machine rotating at the synchronous speed is introduced which will help to carry out this decoupled control concept to the induction machine. This model can be summarized by the following equations:

$$v^{e}_{ds} = p\psi^{e}_{ds} - w_e\psi^{e}_{qs} + r_s i^{e}_{ds} \tag{2-64}$$

$$v^{e}_{qs} = p\psi^{e}_{qs} + w_e\psi^{e}_{ds} + r_s i^{e}_{qs} \tag{2-65}$$

$$0 = p\psi^{e}_{qr} + (w_e - w_r)\psi^{e}_{dr} + r_r i^{e}_{qr} \tag{2-66}$$

$$0 = p\psi^{e}_{dr} - (w_e - w_r)\psi^{e}_{qr} + r_r i^{e}_{dr} \tag{2-67}$$

$$\psi^{e}_{qs} = L_s i^{e}_{qs} + L_m i^{e}_{qr} \tag{2-68}$$

$$\psi^{e}_{ds} = L_s i^{e}_{ds} + L_m i^{e}_{dr} \tag{2-69}$$

$$\psi^{e}_{qr} = L_m i^{e}_{qs} + L_r i^{e}_{qr} \tag{2-70}$$

$$\psi^{e}_{dr} = L_m i^{e}_{ds} + L_r i^{e}_{dr} \tag{2-71}$$

$$T_e = \frac{3P}{2}\frac{L_m}{L_r}\left(\psi^{e}_{dr} i^{e}_{qs} - \psi^{e}_{qr} i^{e}_{ds}\right) \tag{2-72}$$

$$T_e = Jpw_r + Bw_r + T_L \tag{2-73}$$

This model is quite significant to synthesize the concept of field-oriented control. In this model it can be seen from the torque expression (2-72) that if the rotor flux along the q-axis is zero, then all the flux is aligned along the d axis and therefore the torque can be instantaneously controlled by controlling the current along q-axis. Then the question will be how it can be guaranteed that all the flux is aligned along the d-axis of the machine. When a three-phase voltage is applied to the machine, it produces a three-phase flux both in the stator and rotor. The three-phase fluxes can be converted into equivalents developed in two-phase stationary ($d^s$-$q^s$) frame. If this two phase fluxes along ($d^s$-$q^s$) axes are converted into an equivalent single vector then all the machine flux will be considered as aligned along that vector. This vector commonly specifies us de-axis which makes an angle $\theta_e$ with the stationary frame $d^s$-axis. The $q^e$-axis is set perpendicular to the $d^e$-axis. The flux along the qe-axis in that case will obviously be zero. The phasor diagram Figure 2-12 shows these axes. The angle $\theta_e$ keeps changing as the machine input currents change. Knowing the angle $\theta_e$ accurately, d-axis of the $d^e$-$q^e$ frame can be locked with the flux vector.

The control input can be specified in terms of two phase synchronous frame $i^e_{ds}$ and $i^e_{qs}$. $i^e_{ds}$ is aligned along the $d^e$-axis i.e. the flux vector, so does $i^e_{qs}$ with the $q^e$-axis. These two-phase synchronous control inputs are converted into two-phase stationary and then to three- phase stationary control inputs. To accomplish this, the flux angle $\theta_e$ must be known precisely. The angle $\theta_e$ can be found either by Indirect Field Oriented Control (IFOC) or by Direct Field Oriented Control (DFOC). The controller implemented in this fashion that can achieve a decoupled control of the flux and the torque is known as field oriented controller. The block diagram is shown in Figure 2-13

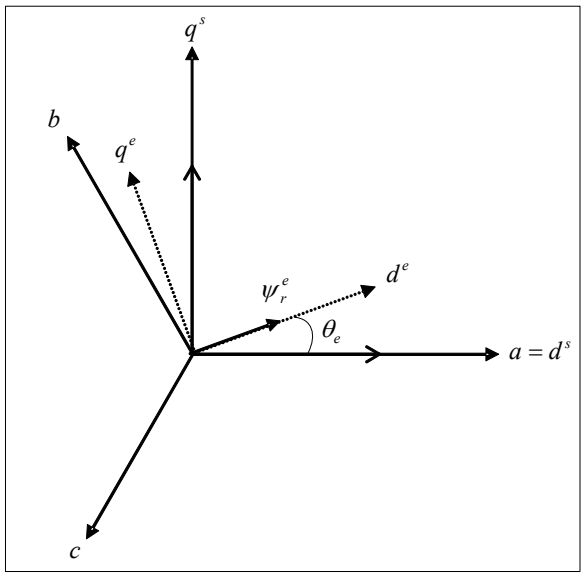

Figure 2-12 Phasor diagram of the field oriented drive system

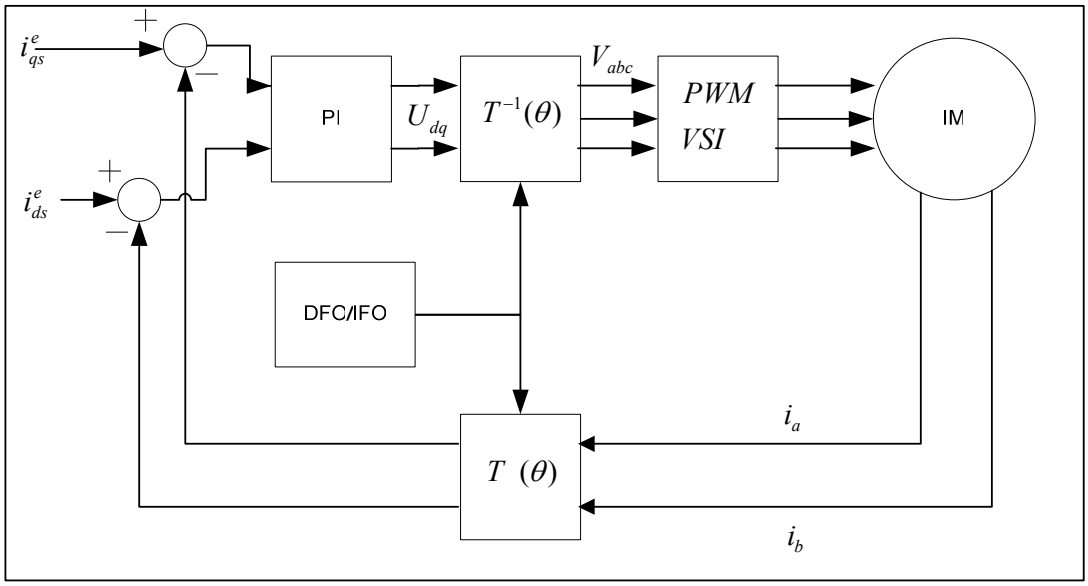

Figure 2-13 Field oriented induction motor drive system

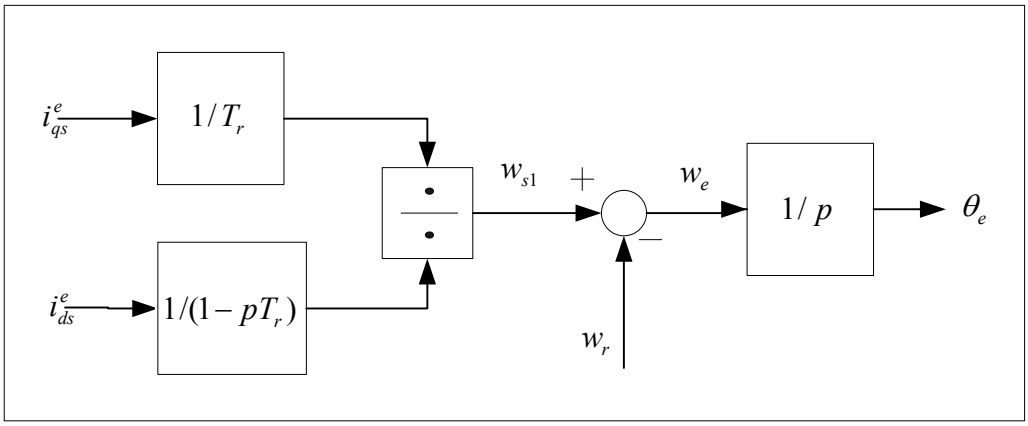


Figure 2-14 Indirect field oriented drive system

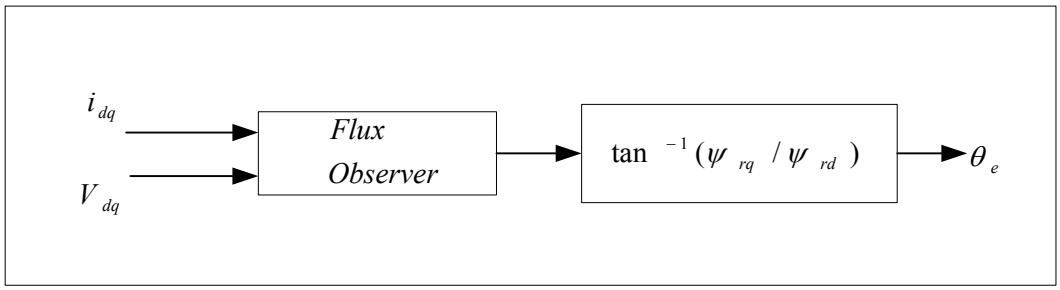


Figure 2-15 Direct field oriented drive system

# CHAPTER 3

# FLUX AND SPEED ESTIMATION FOR SENSORLESS DIRECT FIELD ORIENTED CONTROL OF INDUCTION MACHINE

In this chapter, observers configured for direct field-orientation (DFO) are investigated. The field orientation is implemented in two ways as Direct Field Orientation and Indirect Field Orientation. The basic difference of these methods underlies in the manner of detecting the synchronous speed. In IFO, the slip angle is computed and added to the rotor speed to find the synchronous speed. One must calculate, therefore, the slip-angle and estimate the rotor angle. In the current model employed in the IFO, d-q axes stator currents and precise rotor time-constants are needed to find the slip angle. On the other hand, in DFO, the synchronous speed is computed from the ratio of dq-axes fluxes.

## 3.1. Flux Estimation

Flux estimator used in this chapter can compute both the synchronous speed and the rotor speed. The logic underlying this flux observer is basically an advanced voltage model approach in which integration of the back-emf is calculated and compensated for the errors associated with pure integrator and stator resistance Rs measurement at low speeds. At high speeds, the voltage model provides an accurate stator flux estimate because the machine back emf dominates the measured terminal voltage. However, at low speeds, the stator IR drop becomes significant, causing the accuracy of the flux estimate to be sensitive to the estimated stator resistance. Due to this effect, at low excitation frequencies flux estimation based upon voltage model

are generally not capable of achieving high dynamic performance at low speeds [15]. Consequences of these problems are compensated with the addition of a closed-loop in the flux observer. Basically, the fluxes obtained by current model are compared with those obtained by the voltage model with reference to the current model, or the current model with reference to the voltage model according to the range in which one of these models is superior to other [28]. In this flux observer the voltage model is corrected by the current model through a basic PI block. In the end, the stator fluxes are used to obtain rotor fluxes and rotor flux angle.

### 3.1.1. Estimation of the Flux Linkage Vector

Most of the sensorless control schemes rely directly or indirectly on the estimation of the stator flux linkage vector, ψs being defined as the time integral of the induced voltage,

$$\frac{d\psi^{s,v}}{dt} = u_s - R_s i_s + u_{off}, \psi_s(0) = \psi_{s0} \tag{3-1}$$

where, $u_{off}$ represents all disturbances such as offsets, unbalances and other errors present in the estimated induced emf. A major source of error in the emf is due to the changes in the model parameter Rs. The estimation of the flux vectors requires the integration of (3-1) in real-time. The integrator, however, will have an infinite gain at zero frequency, and the unavoidable offsets contained in the integrator input then make its output gradually drift away beyond limits.

#### 3.1.1.1. Flux Estimation in Continuous Time

The rotor flux linkage dynamics in synchronously rotating reference frame ($w=w_e=w_{\psi r}$) being as;

$$\frac{d\psi_{dr}^{e,i}}{dt} = \frac{L_m}{\tau_r} i_{ds}^e - \frac{1}{\tau_r}\psi_{dr}^{e,i} + (w_e - w_r)\psi_{qr}^{e,i} \tag{3-2}$$

$$\frac{d\psi_{qr}^{e,i}}{dt} = \frac{L_m}{\tau_r} i_{qs}^{e} - \frac{1}{\tau_r}\psi_{qr}^{e,i} + (w_e - w_r)\psi_{dr}^{e,i} \tag{3-3}$$

where $L_m$ is the magnetizing inductance (H), $\tau_r = L_r / R_r$ is the rotor time-constant (sec), and $w_r$ is the electrical angular velocity of the rotor (rad/sec). In the current model, the total rotor flux-linkage is aligned with the d-axis component, and hence;

$$\psi_{r}^{e,i} = \psi_{dr}^{e,i}$$

$$\psi_{qr}^{e,i} = 0$$

Substitution of $\psi_{qr}^{e,i} = 0$ into (3-2) and (3-3) yields the oriented rotor flux dynamics as;

$$\frac{d\psi_{dr}^{e,i}}{dt} = \frac{L_m}{\tau_r} i_{ds}^{e} - \frac{1}{\tau_r}\psi_{dr}^{e,i} \tag{3-4}$$

$$\psi_{qr}^{e,i} = 0 \tag{3-5}$$

Note that (3-4) and (3-5) are the commonly recognized forms of the rotor flux vector equations. When, the rotor flux linkages in (3-4) and (3-5) undergoes the inverse park transformation in the stationary reference frame the result becomes.

$$\psi_{dr}^{s,i} = \psi_{dr}^{e,i}\cos(\theta_{\psi_r}) - \psi_{qr}^{e,i}\sin(\theta_{\psi_r}) = \psi_{dr}^{e,i}\cos(\theta_{\psi_r}) \tag{3-6}$$

$$\psi_{qr}^{s,i} = \psi_{qr}^{e,i}\cos(\theta_{\psi_r}) + \psi_{dr}^{e,i}\sin(\theta_{\psi_r}) = \psi_{dr}^{e,i}\sin(\theta_{\psi_r}) \tag{3-7}$$

where $\theta_{\psi_r}$ is the rotor flux angle (rad). The stator flux linkages in stationary reference frame are then computed using (3-6) and (3-7) as;

$$\psi_{ds}^{s,i} = L_s i_{ds}^s + L_m i_{dr}^s = \left( \frac{L_s L_r - L_m^2}{L_r} \right) i_{ds}^s + \frac{L_m}{L_r} \psi_{dr}^{s,i} \tag{3-8}$$

$$\psi_{qs}^{s,i} = L\, i_{qs}^s + L_m i_{qr}^s = \left( \frac{L_s L_r - L_m^2}{L_r} \right) i_{qs}^s + \frac{L_m}{L_r} \psi_{qr}^{s,i} \tag{3-9}$$

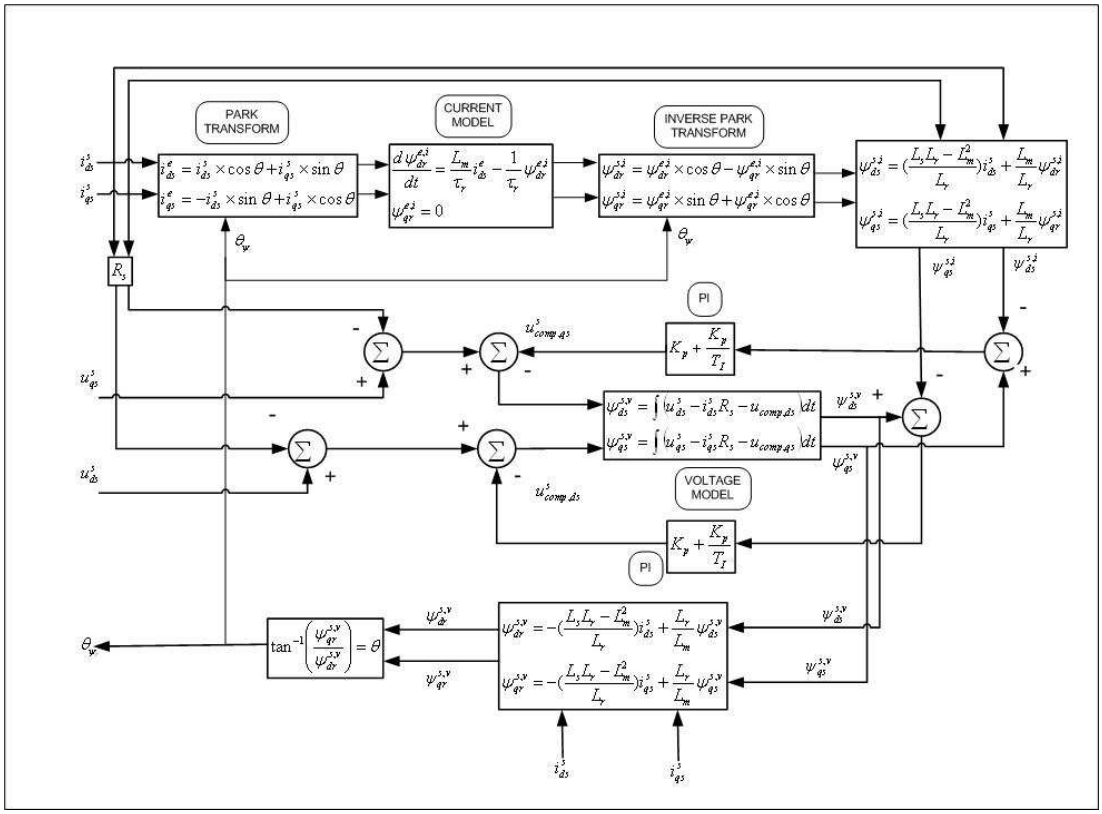


Figure 3-1 Flux estimation

The stator flux linkages in the voltage model, however, are computed by integrating the back emf's and compensated voltages taken into account.

$$\psi_{ds}^{s,v} = \int \left( u_{ds}^s - i_{ds}^s R_s - u_{comp,ds} \right) dt \tag{3-10}$$

$$\psi_{qs}^{s,v} = \int \left( u_{qs}^s - i_{qs}^s R_s - u_{comp,qs} \right) dt \tag{3-11}$$

The compensated voltages, on the otherhand, are computed by the PI control law as follows:

$$u_{comp,ds} = K_p\left(\psi_{ds}^{s,v} - \psi_{ds}^{s,i}\right) + \frac{K_p}{T_I}\int\left(\psi_{ds}^{s,v} - \psi_{ds}^{s,i}\right)dt \tag{3-12}$$

$$u_{comp,qs} = K_p\left(\psi_{qs}^{s,v} - \psi_{qs}^{s,i}\right) + \frac{K_p}{T_I}\int\left(\psi_{qs}^{s,v} - \psi_{qs}^{s,i}\right)dt \tag{3-13}$$

The proportional gain $K_p$ and the reset time $T_I$ are chosen such that the flux linkages computed by the current model becomes dominant at low speed. The reason for that is the back emfs computed by the voltage model result to be extremely low at this speed range (even zero for back emfs at zero speed). While the motor is running at high speed range, the flux linkages computed by voltage model becomes dominant over the flux linkage components computed through the current model.

Once the stator flux linkages in (3-10) and (3-11) are calculated, the rotor flux linkages based on the voltage model are computed once more through (3-14) and (3-15) which are only rearranged forms of (3-8) and (3-9), as

$$\psi_{dr}^{s,v} = -\left(\frac{L_s L_r - L_m^2}{L_m}\right) i_{ds}^{s} + \frac{L_r}{L_m}\psi_{ds}^{s,v} \tag{3-14}$$

$$\psi_{qr}^{s,v} = -\left(\frac{L_s L_r - L_m^2}{L_m}\right) i_{qs}^{s} + \frac{L_r}{L_m}\psi_{qs}^{s,v} \tag{3-15}$$

It is then a straight process to compute the rotor flux angle based on the voltage model as;

$$\theta_{\psi_r} = \tan^{-1}\left(\frac{\psi_{qr}^{s,v}}{\psi_{dr}^{s,v}}\right) \tag{3-16}$$

### 3.1.1.2. Flux Estimation in Discrete Time

The oriented rotor flux dynamics in (3-4) is discretized by using backward approximation as:

$$\frac{\psi_{dr}^{e,i}(k)-\psi_{dr}^{e,i}(k-1)}{T}=\frac{L_m}{\tau_r}i_{ds}^{e}(k)-\frac{1}{\tau_r}\psi_{dr}^{e,i}(k) \tag{3-17}$$

where T being the sampling period (sec). When rearranged (3-17) gives

$$\psi_{dr}^{e,i}(k)=\frac{\tau_r}{\tau_r+T}\psi_{dr}^{e,i}(k-1)-\frac{L_m\times T}{\tau_r+T}i_{ds}^{e}(k) \tag{3-18}$$

The stator flux linkages in (3-10) and (3-11)) are discretized by using trapezoidal approximation as;

$$\psi_{ds}^{s,v}(k)=\psi_{ds}^{s,v}(k-1)+\frac{T}{2}(e_{ds}^{s}(k)-e_{ds}^{s}(k-1)) \tag{3-19}$$

$$\psi_{qs}^{s,v}(k)=\psi_{qs}^{s,v}(k-1)+\frac{T}{2}(e_{qs}^{s}(k)-e_{qs}^{s}(k-1)) \tag{3-20}$$

where the back emf's are computed as;

$$e_{ds}^{s}(k)=u_{ds}^{s}(k)-i_{ds}^{s}(k)R_s-u_{comp,ds}^{s}(k) \tag{3-21}$$

$$e_{qs}^{s}(k)=u_{qs}^{s}(k)-i_{qs}^{s}(k)R_s-u_{comp,qs}^{s}(k) \tag{3-22}$$

Similarly, the PI control laws in (3-12) and (3-13) are also discretized by using trapezoidal approximation as

$$u_{comp,ds}(k)=K_p(\psi_{ds}^{s,v}(k)-\psi_{ds}^{s,i}(k))+u_{comp,ds,i}(k-1) \tag{3-23}$$

$$u_{comp,qs}(k)=K_p(\psi_{qs}^{s,v}(k)-\psi_{qs}^{s,i}(k))+u_{comp,qs,i}(k-1) \tag{3-24}$$

where the accumulating integral terms are;

$$u_{comp,ds,i}(k) = u_{comp,ds,i}(k-1) + \frac{K_p T}{T_I}(\psi_{ds}^{s,v}(k) - \psi_{ds}^{s,i}(k)) \\ = u_{comp,ds,i}(k-1) + K_p K_I(\psi_{ds}^{s,v}(k) - \psi_{ds}^{s,i}(k) \quad (3\text{-}25)$$

$$u_{comp,qs,i}(k) = u_{comp,qs,i}(k-1) + \frac{K_p T}{T_I}(\psi_{qs}^{s,v}(k) - \psi_{qs}^{s,i}(k)) \\ = u_{comp,qs,i}(k-1) + K_p K_I(\psi_{qs}^{s,v}(k) - \psi_{qs}^{s,i}(k) \quad (3\text{-}26)$$

### 3.1.1.3. Flux Estimation in Discrete Time and Per-Unit

All equations are needed to be normalized into per-unit by the specified base quantities. Firstly, the rotor flux linkage in current model (3-18) is normalized by dividing the base flux linkage as

$$\psi_{dr,pu}^{e,i}(k) = \frac{\tau_r}{\tau_r + T}\psi_{dr,pu}^{e,i}(k-1) - \frac{T}{\tau_r + T} i_{ds,pu}^{e}(k) \quad (3\text{-}27)$$

where $\psi_B = L_m I_B$ is the base flux linkage (volt.sec) and $I_B$ is the base current (amp). Next, the stator flux linkages in the current model (3-8) and (3-9) are similarly normalized by dividing the base flux linkage as

$$\psi_{ds,pu}^{s,i}(k) = \frac{L_s L_r - L_m^2}{L_s L_r} i_{ds,pu}^{s}(k) + \frac{L_m}{L_r}\psi_{dr,pu}^{s,i}(k) \quad (3\text{-}28)$$

$$\psi_{qs,pu}^{s,i}(k) = \frac{L_s L_r - L_m^2}{L_s L_r} i_{qs,pu}^{s}(k) + \frac{L_m}{L_r}\psi_{qr,pu}^{s,i}(k) \quad (3\text{-}29)$$

Then, the back emf's in (3-21) and (3-22) are normalized by dividing the base phase voltage $V_B$.

$$e^{s}_{ds,pu}(k) = u^{s}_{ds,pu}(k) - \frac{I_b R_s}{V_b} i^{s}_{ds,pu}(k) - u^{s}_{comp,ds,pu}(k) \tag{3-30}$$

$$e^{s}_{qs,pu}(k) = u^{s}_{qs,pu}(k) - \frac{I_b R_s}{V_b} i^{s}_{qs,pu}(k) - u^{s}_{comp,qs,pu}(k) \tag{3-31}$$

Next, the stator flux linkages in the voltage model (3-19) and (3-20) are divided by the base flux linkage.

$$\psi^{s,v}_{ds,pu}(k) = \psi^{s,v}_{ds,pu}(k-1) + \frac{V_b T}{L_m I_b}\left(\frac{e^{s}_{ds,pu}(k) + e^{s}_{ds,pu}(k-1)}{2}\right) \tag{3-32}$$

$$\psi^{s,v}_{qs,pu}(k) = \psi^{s,v}_{qs,pu}(k-1) + \frac{V_b T}{L_m I_b}\left(\frac{e^{s}_{qs,pu}(k) + e^{s}_{qs,pu}(k-1)}{2}\right) \tag{3-33}$$

Similar to (3-28) and (3-29) the normalized rotor flux linkages in the voltage model are:

$$\psi^{s,v}_{dr,pu}(k) = -\frac{L_s L_r - L_m^2}{L_m L_m} i^{s}_{ds,pu}(k) + \frac{L_r}{L_m}\psi^{s,v}_{ds,pu}(k) \tag{3-34}$$

$$\psi^{s,v}_{qr,pu}(k) = -\frac{L_s L_r - L_m^2}{L_m L_m} i^{s}_{qs,pu}(k) + \frac{L_r}{L_m}\psi^{s,v}_{qs,pu}(k) \tag{3-35}$$

In conclusion, the discrete-time, per-unit equations are rewritten in terms of constants.

The rotor flux linkages developed by the current model in synchronously rotating reference frame ($w=w_{\psi r}$) are:

$$\psi^{e,i}_{dr,pu}(k) = K_1 \psi^{e,i}_{dr,pu}(k-1) - K_2 i^{e}_{ds,pu}(k) \tag{3-36}$$

where

$$K_1 = \frac{\tau_r}{\tau_r + T}$$

$$K_2 = \frac{T}{\tau_r + T} \tag{3-37}$$

The rotor flux linkages developed by the current model in the stationary reference frame (w=0) are:

$$\psi^{s,i}_{ds,pu}(k) = K_4 i^s_{ds,pu}(k) + K_3 \psi^{s,i}_{dr,pu}(k) \tag{3-38}$$

$$\psi^{s,i}_{qs,pu}(k) = K_4 i^s_{qs,pu}(k) + K_3 \psi^{s,i}_{qr,pu}(k) \tag{3-39}$$

$$K_4 = \frac{L_s L_r - L_m^2}{L_s L_r}$$

$$K_3 = \frac{L_m}{L_r} \tag{3-40}$$

The back emf's developed by the voltage model in the stationary reference frame (w=0) is

$$e^s_{ds,pu}(k) = u^s_{ds,pu}(k) - K_5 i^s_{ds,pu}(k) - u^s_{comp,ds,pu}(k) \tag{3-41}$$

$$e^s_{qs,pu}(k) = u^s_{qs,pu}(k) - K_5 i^s_{qs,pu}(k) - u^s_{comp,qs,pu}(k) \tag{3-42}$$

$$K_5 = \frac{I_b R_s}{V_b} \tag{3-43}$$

The stator flux linkages developed by the voltage model in the stationary reference frame (w=0) are:

$$\psi^{s,v}_{ds,pu}(k) = \psi^{s,v}_{ds,pu}(k-1) + K_6 \left(\frac{e^s_{ds,pu}(k) + e^s_{ds,pu}(k-1)}{2}\right) \tag{3-44}$$

$$\psi^{s,v}_{qs,pu}(k) = \psi^{s,v}_{qs,pu}(k-1) + K_6(\frac{e^s_{qs,pu}(k) + e^s_{qs,pu}(k-1)}{2}) \tag{3-45}$$

$$K_6 = \frac{V_b T}{L_m I_b} \tag{3-46}$$

The rotor flux linkages developed by the voltage model in the stationary reference frame (w=0) are:

$$\psi^{s,v}_{dr,pu}(k) = -K_8 i^s_{ds,pu}(k) + K_7 \psi^{s,v}_{ds,pu}(k) \tag{3-47}$$

$$\begin{aligned} K_8 &= \frac{L_s L_r - L_m^2}{L_m L_m} \\ K_7 &= \frac{L_r}{L_m} \end{aligned} \tag{3-48}$$

The rotor flux angle developed by the voltage model

$$\theta_{\psi r,pu}(k) = \frac{1}{2\pi} \tan^{-1}\left[\frac{\psi^{s,v}{}_{qr,pu}(k)}{\psi^{s,v}{}_{dr,pu}(k)}\right] \tag{3-49}$$

The required parameters for this module are summarized as follows:

- The machine Parameters:
- Stator resistance ($R_s$)
- Rotor resistance ($R_r$)
- Stator leakage inductance ($L_{ls}$)
- Rotor leakage inductance ($L_{lr}$)
- Magnetizing inductance ($L_m$)
- The based quantities:
- Base current ($I_b$)
- Base phase voltage ($V_b$)
- The sampling period($T$)

The stator self inductance is $L_s$=$L_{ls}$+$L_m$ and the rotor self inductance is $L_r$=$L_{lr}$+$L_m$.

# CHAPTER 4

# MODEL REFERENCE ADAPTIVE SYSTEMS

## 4.1. Adaptive Control

Adaptive control may be defined in many ways. A possible definition of adaptive control is “a system that adapts itself to changes in the process”. Another definition that is often used but probably too vague to be useful is “a system which is designed from an adaptive point of view”. A more useful one is “a system that consists of a primary feedback that takes care of process signal variations and a secondary feedback that deals with process state changes. In this definition, the primary feedback is used as in non-adaptive control, and the secondary feedback makes the system adaptive. From this definition it is clear that process states variations give rise to adaptation of the system. The aim of reacting to state changes is to attempt to maintain a high system performance, even if the process states are unknown or varying [29]. In the literature there exist several adaptive control techniques. In this thesis Model Reference Adaptive System is applied to induction motor drive as a state observer.

## 4.2. Model Reference Adaptive Systems

Model Reference Adaptive System (MRAS) is one of the most popular adaptive control method used in motor control applications for tracking and observing system parameters and states [22-26, 30-33]. There exist a number of different model reference adaptive control techniques such as parallel model, series model, direct model and indirect model etc. MRAS used in this thesis is parallel

model MRAS that compares both the outputs of a reference model and adaptive model and processes the error between these two according to the appropriate adaptive laws that do not deteriorate the stability requirements of the applied system. A generalized parallel MRAS scheme is shown in Figure 4-1 below in which the primary controller is used to obtain suitable closed loop behavior, as in non-adaptive control schemes. However, because the process parameters are unknown or may vary with time, a fixed parameter setting for the primary controller, such that the closed-loop behavior is acceptable under all circumstances, cannot be found. In the MRAS technique, the desired process response to a command signal is specified by means of a parametrically defined reference model. An adaptation mechanism keeps track of the process output $y_p$ and the model output $y_m$ and calculates a suitable parameter setting such that difference between these outputs tends to zero. In addition to process output $y_p$, the process $x_p$, if available, and the process input u or the reference signal may be used by adaptation mechanism.

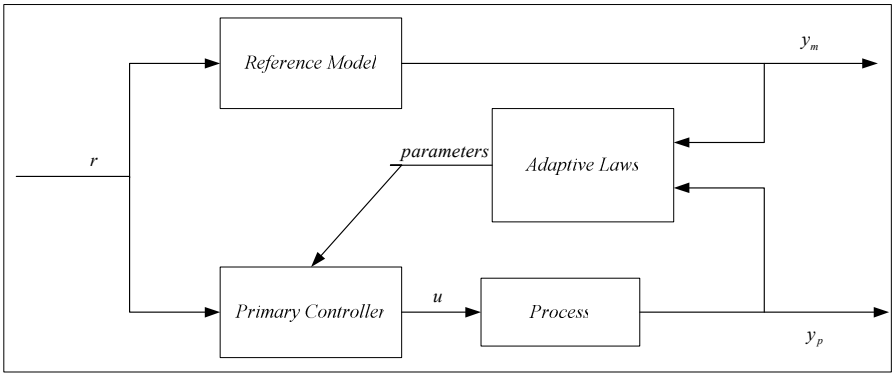

Figure 4-1 General parallel MRAS scheme

An important issue in MRAS is the design of adaptive laws. The first adaptive law designs made use of sensitivity models, and later the stability theory of Lyapunov, and Popov's hyperstability theory, served as standard design methods, yielding a guaranteed stable adaptive system. (see Appendix A)

## 4.3. Introduction to MRAS practice in motor control applications

In a MRAS system, some state variables, $x_d, x_q$ (e.g. back e.m.f components ($e_{md}, e_{mq}$) reactive power components ($q_{md}, q_{mq}$), rotor flux components ($\psi_{rd}, \psi_{rq}$) etc.) of the induction machine, which are obtained from sensed variables such as stator voltage and currents, are estimated in reference model and are then compared with state variables $\hat{x}_d$ *and* $\hat{x}_q$ estimated by using adaptive model. The difference between these state variables is then used in adaptation mechanism, which outputs the estimated value of the rotor speed ($w_r$) and adjusts the adaptive model until satisfactory performance is obtained. Such a scheme is shown in Figure 4-2 where compact space-vector notation is used. However, Figure 4-3 corresponds to an actual implementation, and here components of the space vector are shown.

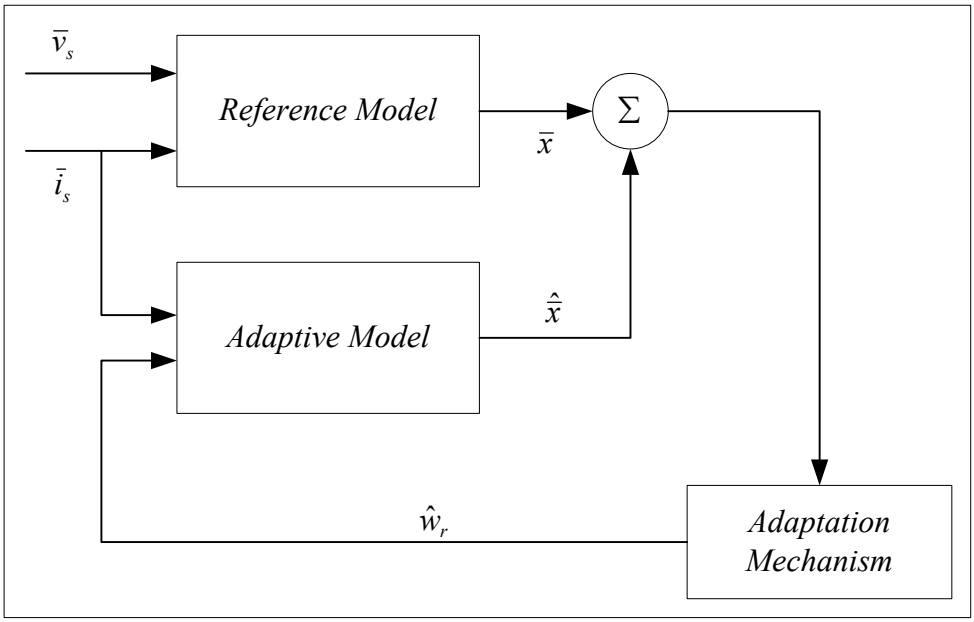


Figure 4-2 Generalized Model Reference Adaptive System

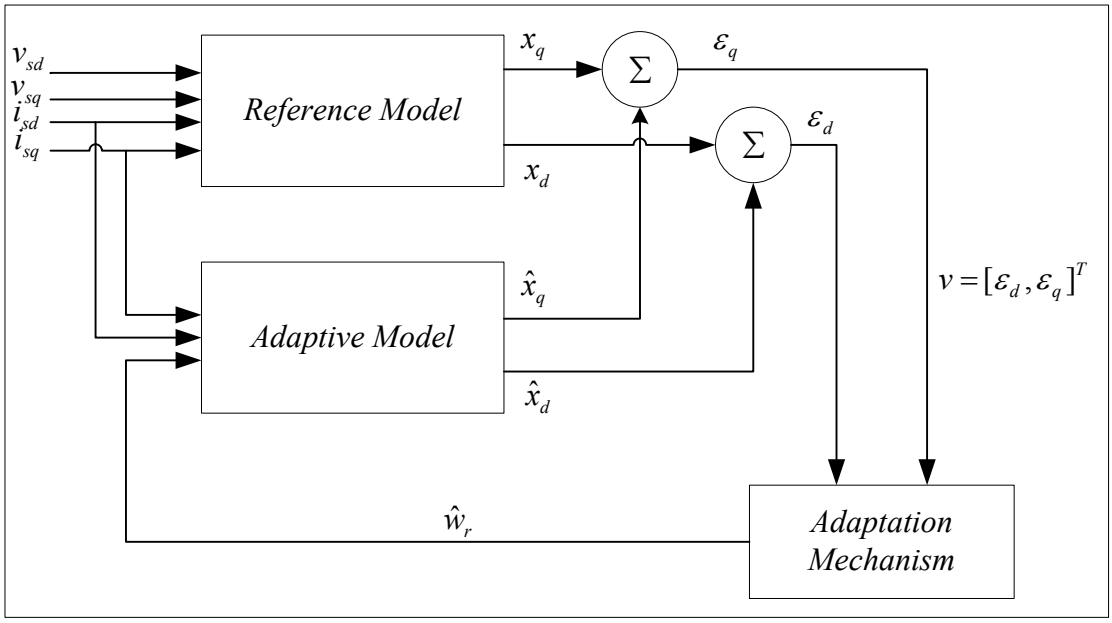


Figure 4-3 MRAS based speed estimator scheme using space vector

The appropriate adaptation mechanism can be derived by using Popov's criterion of hyperstability. This result in a stable and quick response system, where the differences between the state variables of the reference model and adaptive model are manipulated into speed tuning signal ($\varepsilon$), which is then put into a PI type of controller that outputs the estimated rotor speed. Two of the schemes will be discussed in the following sections: reactive power and back-emf errors are used as speed tuning signals. In these expressions $\bar{i}_s$ *and* $\bar{u}_s$ denote the stator voltage and stator current space vectors respectively in the stationary frame $\bar{e}_m$ denotes the back emf space vector also in stationary reference frame as $\Delta\bar{e}_m = \bar{e}_m - \hat{\bar{e}}_m$. The symbol ^ denotes the quantities estimated by the adaptive model. In addition to these classical MRAS schemes artificial intelligence assisted MRAS speed estimators are also discussed in the literature which do not contain any mathematical adaptive model, and the adaptation mechanism is incorporated into the tuning of appropriate artificial intelligence based network (which can be a neural network, a fuzzy-neural network, etc.) [31], [32].

To improve the performance of the observers described in this section, various practical techniques are also discussed which avoid use of pure integrators. Pure integrators leads drift and initial condition problems in digital applications, so recent speed sensorless algorithms tend to avoid pure integrators. Most of the traditional vector control algorithms use low-pass filter instead of pure integrators that also causes serious problems at low speed range. Recent MRAS algorithms mentioned in this thesis avoid both pure integrators and low-pass filters. Reactive power scheme described below is robust to stator resistance and rotor resistance variations and can even be applied at very low speeds (but not zero speed).Both of the observers (reactive power and back-emf schemes) described below use monitored stator currents and stator voltages, but in a voltage-source inverted fed drive, it is not necessary to monitor the stator voltages, since it is possible to reconstruct them by using the inverter switching states and also the monitored value of dc link voltage.

## 4.4. Application of Popov's Hyperstability Theorem and Integral Inequality

This part contains a short description of the selection of the appropriate adaptation mechanism, proves why there is a PI controller in the scheme described in MRAS schemes used in this thesis, and also shows the form of speed tuning signal to be used.

In general, a model reference adaptive speed estimator system can be represented by an equivalent non-linear feedback system which comprises a feed-forward time invariant linear subsystem and a feedback non-linear time varying subsystem. This is shown below in Figure 4-4.

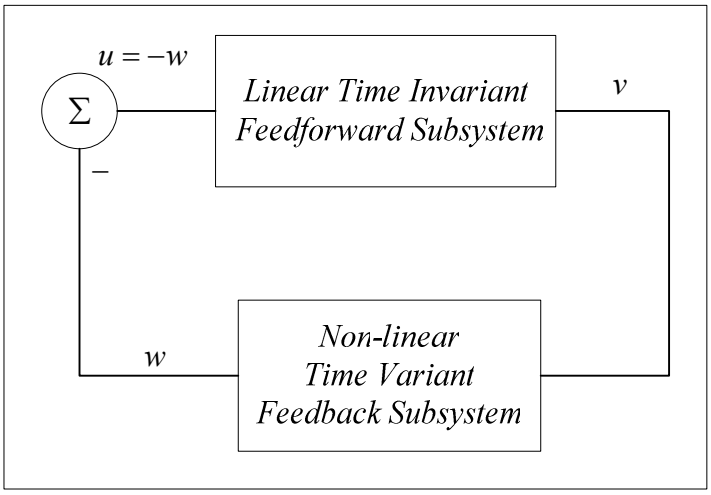

Figure 4-4 Equivalent non-linear feedback system

In Figure 4-4 the input to the linear time-variant system is $u$ (which contains the stator voltage and currents), its output is $v$, which is the speed-tuning signal $v = [\varepsilon_d, \varepsilon_q]^T$. The output of the non-linear time invariant system is $w$, and $u = -w$. The rotor speed estimation algorithm (adaptation mechanism) is chosen according to Popov's hyperstability theory, whereby the transfer function matrix of the linear time invariant system must be strictly positive real and the non-linear time varying feedback system satisfies Popov's integral inequality, according to which $\int v^T w\, dt \geq 0$ in the time interval [0, $t_1$] for all (see appendix A). Thus to obtain the adaptation mechanism, first the transfer function *F(s)* of the linear time invariant feed-forward subsystem has to be obtained. It can be shown by lengthy calculations that in both of the schemes described in the following part this is strictly positive real. A possible proof uses the state-variable form of the error equation, $dv/dt = Av - w$, which is obtained by subtracting the state variable equations of the adjustable model from the state-variable equations of the reference model (where A is the state matrix).

The feedforward path transfer matrix of the linear time-invariant subsystem shown in Figure 4-4 above is $F(s) = [sI - A]^{-1}$, where $I$ is an identity matrix. It follows from the derivation of the error state equation that $w = [\hat{w}_r - w_r][-\hat{x}_q\ x_d]^T$

(where $\hat{x}_d$ *and* $\hat{x}_q$ are estimated by adaptive model), thus w is substituted into Popov's integral inequality, $\int v^T w\,dt \geq 0$, it can be shown that this inequality can be satisfied by letting $\hat{w}_r = (K_p + K_i / p)\varepsilon$. In this equation *1/p* represent an integrator and $\varepsilon$ is the appropriate speed-tuning signal. In general, the state variables in the reference and adaptive models are $x_d, x_q$ *and* $\hat{x}_d, \hat{x}_q$ respectively and speed tuning signal is $Im(\bar{x}\hat{\bar{x}}^*)$, where the asterisk denotes the complex conjugate. Included speed-tuning signals in this thesis are, basically, $Im(\bar{e}_m \hat{\bar{e}}_m^{\,*})$ and $Im(\bar{q}_m \hat{\bar{q}}_m^{\,*})$ where $e_m$ *and* $q_m$ represent back-emf and reactive power respectively. It can be seen that when a specific state variable is used (on the outputs of the reference and adaptive models), then a corresponding speed tuning signal of a specific form is obtained by Popov's integral inequality. It has been discussed above that when the rotor speed to be estimated is changed in the adaptive model in such a way that the difference between the output of the reference model and the adaptive model is zero, then the estimated rotor speed is equal to the actual rotor speed. The error signal actuates the rotor-speed identification algorithm, which makes this error converge asymptotically to zero. The physical reason for the integrator (in PI controller) is that this ensures that the error converges asymptotically to zero.

In recent years several MRAS schemes are studied for tacholess vector control of ac drives. Most of these schemes have low speed problems due to the low-pass filters or pure integrators. These schemes obtain speed tuning signal form state variables, $x_d$ ,$x_q$ (e.g. active power components ($p_d$ ,$p_q$) , rotor flux components ($\psi_{rd}$,$\psi_{rq}$), torque components ($t_{ed}$,$t_{eq}$ ), voltage components ($v_d$,$v_q$ etc.). In addition to these schemes, recently proposed schemes using back-emf and reactive power enhanced the performance of the MRAS solutions excluding pure integrators in their algorithms [34]. Also reactive power MRAS model is truly robust to stator resistance changes. The details of these schemes will be given in the following part.

## 4.5. Back-emf MRAS Scheme

In this MRAS scheme the back-emf ($e_m$) is used as speed tuning signal. When the back-emf used then the problems associated with the pure integrators in the reference model disappear, since in this case the reference model does not contain any integrator. Equations for an induction motor in the stationary frame can be expressed as:

$$V_S = R_S\, i_S + \sigma\, L_S \frac{di_S}{dt} + e_m \tag{4-1}$$

$$\frac{di_m}{dt} = \overline{w}_r \otimes i_m - \frac{1}{T_r} i_m + \frac{1}{T_r} i_S \tag{4-2}$$

where $\overline{w}_r$ is a vector whose magnitude $w_r$ is rotor electrical angular velocity, and whose direction is determined according to right hand system of coordinates as shown in Figure 4-5 "$\otimes$" denotes the cross product of vectors respectively

From (4-1) and (4-2), $e_m$ and structure of MRAS can be derived as follows:

$$e_m = V_s - \left( R_s i_s + \sigma L_s \frac{di_s}{dt} \right) \tag{4-3}$$

$$e_m = L'_m \frac{di_m}{dt} \tag{4-4}$$

$$= L'_m \left( w_r \otimes i_m - \frac{1}{T_r} i_m + \frac{1}{T_r} i_s \right) \tag{4-5}$$

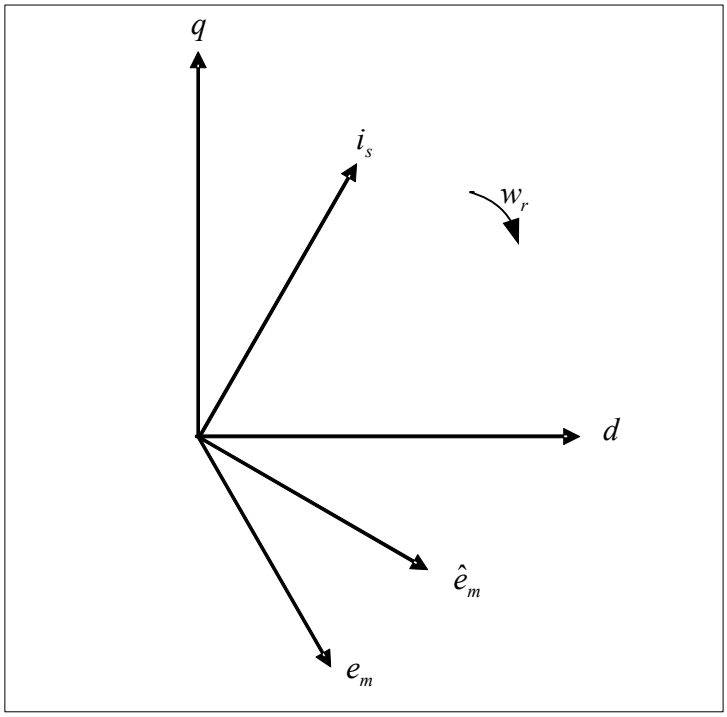

Figure 4-5 Coordinates in stationary reference frame

If we rewrite the equations above for the direct and quadrature-axis back-emf in the following form:

$$\begin{aligned} e_{md} &= L_m \frac{di_{md}}{dt} = \frac{L_m}{L_r}\frac{d\psi_{rd}}{dt} \\ &= V_{sd} - \left( R_s i_{ds} + \sigma L_s \frac{di_{sd}}{dt} \right) \end{aligned} \tag{4-6}$$

$$\begin{aligned} e_{mq} &= L_m \frac{di_{mq}}{dt} = \frac{L_m}{L_r}\frac{d\psi_{rq}}{dt} \\ &= V_{sq} - \left( R_s i_{sq} + \sigma L_s \frac{di_{sq}}{dt} \right) \end{aligned} \tag{4-7}$$

If we use the counterelectromotive force (emf) vector $e_m$ instead of rotor flux vector which was used in the previous MRAS schemes [35] for speed identification, then a new MRAS system is obtained. Fig.5.6 illustrates the new structure of the new

MRAS for speed estimation. Two independent observers are configured to estimate the components of the counter-EMF vector, one based on (4-6) and the other based on (4-5) and (4-7) The observer based on (4-6) can be regarded as a reference model of the induction motor since (4-6) does not involve the quantity $w_r$ , and the one based on (4-5) and (4-7) can be regarded as adjustable model because (4-5) and (4-7) do involve $w_r$. The error between the outputs of the two observers is then used to drive a suitable adaptation mechanism which generates the estimate $\hat{w}_r$ for the adjustable model.

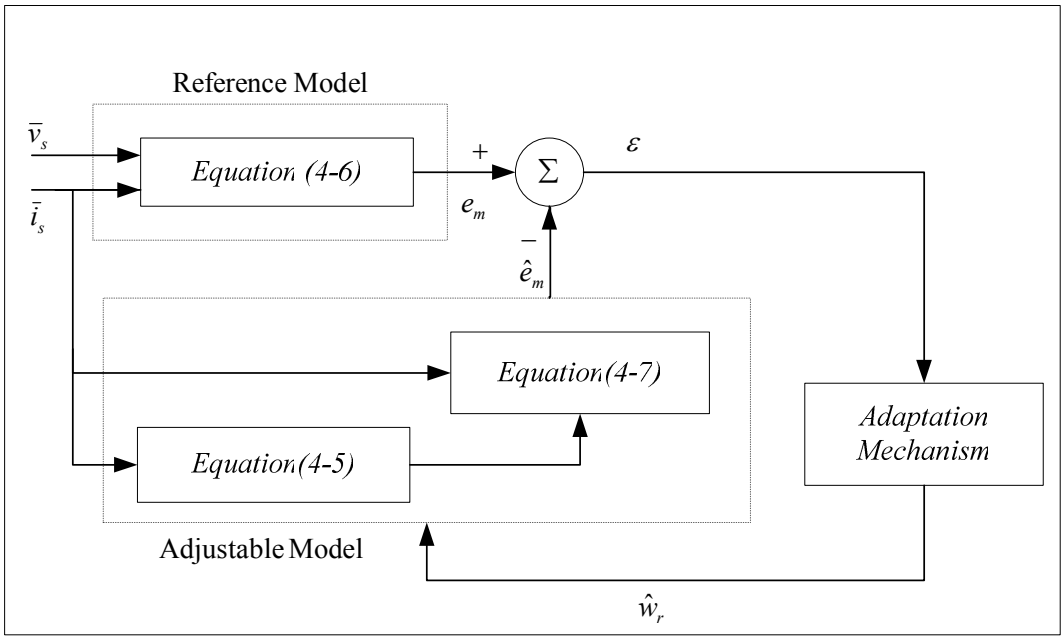

Figure 4-6 Structure of the MRAS system for speed estimation

When the scheme shown in Figure 4-6 is employed in a speed-sensorless vector controlled drive, satisfactory performance can be obtained even at low speeds if an accurate value of the stator resistance is used, since the reference model does not contain pure integration. However, the stator resistance varies with temperature, and this affects the stability performance of the speed observer, especially at low speeds. A MRAS scheme which is intensive to stator resistance variation can be obtained by using such

a speed-tuning signal, which is obtained from a quantity which does not contain the stator resistance. On the other hand some of the applications use parameter estimation or parameter tracking algorithms to compensate the error caused by parameter deviation. Thus, in literature there exist several on-line parameter estimation algorithms at real time.

### 4.5.1. Adaptation Mechanisms and Stability of MRAS

It is important to ensure that the system will be stable and the estimated quantity will converge to the actual value for the adaptation mechanism of MRAS algorithms. In general $w_r$ is a variable; thus, the models are linear time-varying systems. For the purpose of deriving an adaptation mechanism, however, it is valid to initially treat $w_r$ as a constant parameter of the models. By differentiating both sides of (4.7), we get

$$\frac{de_m}{dt} = w_r \otimes e_m - \frac{1}{T_r} e_m + \frac{L_m}{T_r} \frac{di_s}{dt} \tag{4-8}$$

Here, letting $\varepsilon = e_m - \hat{e}_m$, and subtracting (4.8) for the adjustable model from (4.8) for the reference model, we obtain the following state error equation:

$$\begin{aligned} \frac{d\varepsilon}{dt} &= w_r \otimes \varepsilon - \frac{1}{T_r} \varepsilon - (\hat{w}_r - w_r) \otimes \hat{e}_m \\ &= A\varepsilon - W \end{aligned} \tag{4-9}$$

Where

$$A = \begin{bmatrix} -\frac{1}{T_r} & -w_r \\ w_r & -\frac{1}{T_r} \end{bmatrix} = -\frac{1}{T_r} I + w_r J,$$

$$W = (\hat{w}_r - w_r) \otimes \hat{e}_m = (\hat{w}_{r-} w_r) \begin{bmatrix} -\hat{e}_{mq} \\ \hat{e}_{md} \end{bmatrix} \quad and$$

$$I = \begin{bmatrix} 1 & 0 \\ 0 & 1 \end{bmatrix}, \; J = \begin{bmatrix} 0 & -1 \\ 1 & 0 \end{bmatrix}.$$

Since $\hat{w}_r$ is produced by adaptation mechanism, (4.9) describes a nonlinear feedback system as shown in Figure 4-7. Hyperstability requires that the linear time invariant forward–path transfer matrix be strictly positive real and that the nonlinear feedback including the adaptation mechanism satisfies Popov's criterion for hyperstability.

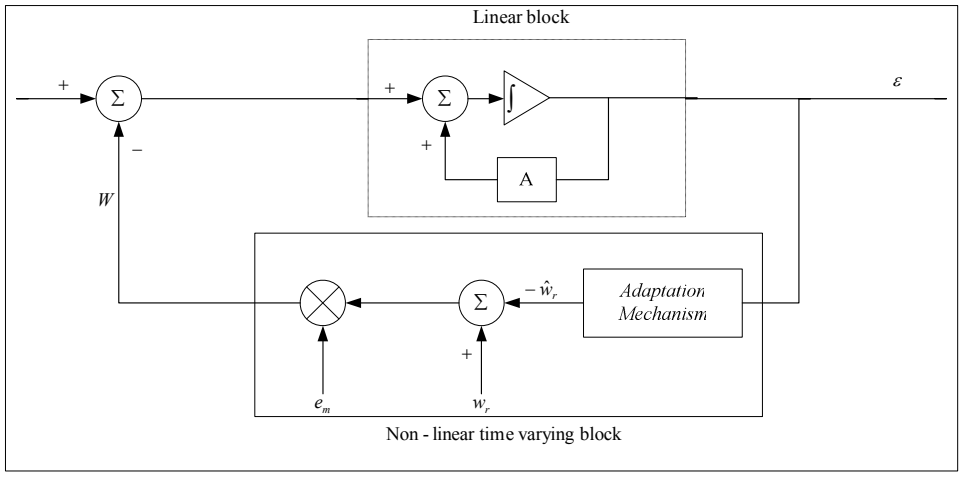


Figure 4-7 Equivalent nonlinear feedback system of MRAS

Popov's criterion requires that

$$\int_0^{t_1} \varepsilon \bullet W \, dt \geq -\gamma_0^2 \quad for \; all \; t_1 \geq 0 \tag{4-10}$$

where $\gamma_0^2$ is a real positive constant and $\bullet$ is dot product. Here, letting

$$\hat{w}_r = \left( K_p + \frac{K_i}{p} \right) (\hat{e}_m \otimes \varepsilon) \tag{4-11}$$

and substituting for $W$ in inequality (4-10), (4-10) becomes

$$\int_0^{t_1} \varepsilon \bullet W \, dt = \int_0^{t_1} \varepsilon \bullet \{(\hat{w}_r - w_r) \otimes \hat{e}_m\} d \tag{4-12}$$

$$= \int_0^{t_1} (\varepsilon \otimes \hat{e}_m) \bullet \left( w_r - (K_p + \frac{K_i}{p})(\hat{e}_m \otimes \varepsilon) \right) dt$$

$$\geq -\gamma_0^2$$

Using the following well known inequality

$$\int_0^{t_1} \frac{d}{dt} f(t) \cdot f(t) \, dt \geq -\frac{1}{2} f^2(0) \tag{4-13}$$

it can be shown that inequality (4.12) is satisfied.

## 4.6. Reactive Power MRAS Scheme

In the previous part, back-emf is used as tuning signal and the performance of the MRAS is proved to be perfect in the simulation. Since the reference model does not require pure integration, this system can achieve good performance even at low speeds, as long as the value of stator resistor is known precisely. The stator resistance, however, varies with the temperature of the stator. The stator resistance thermal variations affect the performance and stability of MRAS speed estimator, especially at low speeds as shown later in this thesis. Therefore, a speed identification system with low sensitivity to the stator resistance variations is necessary for applications of low-speed drives. Here, another approach to speed

identification with completely robust to stator resistance variations is proposed. This scheme can be represented in two different ways whose basics are the same.

First let us define a new quantity $q_m$ as the cross product of the counter EMF vector $e_m$ and the stator current vector is. That is

$$q_m \overset{\Delta}{=} i_s \otimes e_m \tag{4-14}$$

$q_m$ is a vector, whose direction is shown in Figure 4-5 and whose magnitude $q_m$ represents the instantaneous reactive power maintaining the magnetizing current. Substituting the (4-6) and (4-7) for $e_m$ in (4-14) noting that $i_s \otimes i_s = 0$ ,we have

$$q_m = i_s \otimes \left( v_s - \sigma L_s \frac{di}{dt} \right) \tag{4-15}$$

$$q_m = \frac{L_m^2}{L_r} \left( (i_m \bullet i_s) w_r + \frac{1}{T_r} i_m \otimes i_s \right) \tag{4-16}$$

Using (4-15) and (4-16) as the reference model and the adjustable model, respectively, an MRAS system can be drawn as in Fig.4.7, where proportional and integral (PI) operations are utilized as the adaptation mechanism. From (4-15) and (4-16), it is evident that the speed estimation system of Fig.4.8 is completely robust to the stator resistance, besides requiring no integral calculation.

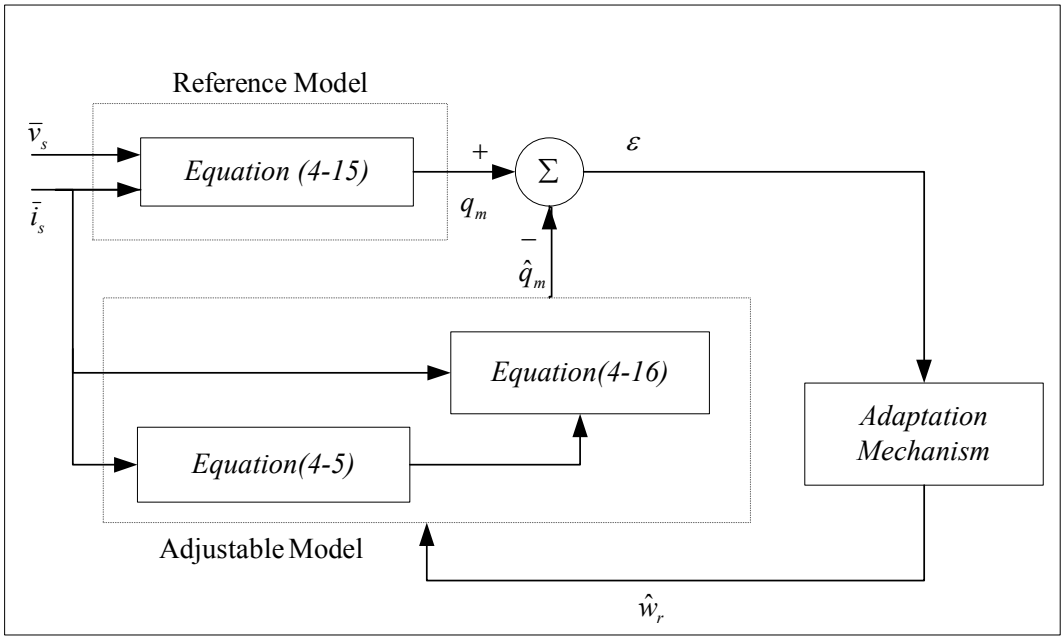


Figure 4-8 System structure of rotor speed observer using the tuning signal $Im(\Delta\bar{e}_m\bar{i}_s)$

The information required for this module is stator voltage and stator current components in the $d^s$-$q^s$ stationary reference frame. Two sets of equations are developed to compute reactive power of the induction motor in the reference and adaptive models. The reference model does not involve the rotor speed while the adaptive model needs the estimated rotor speed to adjust the computed reactive power to that computed from the reference model. Notice that the representation of complex number is defined for the stator voltages and currents in the stationary reference frame i.e., $v_s = v_{sd} + jv_{sq}$ *and* $\bar{i}_s = i_{sd} + ji_{sq.}$

### 4.6.1. Reference Model Continuous Time Representation

The back-emf of the induction motor can be expressed in the stationary frame as follows

$$\hat{e}_{md} = \frac{L_m}{L_r}\frac{d\psi_{rd}}{dt} = v_{sd} - R_s i_{sd} - \sigma L_s \frac{di_{sd}}{dt} \qquad (4\text{-}17)$$

$$\hat{e}_{mq} = \frac{L_m}{L_r}\frac{d\psi_{rq}}{dt} = v_{sq} - R_s i_{sq} - \sigma L_s \frac{di_{sq}}{dt} \tag{4-18}$$

$$\bar{e}_m = e_{md} + j e_{mq} \tag{4-19}$$

The reactive power of the induction motor can be computed from cross product of stator currents and back-emf vectors as follows:

$$q_m = \bar{i}_s \times \bar{e}_m = \bar{i}_s \times \left( v_s - R_s \bar{i}_s - \sigma L_s \frac{d\bar{i}_s}{dt} \right) = \bar{i}_s \times \bar{v}_s - \bar{i}_s \times \sigma L_s \frac{d\bar{i}_s}{dt} \tag{4-20}$$

where $\bar{i}_s \times \bar{i}_s = i_{sd} i_{sq} - i_{sq} i_{sd} = 0 \quad and \quad \sigma = 1 - \frac{L_m^2}{L_r L_s}$ $(leakage\ \ cofficient)$. As a result the reactive power shown in (4-20) can further be derived as

$$q_m = i_{sd} v_{sq} - i_{sq} v_{sd} - \sigma L_s \left( i_{sd} \frac{di_{sq}}{dt} - i_{sq} \frac{di_{sd}}{dt} \right) \tag{4-21}$$

### 4.6.2. Adaptive Model Continuous Time Representation

The estimated back-emf computed in the adaptive model can be expressed as follows:

$$\hat{e}_{md} = \frac{L_m^2}{L_r}\frac{di_{md}}{dt} = \frac{L_m^2}{L_r}\left( -T_r \hat{w}_r i_{mq} - i_{md} + i_{sd} \right) \tag{4-22}$$

$$\hat{e}_{mq} = \frac{L_m^2}{L_r}\frac{di_{mq}}{dt} = \frac{L_m^2}{L_r}\left( -T_r \hat{w}_r i_{md} - i_{mq} + i_{sq} \right) \tag{4-23}$$

$$\hat{\bar{e}}_m = \hat{e}_{md} + j\hat{e}_{mq} \tag{4-24}$$

where $T_r = \frac{L_r}{R_r}$ is the rotor time constant, $i_{md}, i_{mq}$ are computed from the following equations:

$$\frac{di_{md}}{dt} = -\hat{w}_r i_{mq} - \frac{1}{T_r} i_{md} + \frac{1}{T_r} i_{sd} \tag{4-25}$$

$$\frac{di_{mq}}{dt} = -\hat{w}_r i_{md} - \frac{1}{T_r} i_{mq} + \frac{1}{T_r} i_{sq} \tag{4-26}$$

Once the estimated back-emf computed by (4-22)-(4-26), the estimated reactive power can be computed as follows:

$$\hat{\bar{q}}_m = \bar{i}_s \times \hat{\bar{e}}_m = i_{sd} \hat{e}_{mq} - i_{sq} \hat{e}_{md} \tag{4-27}$$

Then, the PI controller tunes the estimated rotor speed such that the reactive power generated by adaptive model matches that generated by reference model. The speed tuning signal is the error of reactive power that can be expressed as follows:

$$\varepsilon_{\Delta e} = \bar{i}_s \times (\bar{e}_m - \hat{\bar{e}}_m) = q_m - \hat{q}_m \tag{4-28}$$

When this observer is used in a vector-controlled drive, it is possible to obtain satisfactory performance even at very low speeds. The observer can track the actual rotor speed with a bandwidth that is only limited by noise, so the PI controller gains should be as large as possible .The scheme is insensitive to stator resistance variations. The parameter $T_r$ has a negligible influence on the operation of both of the overall MRAS vector control systems. If the MRAS successfully maintains nearly zero error, and if the same value of $T_r$ is used in the MRAS adjustable models and in the function block for calculating $w_{slip}$, then we have the following relations:

$$w_e = \hat{w}_e \ \textit{and} \ T_r w_{slip} = \hat{T}_r \hat{w}_{slip}$$

where variables without "^" are actual values, and ones with "^" represent the corresponding values used in the MRAS vector control systems. Thus, if $T_r \neq \hat{T}_r$, then $w_{slip} \neq \hat{w}_{slip}$, but $w_o = \hat{w}_o$, which is used for orienting the stator current vector. Therefore, complete field orientation can be achieved even if the value of $T_r$ is quite wrong. The error in the value of $T_r$, however, produces an error in the speed feedback, thus affecting the accuracy of the speed control as follows:

$$\varepsilon_w = \hat{w}_r - w_r = \left(1 - \frac{T_r}{\hat{T}_r}\right) w_{slip} \tag{4-29}$$

This also holds for the previous MRAS scheme. However, the accuracy of the speed estimation system discussed depends on the transient stator inductance and also referred magnetizing inductance. The latter quantity is not too problematic, since it does not change with temperature. Furthermore, deviations of $T_r$ from its correct value produces a steady-state error in the estimated speed and this error become significant at low speeds.

### 4.6.3. Discrete Time Representation

For implementation on digital system, the differential equations need to be transformed to difference equations. Due to high sampling frequency compared to bandwidth of the system, the simple approximation of numerical integration , such as forward ,backward, or trapezoidal rules, can be adopted [36] . Consequently, the reactive power equations in both reference an adaptive models are discretized as follows:

#### 4.6.3.1. Reference Model

According to (4-21) reference model reactive power is given as :

$$q_m = i_{sd} v_{sq} - i_{sq} v_{sd} - \sigma L_s \left( i_{sd} \frac{di_{sq}}{dt} - i_{sq} \frac{di_{sd}}{dt} \right)$$

Using backward approximation:

$$q_m(k) = i_{sd}(k) v_{sq}(k) - i_{sq}(k) v_{sd}(k) - \sigma L_s \left( i_{sd}(k) \frac{i_{sq}(k) - i_{sq}(k-1)}{T} - i_{sq}(k) \frac{i_{sd}(k) - i_{sd}(k-1)}{T} \right) \quad (4\text{-}30)$$

And this equation can be further simplified as:

$$q_m(k) = i_{sd}(k) v_{sq}(k) - i_{sq}(k) v_{sd}(k) - \frac{\sigma L_s}{T} \left( i_{sd}(k-1) i_{sq}(k) - i_{sd}(k) i_{sq}(k-1) \right) \quad (4\text{-}31)$$

where $T$ is the sampling time.

#### 4.6.3.2. Adaptive Model

According to (4-27), reactive power in adaptive model is derived as

$$\hat{\bar{q}}_m = \bar{i}_s \times \hat{\bar{e}}_m = i_{sd} \hat{e}_{mq} - i_{sq} \hat{e}_{md}$$

whose discrete time representation is:

$$\hat{q}_m(k) = i_{sd}(k) \hat{e}_{mq}(k) - i_{sq}(k) \hat{e}_{md}(k) \quad (4\text{-}32)$$

where $\hat{e}_{md}(k)$ *and* $\hat{e}_{mq}(k)$ are computed as follows:

Continuous time representation:

$$\hat{e}_{md} = \frac{L_m^2}{L_r}\frac{di_{md}}{dt} = \frac{L_m^2}{L_r}\left(-T_r\hat{w}_r i_{mq} - i_{md} + i_{sd}\right)$$

$$\hat{e}_{mq} = \frac{L_m^2}{L_r}\frac{di_{mq}}{dt} = \frac{L_m^2}{L_r}\left(-T_r\hat{w}_r i_{md} - i_{mq} + i_{sq}\right) \tag{4-33}$$

Discrete time representation:

$$\hat{e}_{md}(k) = \frac{L_m^2}{L_r}\left(-T_r\hat{w}_r(k) i_{mq}(k) - i_{md}(k) + i_{sd}(k)\right)$$

$$\hat{e}_{mq}(k) = \frac{L_m^2}{L_r}\left(-T_r\hat{w}_r(k) i_{md}(k) - i_{mq}(k) + i_{sq}(k)\right) \tag{4-34}$$

and $i_{md}(k), i_{mq}(k)$ can be solved by using trapezoidal integration method, it yields

Continuous time representation:

$$\frac{di_{md}}{dt} = -\hat{w}_r i_{mq} - \frac{1}{T_r} i_{md} + \frac{1}{T_r} i_{sd}$$

$$\frac{di_{mq}}{dt} = -\hat{w}_r i_{md} - \frac{1}{T_r} i_{mq} + \frac{1}{T_r} i_{sq} \tag{4-35}$$

Discrete time representation

$$i_{md}(k) = i_{md}(k-1)\left[-\frac{T^2}{2}\hat{w}_r^2(k) + 1 - \frac{T}{T_r} + \left(\frac{T}{T_r}\right)^2\right] -$$

$$i_{mq}(k-1)\hat{w}_r(k)\left[T - \frac{T^2}{T_r}\right] + i_{sd}(k)\left[\frac{T}{T_r} - \frac{T^2}{2T_r^2}\right] - \tag{4-36}$$

$$i_{sq}(k)\hat{w}_r(k)\left[\frac{T^2}{2T_r}\right]$$

$$i_{mq}(k) = i_{mq}(k-1)\left[-\frac{T^2}{2}\hat{w}_r^2(k) + 1 - \frac{T}{T_r} + \left(\frac{T}{T_r}\right)^2\right] -$$

$$i_{md}(k-1)\hat{w}_r(k)\left[T - \frac{T^2}{T_r}\right] + i_{sq}(k)\left[\frac{T}{T_r} - \frac{T^2}{2T_r^2}\right] - \qquad (4\text{-}37)$$

$$i_{sd}(k)\hat{w}_r(k)\left[\frac{T^2}{2T_r}\right]$$

### 4.6.4. Per unit, discrete time representation

#### 4.6.4.1. Reference Model

Dividing (4-30) by base power of $V_bI_b$, then its per unit representation is as follows:

$$\begin{aligned} q_m(k) = {} & i_{sd}(k)v_{sq}(k) - i_{sq}(k)v_{sd}(k) - \\ & K_1\left(i_{sd}(k-1)i_{sq}(k) - i_{sd}(k)i_{sq}(k-1)\right) \end{aligned} \qquad (4\text{-}38)$$

Rearranging (4-38), then another form can be shown

$$q_m(k) = i_{sd}(k)\left(v_{sq}(k) - K_1 i_{sq}(k-1)\right) - i_{sq}(k)\left(v_{sd}(k) + K_1 i_{sd}(k-1)\right) pu \qquad (4\text{-}39)$$

where $K_1 = \dfrac{\sigma L_s I_b}{TV_b}$, $V_b$ is base voltage, and $I_b$ is base current.

#### 4.6.4.2. Adaptive Model

Dividing (4-34) by base voltage $V_b$, then yields

$$\begin{aligned} \hat{e}_{md}(k) &= K_2\left(-K_3\hat{w}_r(k)i_{mq}(k) - i_{md}(k) + i_{sd}(k)\right) pu \\ \hat{e}_{mq}(k) &= K_2\left(-K_3\hat{w}_r(k)i_{md}(k) - i_{mq}(k) + i_{sq}(k)\right) pu \end{aligned} \qquad (4\text{-}40)$$

where $K_2 = \frac{L_m^2 I_b}{L_r T_r V_b}$, $K_3 = T_r w_b = \frac{L_r w_b}{R_r}$ *and* $w_b = 2\pi f_b$ is base electrical angular velocity. Similarly, dividing (4-36) and (4-37) by base current $I_b$ , then yields:

$$\begin{aligned} i_{md}(k) &= i_{md}(k-1)\left[-K_4 \hat{w}_r^2(k) + K_5\right] - \\ &\quad i_{mq}(k-1)\hat{w}_r(k)K_6 + i_{sd}(k)K_7 - i_{sq}(k)\hat{w}_r(k)K_8 \\ i_{mq}(k) &= i_{mq}(k-1)\left[-K_4 \hat{w}_r^2(k) + K_5\right] - \\ &\quad i_{md}(k-1)\hat{w}_r(k)K_6 + i_{sq}(k)K_7 - i_{sd}(k)\hat{w}_r(k)K_8 \end{aligned} \tag{4-41}$$

Where

$$K_4 = \frac{w_b^2 T^2}{2},\ K_5 = 1 - \frac{T}{T_r} + \left(\frac{T}{T_r}\right)^2,\ K_6 = w_b\left(T - \frac{T^2}{T_r}\right),\ K_7 = -\frac{T}{T_r} + \left(\frac{T}{T_r}\right)^2$$

$$and\ K_8 = \frac{w_b T^2}{2}$$

# CHAPTER 5

# SIMULATIONS AND EXPERIMENTAL WORK

## 5.1. Simulations

Two different simulations were done to observe the effectiveness of the derived algorithms for the flux and speed estimation with MRAS scheme. MATLAB Simulink is used as simulation tool. Block diagram of the simulated system shown in Figure 5-1. Voltage inputs and current outputs of induction machine model are used as the inputs of speed and flux estimators. The simulation parameters are same as real motor used in the experiments. These parameters are kept constant during simulations. They are given in Table 5-1. The PI regulators are tuned as to match reference and adaptive variables together when parameter errors are absent. All simulations are carried out in discrete-time. Sampling time of simulations is the same with the one used in discrete time estimators of experiments.

Table 5-1 Simulation Parameters

| | |
|---|---|
| Rotor resistance per phase | 2.19 Ω |
| Stator resistance per phase | 1.80 Ω |
| Stator self inductance per phase | 0.192 H |
| Rotor self inductance per phase | 0.192 H |
| Magnetizing inductance | 0.184 H |
| Base line current | 7.5 A |
| Base per phase voltage | 220 V |
| Base torque | 12.375 Nm |
| Base linkage flux | 1.38 Vsec/rad |
| Base electrical angular velocity | 314 rad/sec |
| Number of motor poles | 4 |
| Sampling frequency | 0.0001 sec |

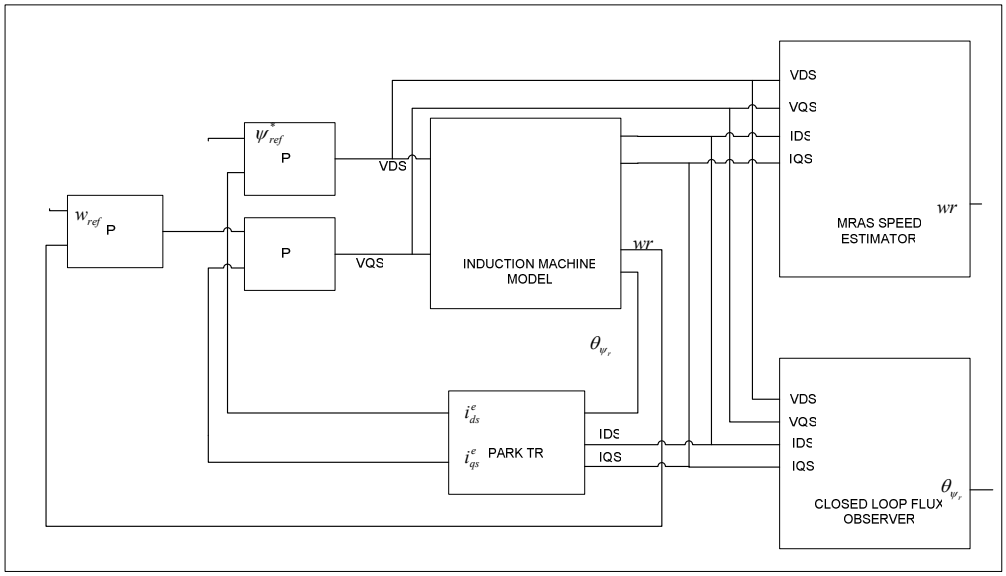


Figure 5-1 Block diagram of the system used in simulations

* $\psi_{ref}$ represents $i_{ds}^{e}$ set point in the simulation

### 5.1.1. Four Quadrant Operation

The simulation is implemented under no-load conditions. Figure 5-2 shows the outputs of the machine model used in simulations when the model is operating in four quadrant. As expected torque is positive and constant during speeding up with constant acceleration. Meanwhile frequency of d- and q-axes components of stator currents increase. The frequency of rotor flux increases as the machine accelerates.

During constant speed operation, torque remain constant at low value which overcomes friction and windage. Frequencies of currents and rotor flux angle remain constant in this period.

When the machine starts decelerate, torque becomes negative and frequencies of currents together with rotor flux angle decrease.

All the phenomena repeat itself in the negative sense when the speed is reversed. In Figure 5-4 four quadrant speed tracking performance of reactive power MRAS scheme is simulated. Actual and estimated speeds are drawn together. Figure 5-3 shows outputs of both reference and adaptive models of MRAS. In Figure 5-5,

both actual and estimated rotor flux angle are given. Rotor flux angle is estimated using closed-loop flux observer.

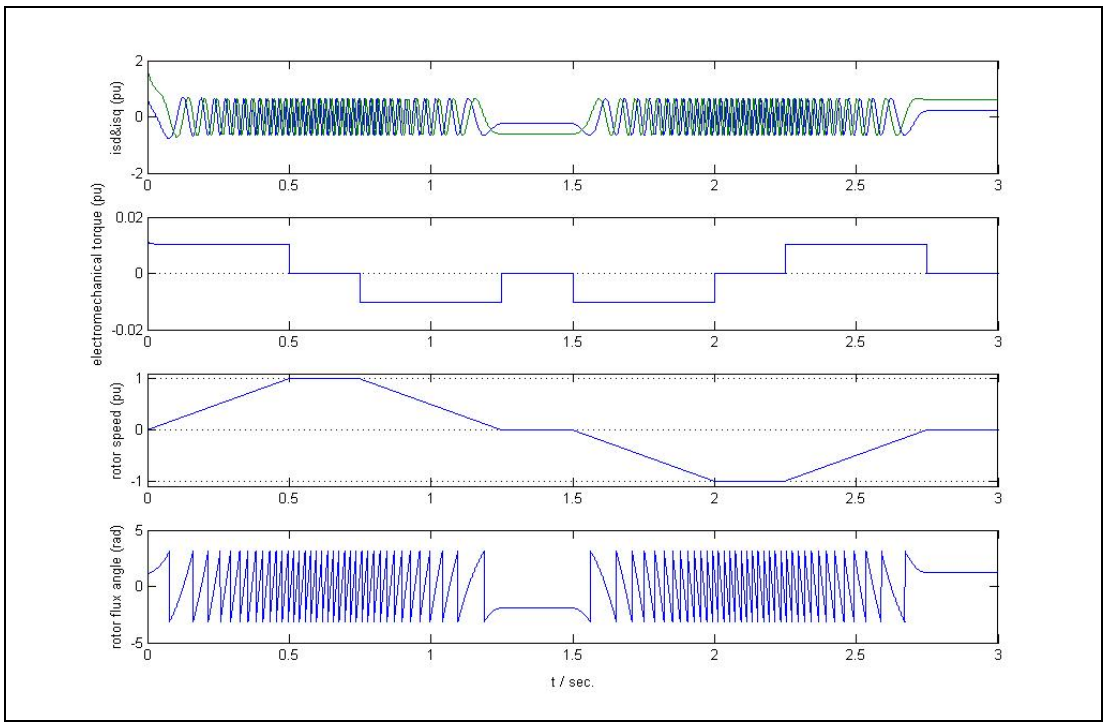


Figure 5-2 Four-quadrant speed reversal of induction motor q- and d-axis stator currents, produced torque due to inertia (J), rotor speed, rotor flux angle

Referring to the equivalent circuit of the machine when the machine runs at high speed rotor impedance becomes highly resistive and stator current decreases to a low value of which the magnetizing branch current makes up considerably high proportion. Therefore the current drawn by the stator is highly inductive leading to increased consumption of the reactive power. Figure 5-3 displays this fact so that reactive power is increasing with motor's speeding up, and reactive power remains high when the motor runs at high speed. In deceleration mode reactive power decreases as the speed decreases. Figure 5-3 therefore resulted as expected. Further note that Figure 5-3 shows both reference model reactive power output and adaptive

model reactive power output. It is apparently seen in Figure 5-3 that adaptive model reactive power output follows the reference model reactive output exactly.

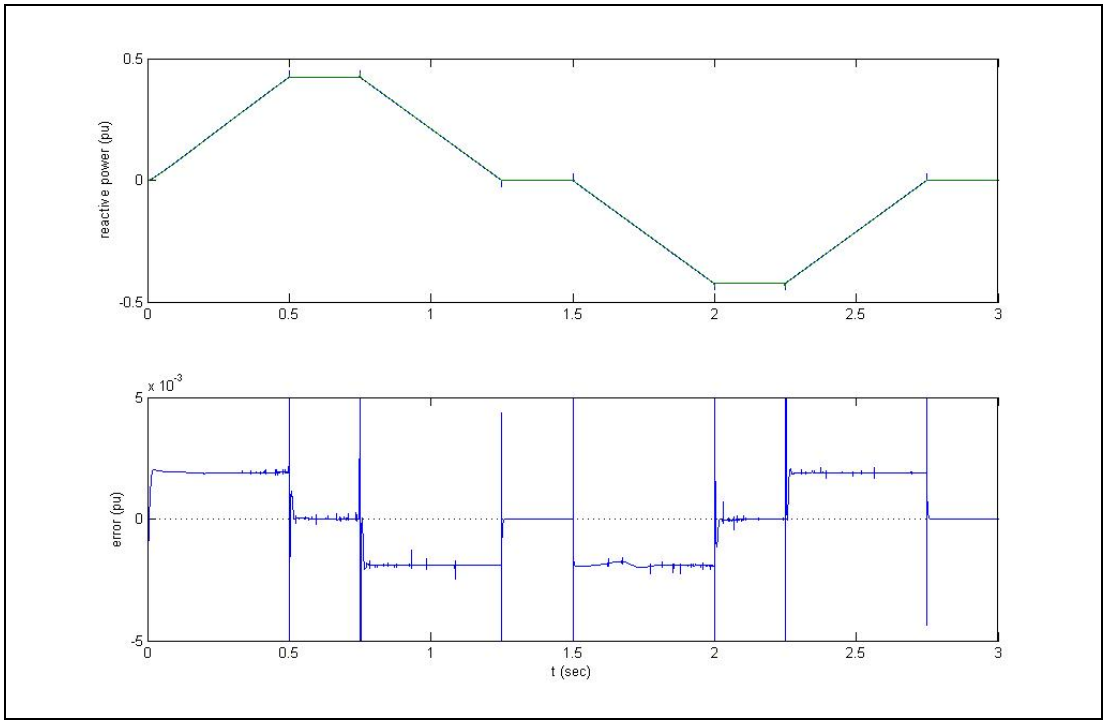


Figure 5-3 Reference and adaptive model reactive power outputs of reactive power MRAS scheme and difference between them

Note in Figure 5-4 estimated speed tracks the actual one which is output of the machine model shown in Figure 5-1. in constant speed region small error appears but this may be neglected.

Figure 5-5 shows actual and estimated rotor flux angles. Here estimated flux angle is the output of closed loop flux observer. However the graph is not clear thoroughly but during the acceleration or deceleration we clearly see that both actual and estimated values are quite close coincidence. There no doubt that they are coincident in other regions of operation as well. Thus when the rotor flux angle goes through park transformation as shown in Figure 5-1. The results are $i_{ds}$ and $i_{qs}$

(obtained in rotor flux reference frame) input to PI regulators which are yielding $V_{ds}$and $V_{qs}$.

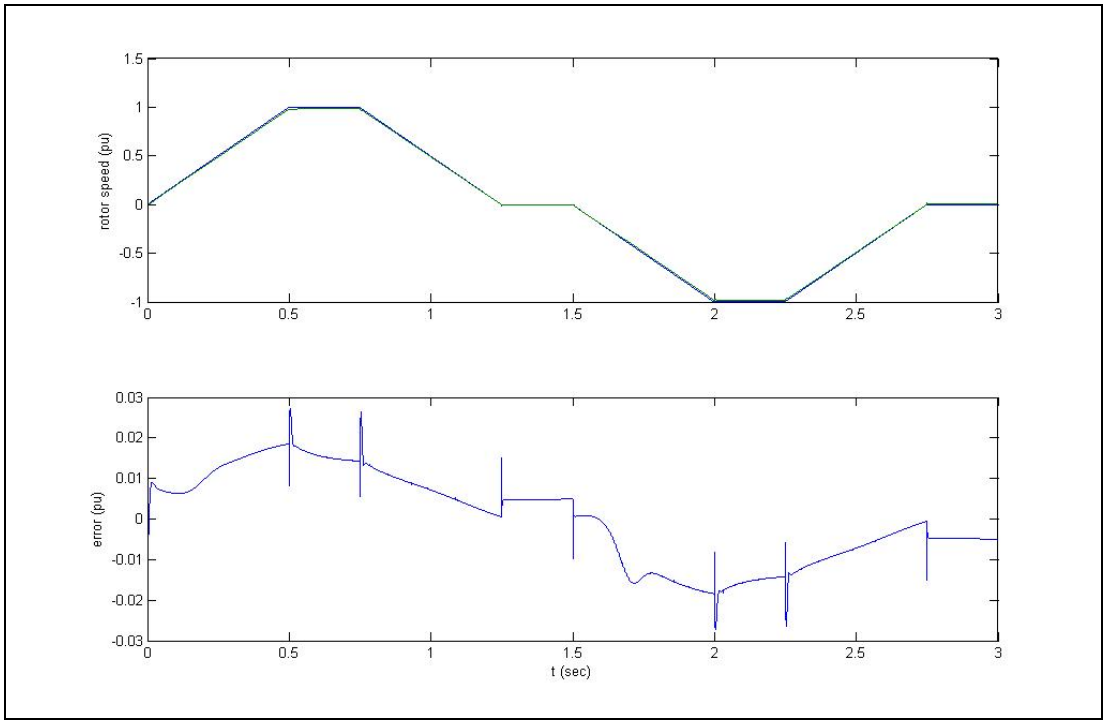


Figure 5-4 Actual speed and speed estimated using reactive power MRAS scheme and difference between them

### 5.1.2. Varying Load Condition

The simulation was done under varying load conditions. Rated torque is applied at 0.75 second after reaching the rated speed under no load condition. At the time t=1 sec. the applied load torque is reduced to 50% of the rated torque. At t=1.25 sec. it is raised to %100 $T_{rated}$ again. At t=2 sec. the load torque is removed. Figure 5-6 shows the variables of Figure 5-2 under the above stated loading and timing conditions. Depending on the loading conditions torque vs. time profile is to be taken reference to follow the variations in $i_{ds}$ and $i_{qs}$, and the rotor flux angle. We note that as the point of significance from Figure 5-6 the frequencies of $i_{ds}$ and $i_{qs}$ pair and the rotor flux angle do not change with loading.

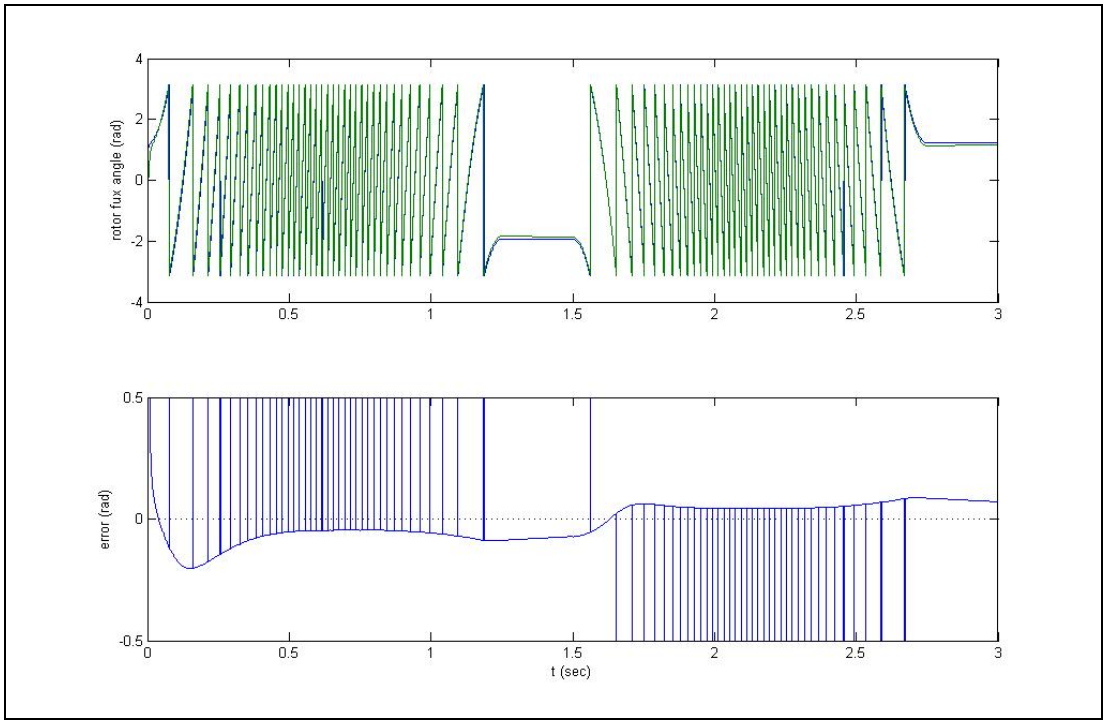


Figure 5-5 Actual rotor flux angle and estimated rotor flux angle as output by the closed loop flux estimator and difference between them

Figure 5-7 plots the variation in reference and adaptive model reactive power outputs for the reactive power MRAS scheme during the loading variations. Here both reactive power outputs are resulting very close to each other, which is the main objective of using the scheme. If they are almost identical the natural consequence is that the scheme can be considered that the rotor speed is accurately estimated without using any added external sensor. Referring to Figure 5-7 the spikes seen on the reactive power outputs deserve a sound explanation which we lack.

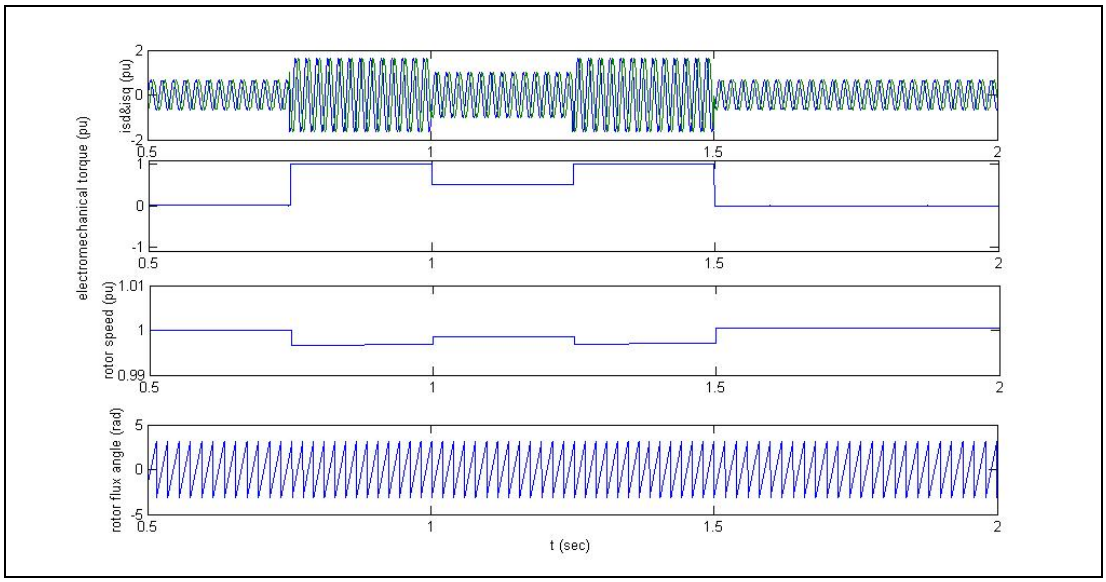


Figure 5-6 q- and d-axes stator currents, applied torque, actual rotor speed and actual rotor flux angle of motor in case of varying load torque

As a verification of the hypothesis that the rotor speed can be accurately estimated with reference to Figure 5-7, we see in Figure 5-8 a comparison of actual and estimated values of the rotor speed. They are really close during speed up, but they differ very slightly under all varying load conditions. Our opinion is that the difference is negligible.

The spikes, which cannot be explained, present in Figure 5-7 are also seen in Figure 5-8 as well.

Figure 5-9 displays the close coincidence of the actual and estimated rotor flux angles under varying loading conditions.

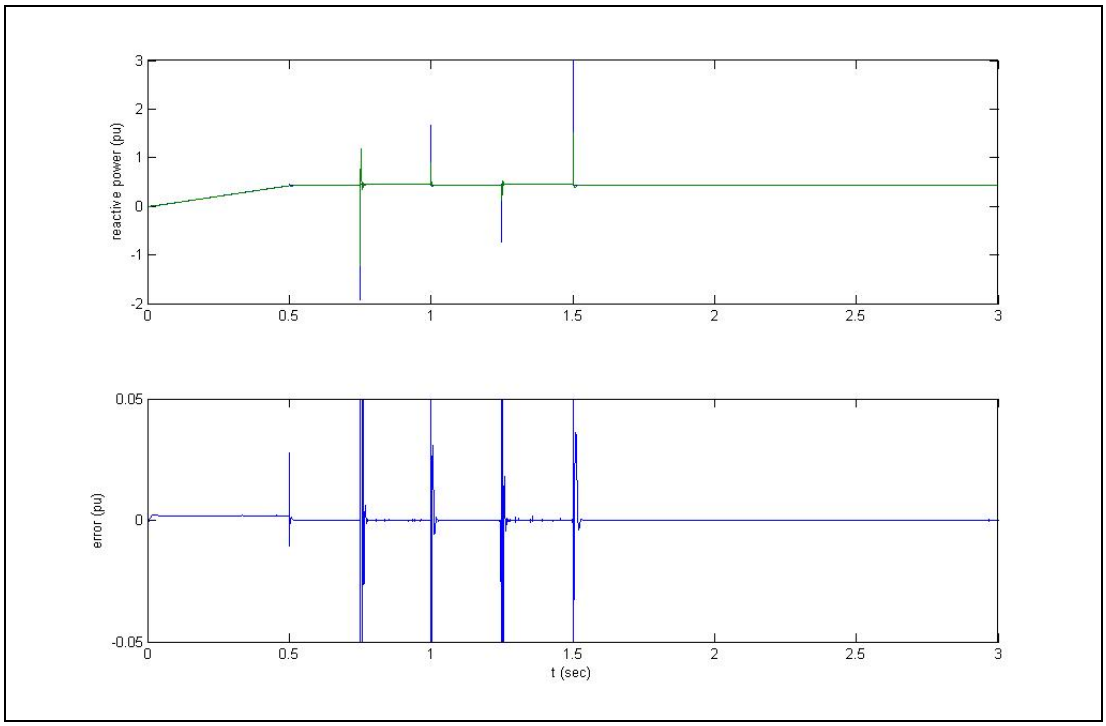


Figure 5-7 Reference and adaptive model reactive power outputs of reactive power MRAS scheme and difference between them

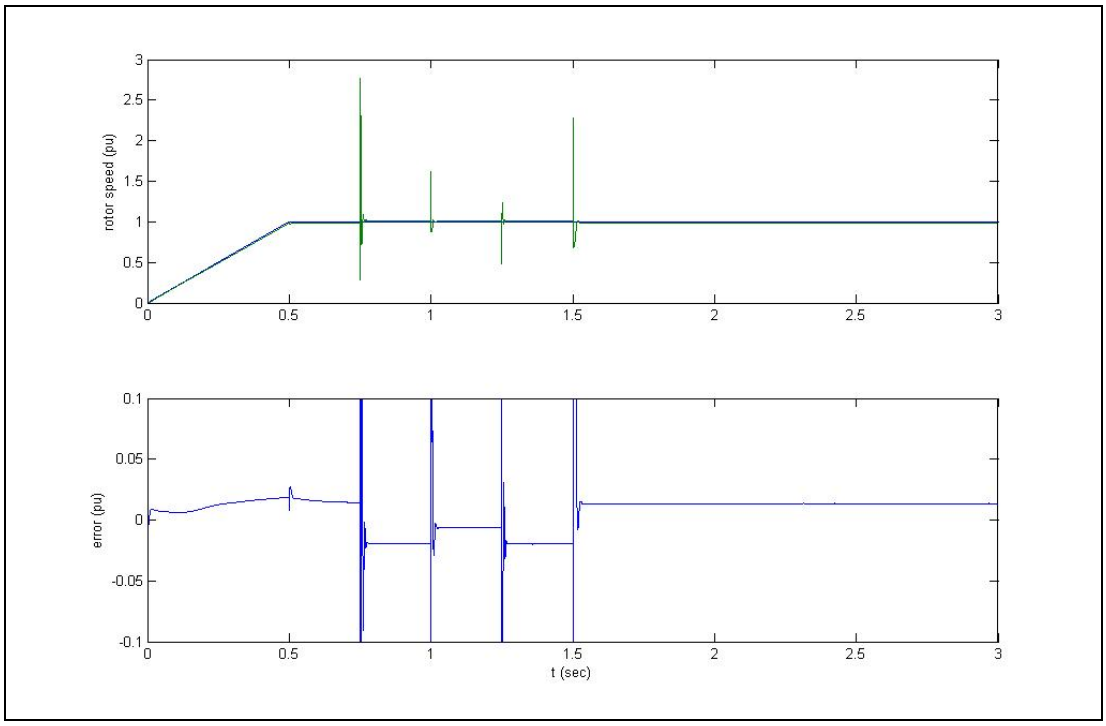


Figure 5-8 Actual speed and speed estimated using reactive power MRAS scheme and difference between them

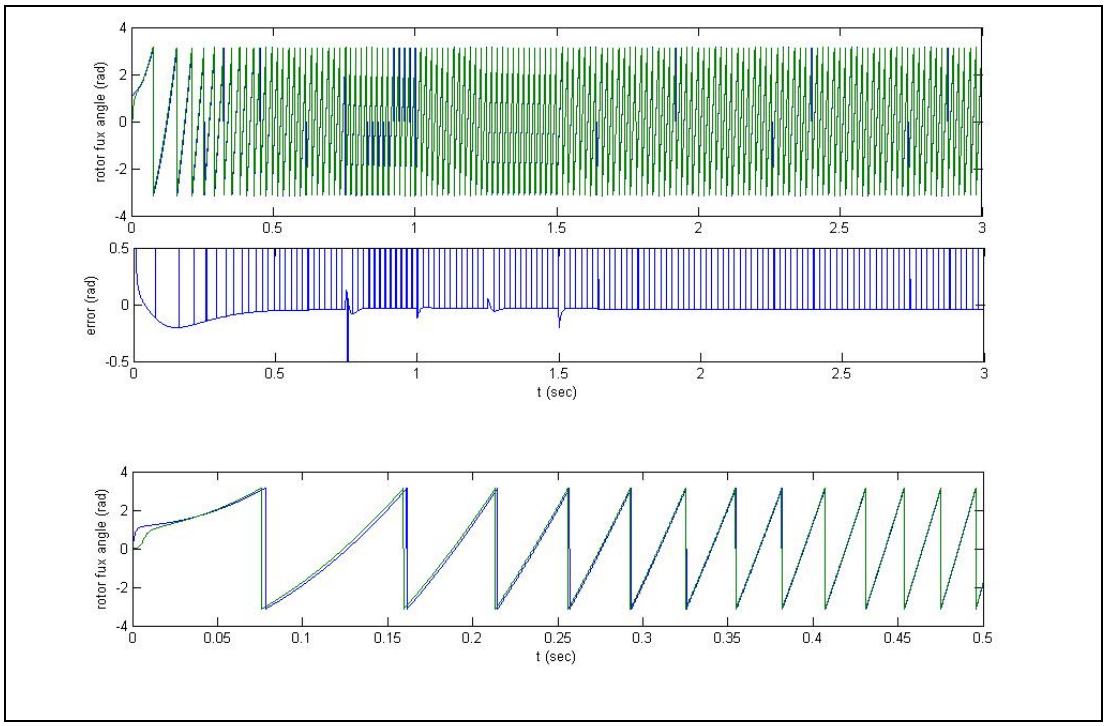


Figure 5-9 Actual rotor flux angle and estimated rotor flux angle according to closed loop flux estimator, difference between them and actual and estimated rotor flux angles during speeding up

## 5.2. Experimental Work

Speed and flux estimators designed in MRAS scheme have been tested experimentally as well. Experiments were done in two steps. In first step closed loop flux observer was tuned for satisfactory operation at different speeds. Then at the second step, using rotor flux position estimate of flux observer in DFOC algorithm, closed loop torque control was applied. In parallel mechanical speed was estimated.

Measured quantities were two of the three phase currents. Phase voltages were calculated internally from the conduction times of upper half switching elements of bridge inverter, under assumption that the bus voltage is constant during operation and no dead time between upper and lower half switching elements are present.

### 5.2.1. Tuning of Flux Observer

In this thesis DFOC algorithm was implemented as FOC scheme. To implement DFOC, rotor flux position with respect to stator frame has to be known, and closed loop flux observer provides this position. Without the knowledge of this data, current loop cannot be closed. Because of this, observer was tuned at different speeds while open loop control was applied to the motor at no load condition.

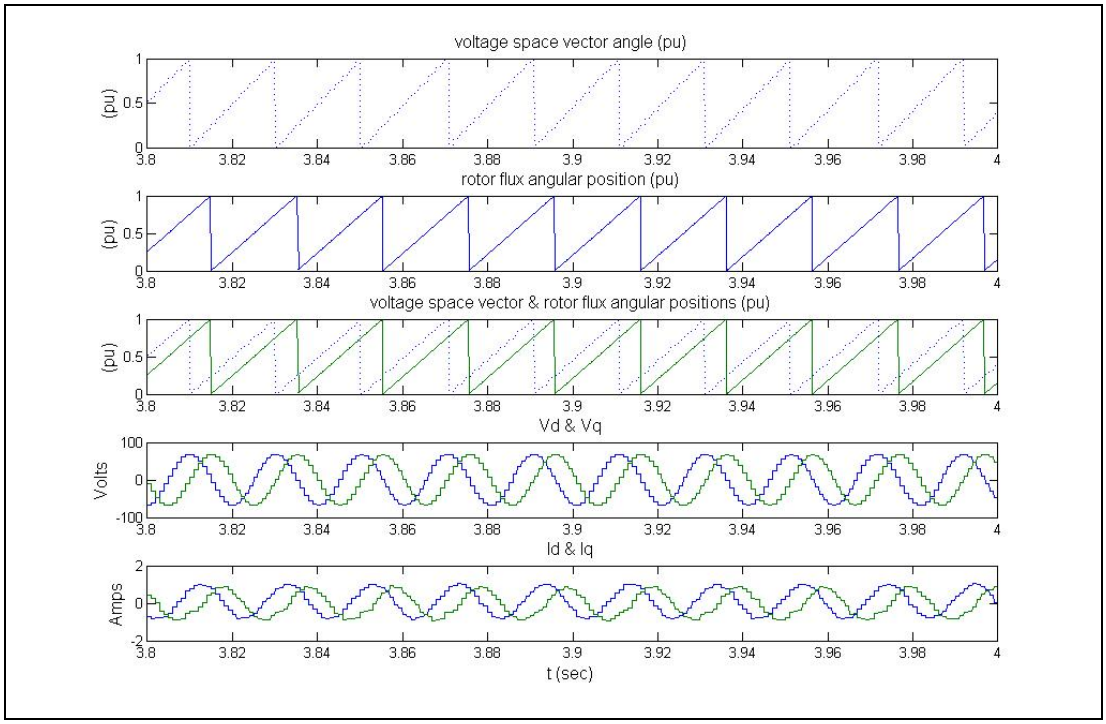


Figure 5-10 applied 50Hz voltage space vector angle, estimated rotor flux angular position, d- and q- axes voltages and currents at steady state

At the beginning, motor was run at 50Hz. Angle of the applied voltage space vector (trace 1) with respect to time is shown in Figure 5-10. Unit for the angle is p.u. where 1 refers to $2\pi$ rads. The estimated rotor flux position (trace 2) using d- and q-axes voltages (trace 4) and currents (trace 5) are shown in Figure 5-10. It is seen that, at steady state estimated flux rotates at the same frequency with stator voltage and currents, and lags voltage space vector (trace 3) as expected.

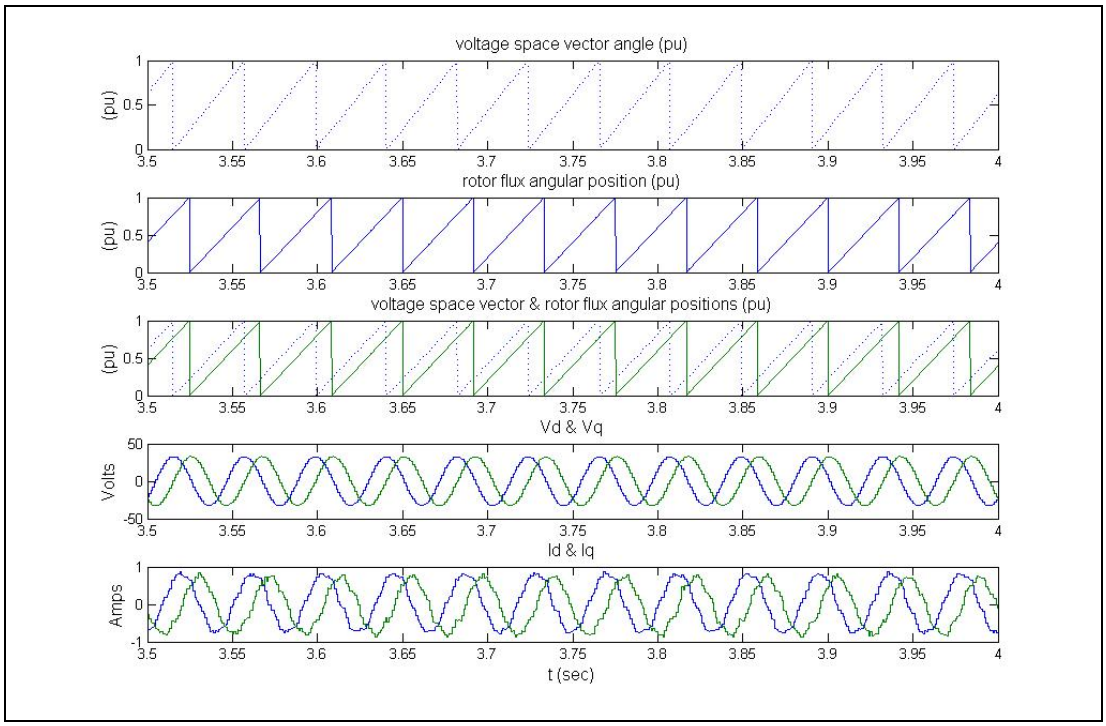


Figure 5-11 applied 25Hz voltage space vector angle, estimated rotor flux angular position, d- and q- axes voltages and currents at steady state

Next, the motor was run at 25Hz and the rotor flux position (trace 2) was estimated with closed loop flux observer which have the same parameters tuned for 50Hz. Steady state values of measured currents (trace 5) and calculated voltages (trace 4) are shown with estimated rotor flux angular position in Figure 5-11. Note that trace 3, being the combined form of traces 1 and 2, shows that rotor flux angular position lags as expected the voltage space vector while being generated at the same frequency. However, this does not bear the fact that the amount of the lagging is definitely correct. The reason for this, there is no way to measuring the actual rotor flux itself. Hence we may conclude that relative standing of the rotor flux angle variation with reference to the voltage space vector gives us a global idea that the rotor flux angular position is estimated reasonably. On the other hand, $V_{ds}$ and $V_{qs}$ (trace 4) and $i_{ds}$ and $i_{qs}$ (trace 5) waveforms are at the same frequency with the rotor flux angular position variation indicating once again the latter caries correct information although it is a rough knowledge.

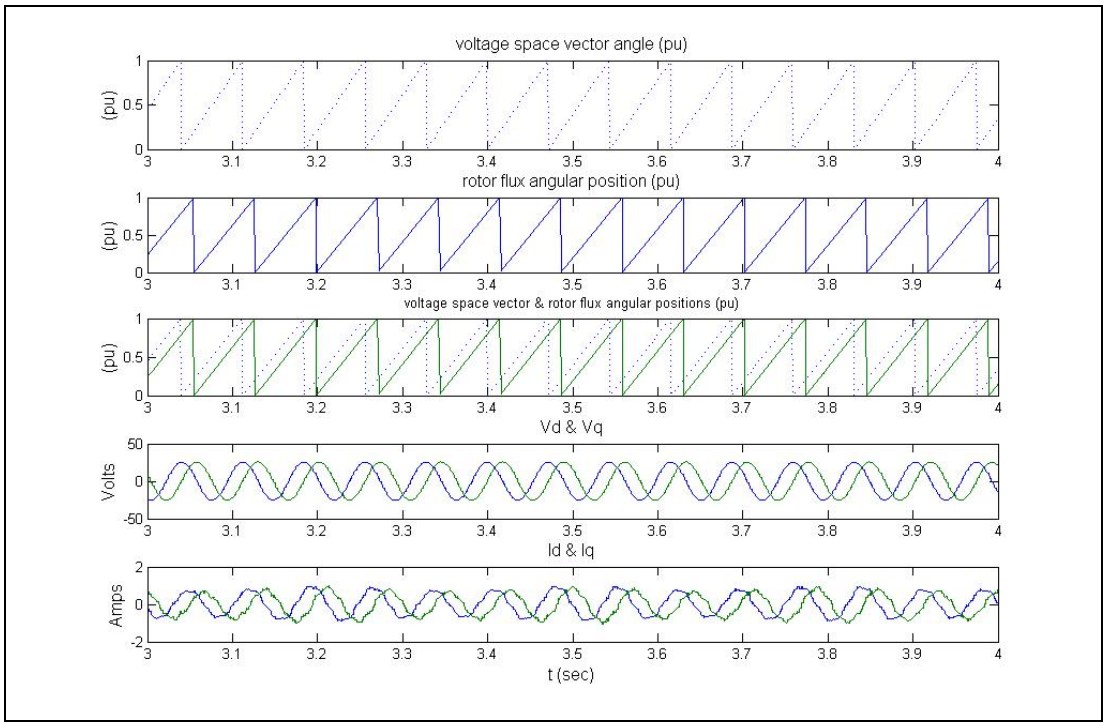


Figure 5-12 applied 13Hz voltage space vector angle, estimated rotor flux angular position, d- and q- axes voltages and currents at steady state

Performance of closed loop flux observer, without changing parameters set, was tested for different speeds. Figure 5-12 shows applied voltage space vector (trace 1) rotating at 13Hz, estimated rotor flux angular position and d- and q-axes stator voltages (trace 4) and currents (trace 5) at steady state. The same discussion made for operation at 25Hz is valified here for a case held at frequency of 13Hz.

Performance of the flux estimator at low frequencies is especially important. Referring to (5-1) and (5-2), at low frequency the term $w_e$ is low together with $V_s$, leaving $R_s i_s$ product term dominant in the integration process which is the cause of both amplified errors in the flux estimated and drift and offset problems resulting from pure integration. However, instead of $w_e \psi_q$ product in the same equation in this study a compensated voltage derived from current model and PI regulator is used as shown in Figure 3-1. This is expected to improve the performance of the estimation. For this reason, closed loop observer is tested at 6Hz and 3Hz. While Figure 5-13 shows voltage space vector, estimated rotor flux angular position, d- and q-axis

voltages and currents for 6Hz at steady state, figure 5-14 shows them for 3Hz. They both show that estimator performance maintains its successful performance at these low frequencies when results are compared with those obtained at higher frequencies.

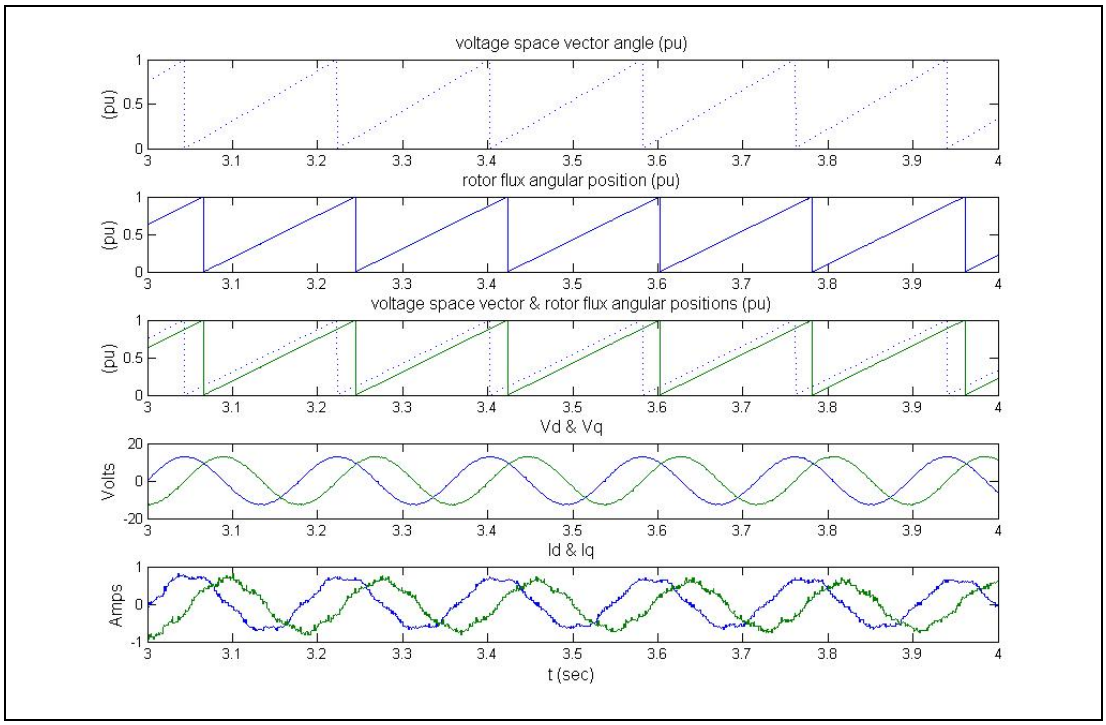


Figure 5-13 applied 6Hz voltage space vector angle, estimated rotor flux angular position, d- and q- axes voltages and currents at steady state

$$\psi_{ds}^{s,v} = \int \left( u_{ds}^{s} - i_{ds}^{s} R_s + w_e \psi_{qs}^{s,v} \right) dt \qquad (5\text{-}1)$$

$$\psi_{qs}^{s,v} = \int \left( u_{qs}^{s} - i_{qs}^{s} R_s - w_e \psi_{ds}^{s,v} \right) dt \qquad (5\text{-}2)$$

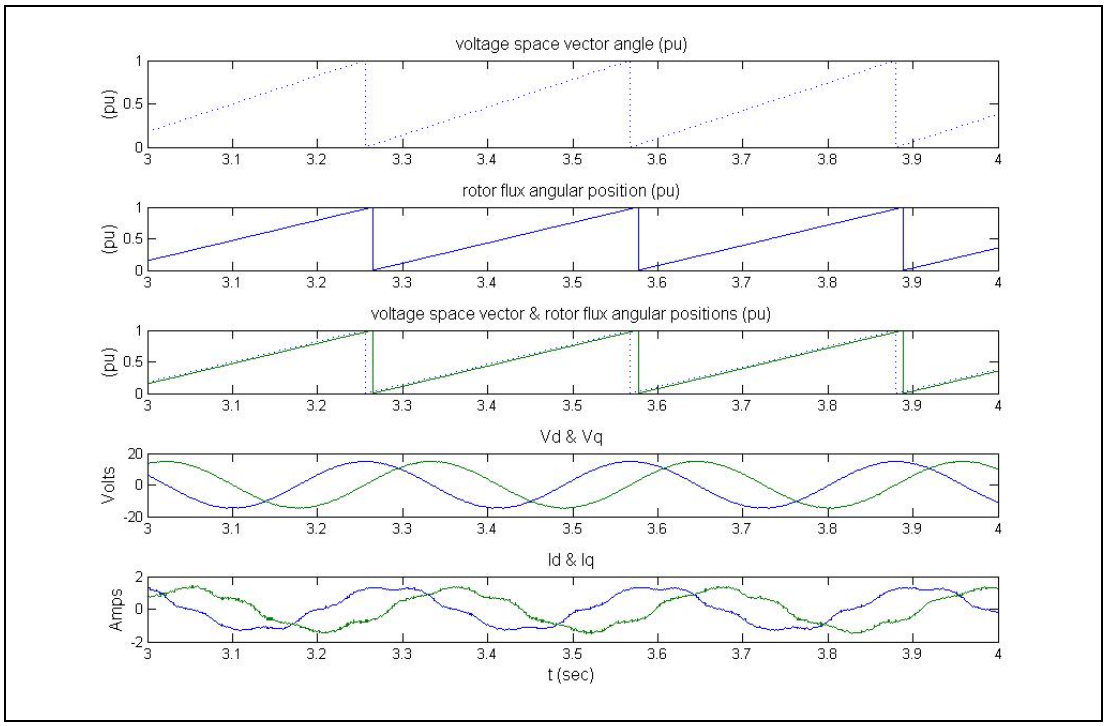


Figure 5-14 applied 3Hz voltage space vector angle, estimated rotor flux angular position, d- and q- axie voltages and currents at steady state

### 5.2.2. Closed Loop Torque Control

After tuning flux observer, closed loop torque control was applied by means of DFOC. In this step, experiments were done for different values of torque demands such as;

i. Low torque demand ($i_{qs}^{e}$ = 0.1A). With this test we want to see the behavior of the system while overcoming the effect of static friction and moment of inertia.

ii. Moderate level torque demand ($i_{qs}^{e}$ = 0.25), to observe the behavior of the system at a higher speed compared to that of part i.

iii. Large torque demand ($i_{qs}^{e}$ = 1A). Machine is expected to speed up to speeds above the base speed (>314 rd/sec). The speed is expected to be such that machine will find an equilibrium to meet the friction and windage torque demand at the end.

iv. Negative torque demand ($i_{qs}^{e}$ = -0.5A). Machine is expected to rotate opposite direction similar to that when compared with the behavior observed in part ii. With this test we want to see that the flux estimator works identically same in the negative direction to the contrary of the previous tests.

**i**. Figure 5-15 shows d- and q-axes stator currents (trace 2) and voltages (trace 1) at starting instant. Demanded $i_{ds}^{e}$ is 1A, and demanded $i_{qs}^{e}$ is 0.1A in rotor flux frame. The estimated rotor flux position and measured currents in rotor flux frame are shown in Figure 5-16. Both of two components reach their set values. Settling time may be reduced with the expense of overshoot. As stated in Chapter 2, FOC

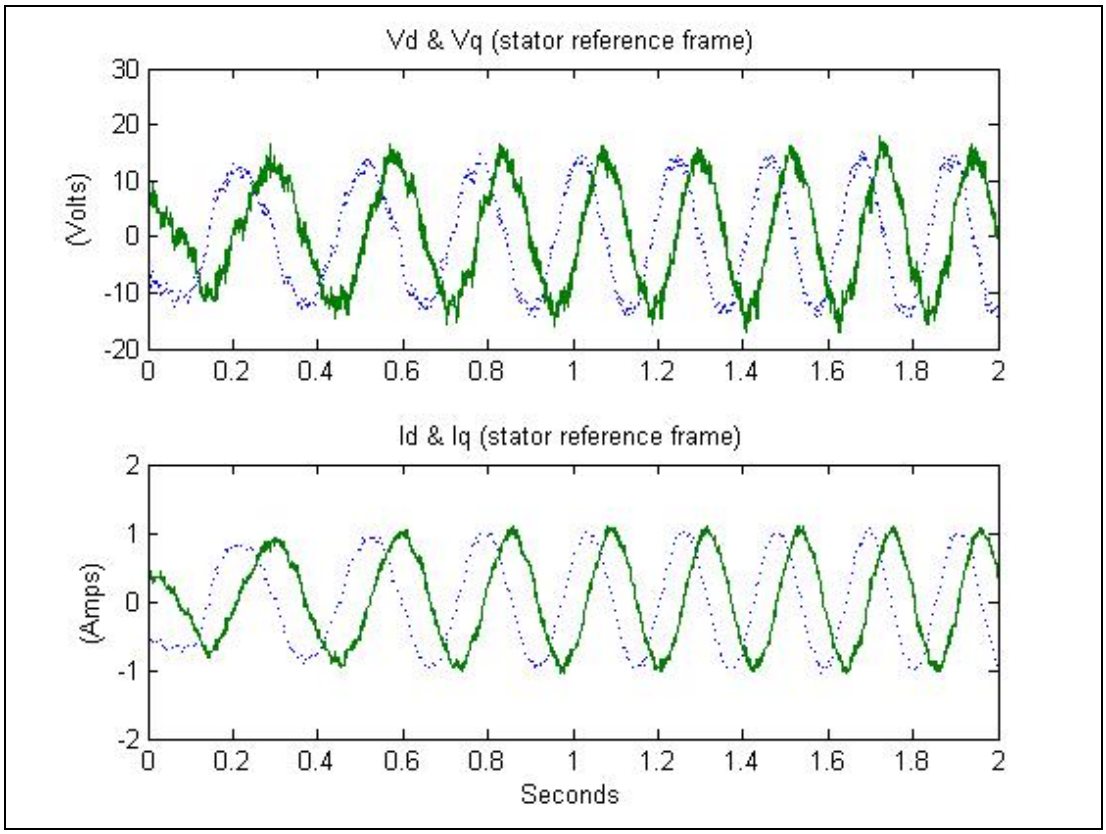


Figure 5-15 d- and q-axes voltages and currents at starting instant

topic, $i_{ds}^{e}$ is flux producing component, and $i_{qs}^{e}$ is torque producing component under constant flux. 0.1A current produces very little torque so motor rotates very slowly near 50rpm. This result verifies the success of this flux estimation scheme, while the motor is running at low frequencies. This result is quite important when it is compared with the failures of the open-loop observers discussed before. Hence the use of compensated voltage method proposed in this study is quite effective as a solution for the discussed problem. The rotor speed, estimated using reactive power MRAS scheme, is shown in Figure 5-17. As seen on Figure 5-17, adaptive model's output tracks reference model's output.

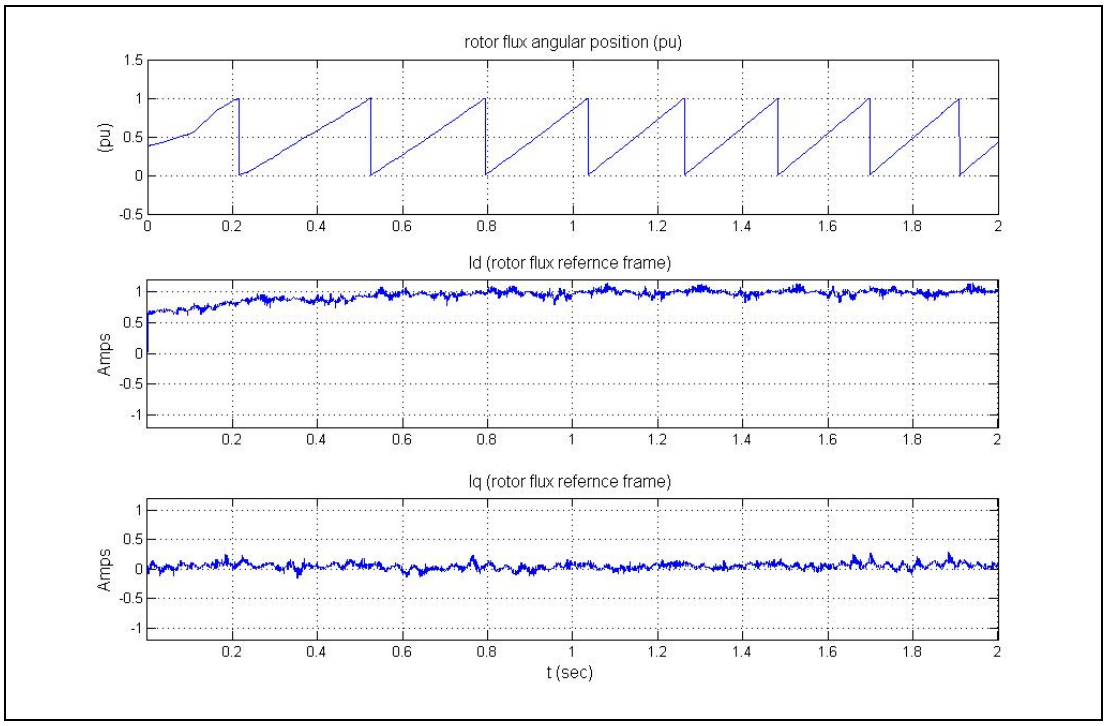


Figure 5-16 Estimated rotor flux angular position, measure d- and q- axes currents in rotor flux reference frame

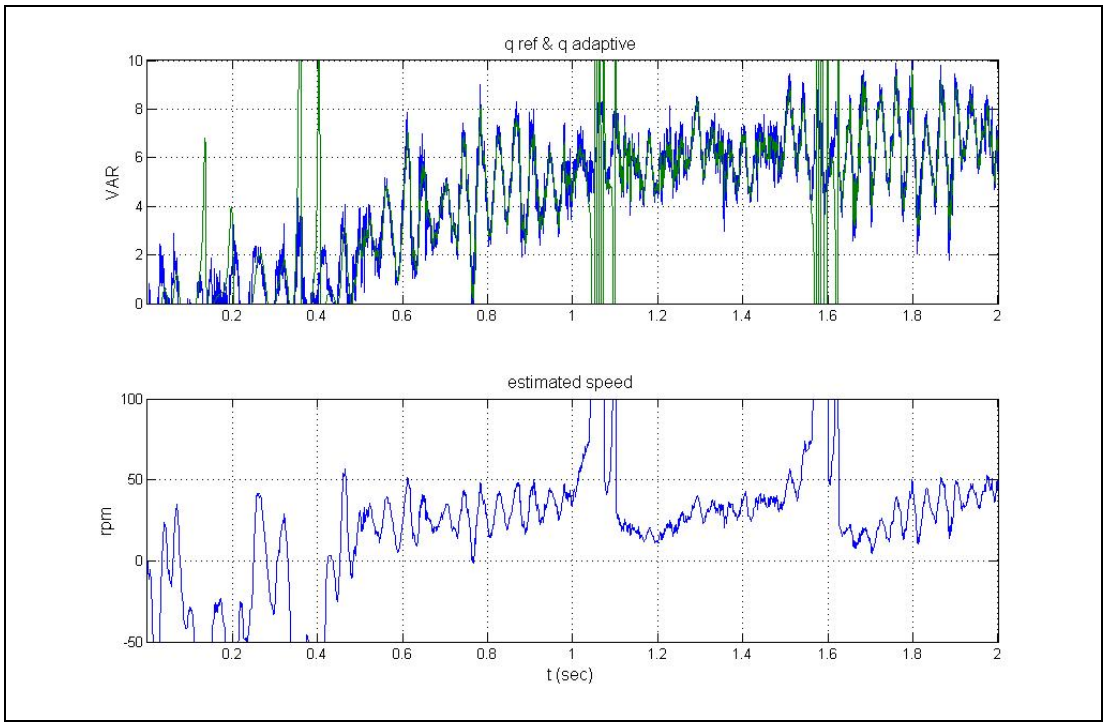


Figure 5-17 Reactive power outputs of reference and adaptive models and estimated rotor speed

**ii**. Then $i_{qs}^{e}$ set point was increased to 0.25A, while $i_{ds}^{e}$ set point was kept constant. Figure 5.18 shows d- and q-axes stator currents and voltages in stator reference frame during starting.

The estimated rotor flux position (trace 1) and d- and q- axes stator currents (traces 2, 3, respectively) in this frame is shown in Figure 5-19. Both of the two components have reached to set values. The rotor speed estimated using reactive power MRAS scheme, is shown in Figure 5-20. As seen on Figure 5-20, adaptive model's output tracks reference model's output.

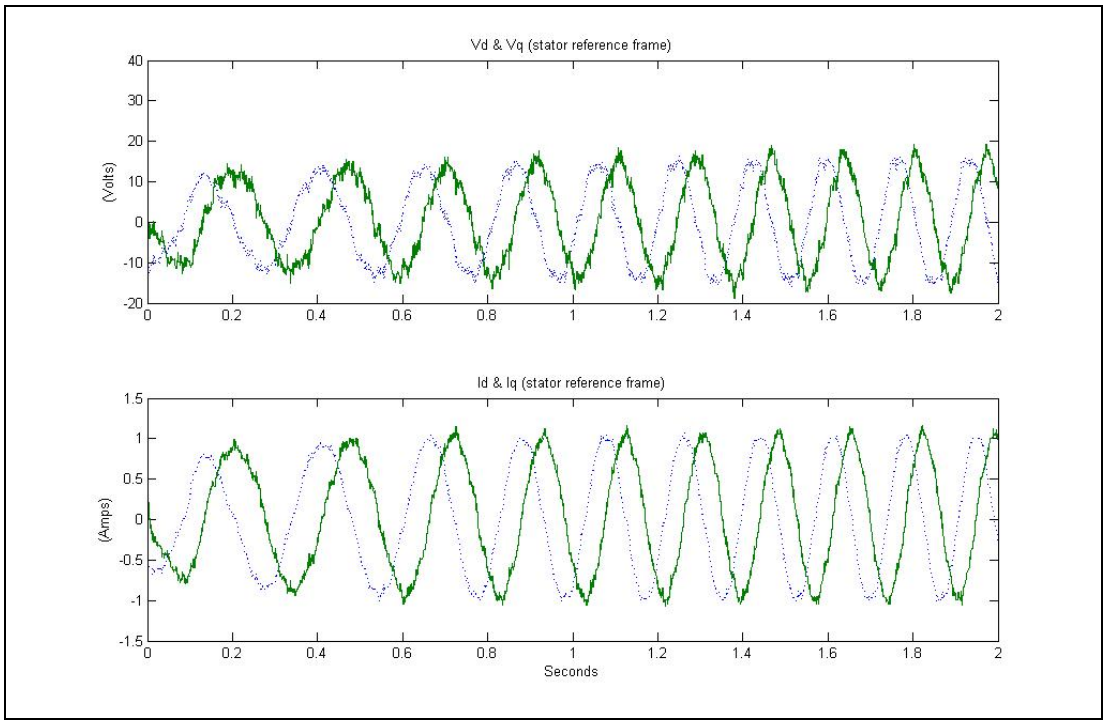


Figure 5-18 d- and q-axes voltages and currents at starting instant

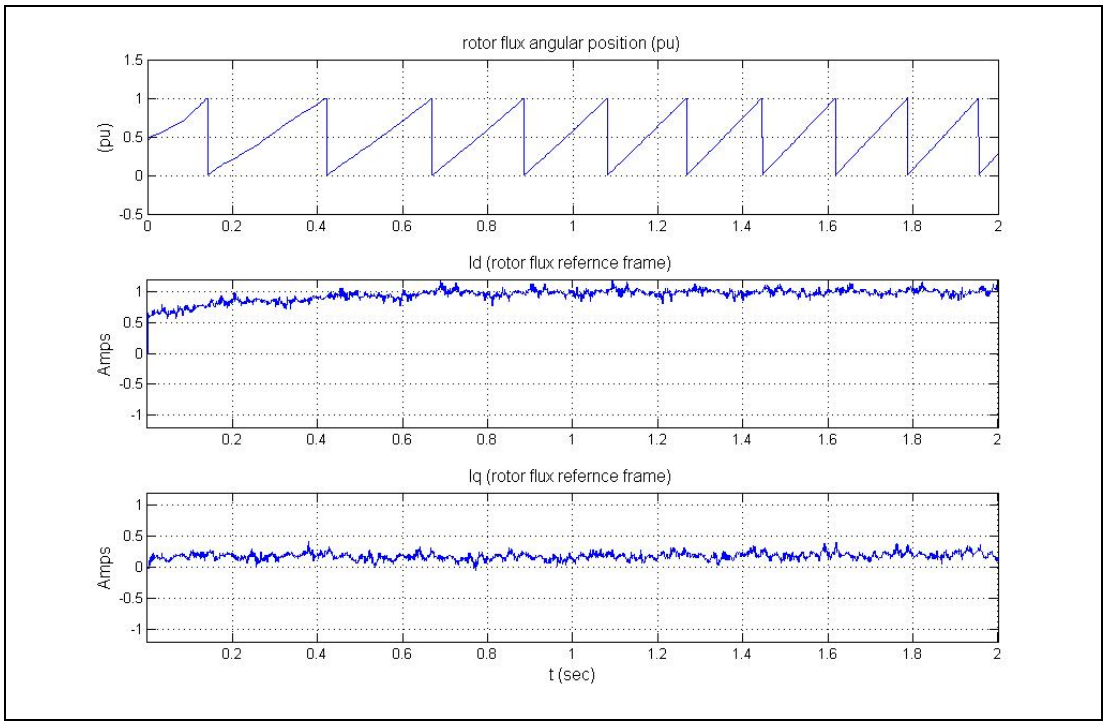


Figure 5-19 Estimated rotor flux angular position, measure d- and q- axes currents in rotor flux reference frame

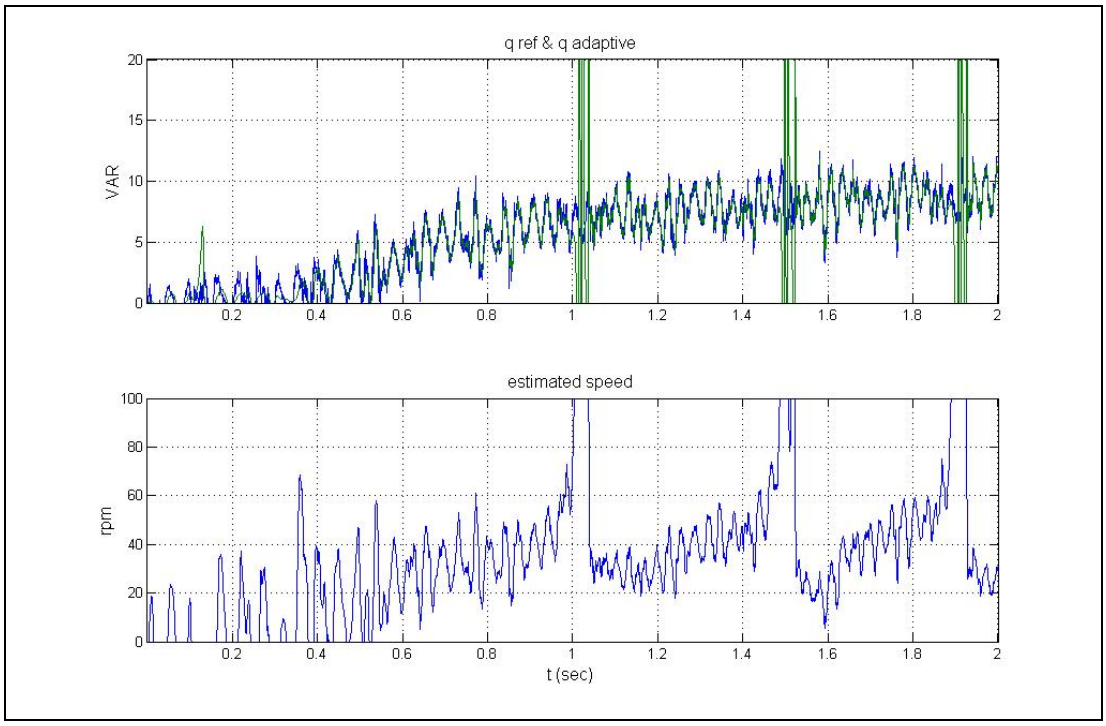

Figure 5-20 Reactive power outputs of reference and adaptive models and estimated rotor speed

**iii**. $i_{qs}^{e}$ set point value was further increased to 1A while $i_{ds}^{e}$ setting was kept constant. Figure 5-21 shows d- and q-axes stator currents and voltages in stator reference frame during starting. The main pint seen in Figure 5-21 is that the frequency is continuously increasing within the time frame. That is machine continue to accelerate not settling to a steady-state speed within this time period.

Estimated rotor flux position and measured currents in rotor flux frame are shown in Figure 5-22 and the estimated rotor speed using reactive power MRAS scheme is shown in Figure 5-23. Note that $i_{ds}^{e}$ has reached the set value however, $i_{qs}^{e}$ has not in Figure 5-22. This discrepancy may be explained as follows; the torque produced in this case has been much larger than that of previous cases (i, ii). This carried the motor to a very high speed since the motor was operating in no load condition. Back-emf would be high due to high speed, and therefore, forcing the

demanded current, $i_{qs}^{e}$ could not be drawn from the line. If the motor would possibly be loaded externally, the resulting speed at equilibrium would be lower. This in turn means that the back-emf voltage would be lower. As a result $i_{qs}^{e}$ could reach to the set point.

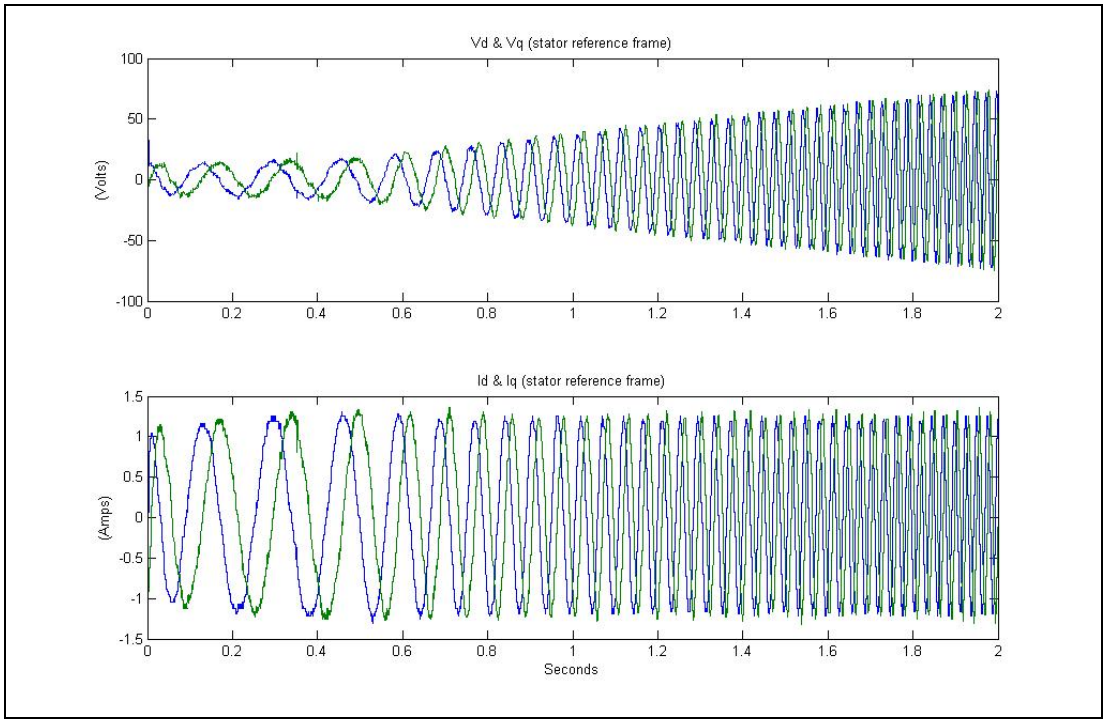


Figure 5-21 d- and q-axis voltages and currents at starting instant

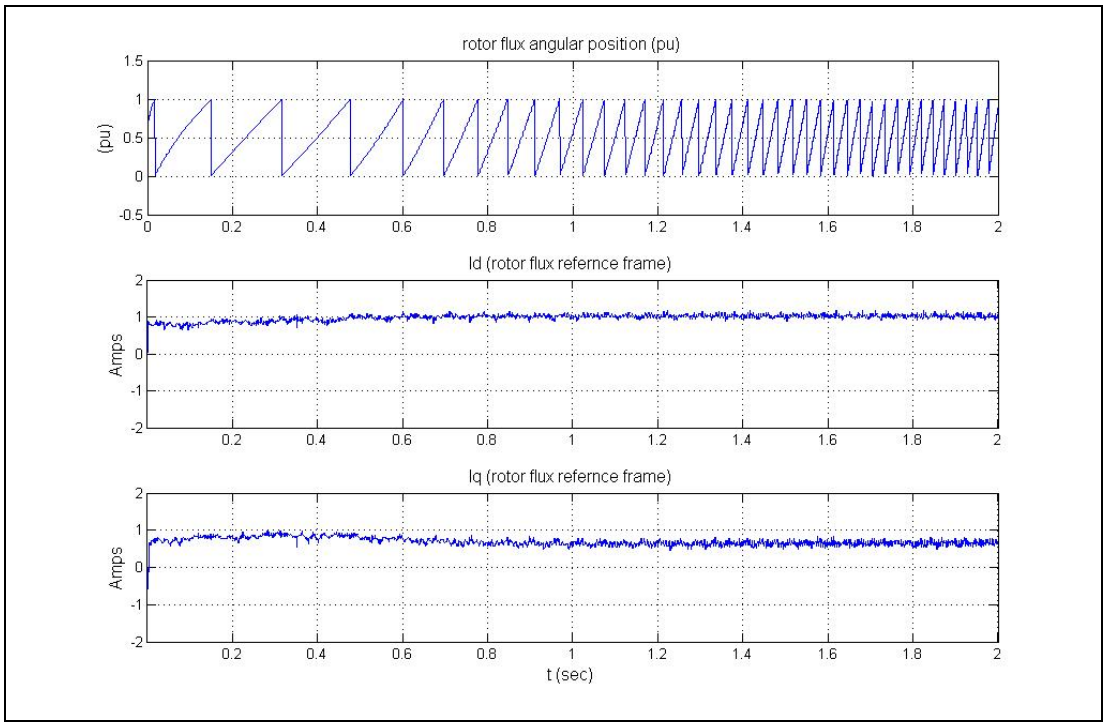


Figure 5-22 Estimated rotor flux angular position, measure d- and q- axis currents in rotor flux reference frame

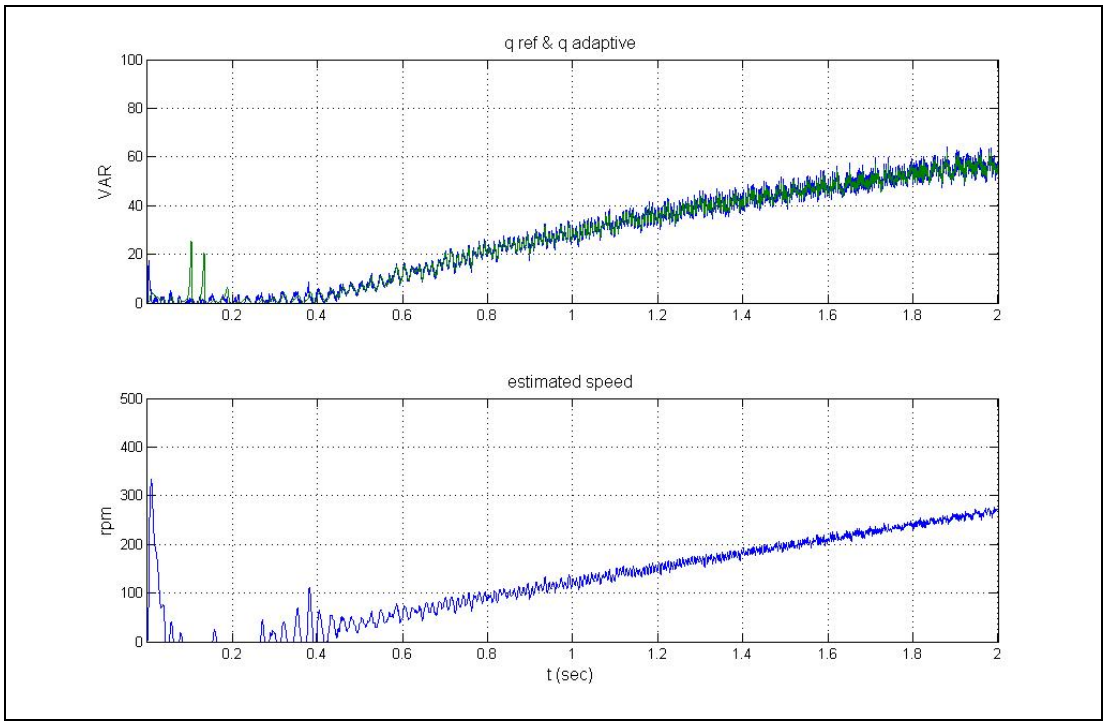


Figure 5-23 Reactive power outputs of reference and adaptive models and estimated rotor speed

**iv**. In this last test the direction of rotation has been changed by demanding negative torque. For this reason $i_{qs}^{e}$ set point was changed to -0.5A while $i_{ds}^{e}$ was kept constant. Figure 5-24 shows d- and q-axis stator currents and voltages in stator reference frame during starting. The estimated rotor flux position and $i_{ds}^{e}$ and $i_{qs}^{e}$ are shown in Figure 5-25. Both of two components have reached to set values. The rotor speed, estimated using reactive power MRAS scheme, is shown in Figure 5-26 on which, adaptive model's output tracks reference model's output.

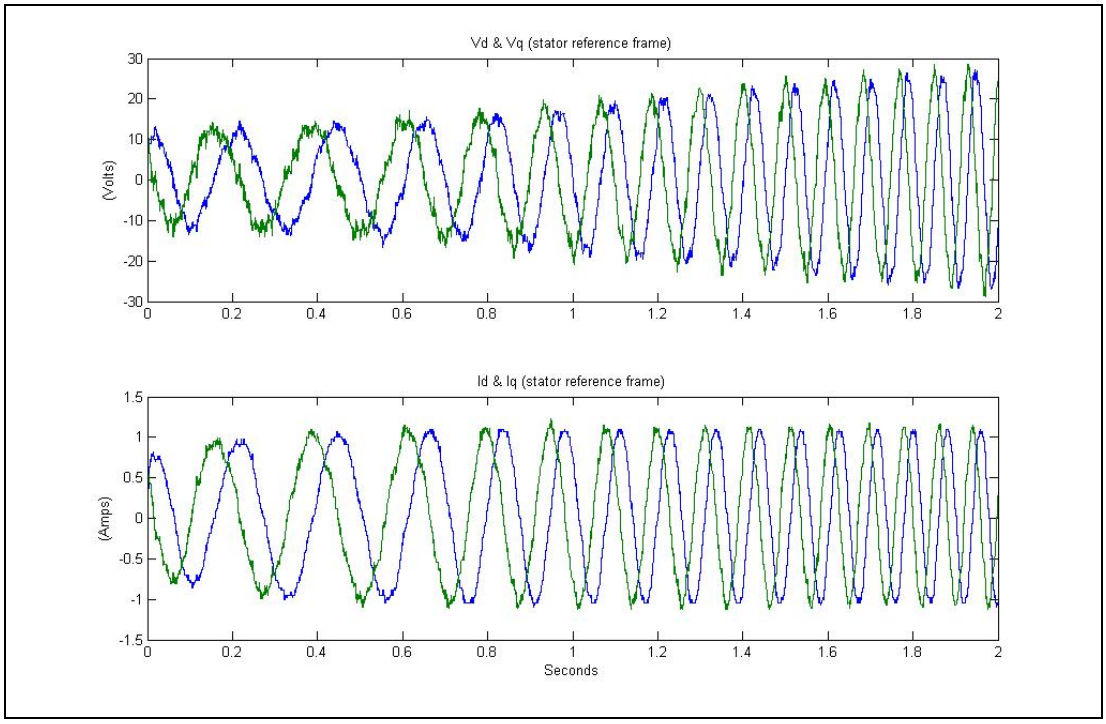


Figure 5-24 d- and q-axis voltages and currents at starting instant

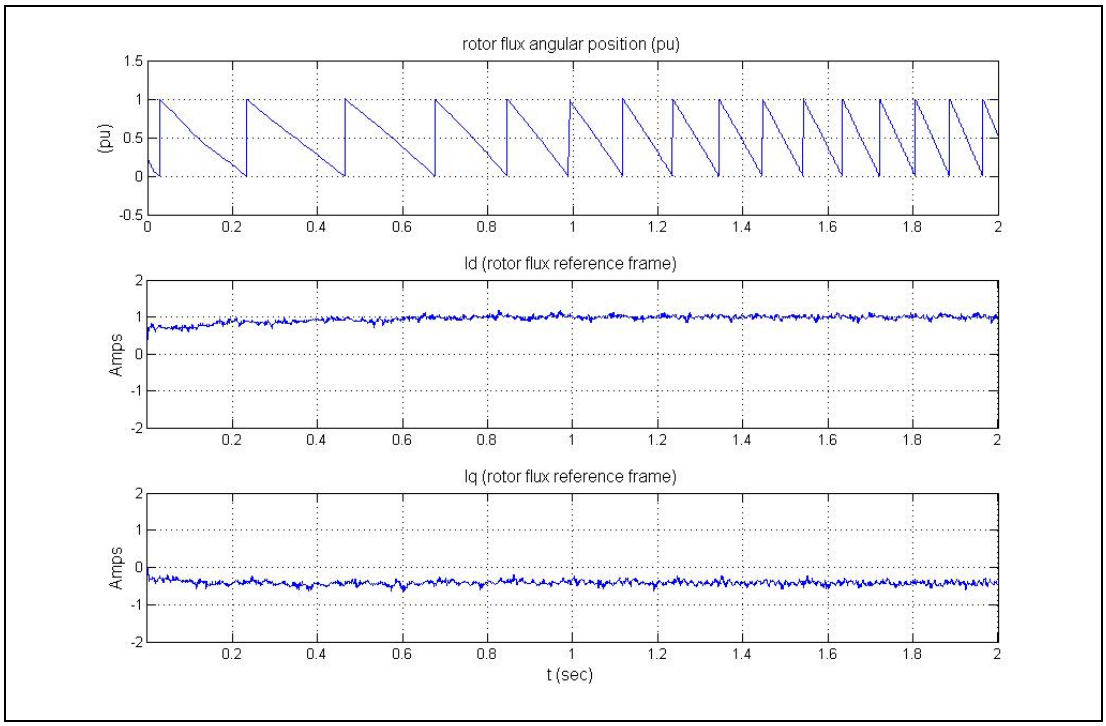


Figure 5-25 Estimated rotor flux angular position, measure d- and q- axis currents in rotor flux reference frame

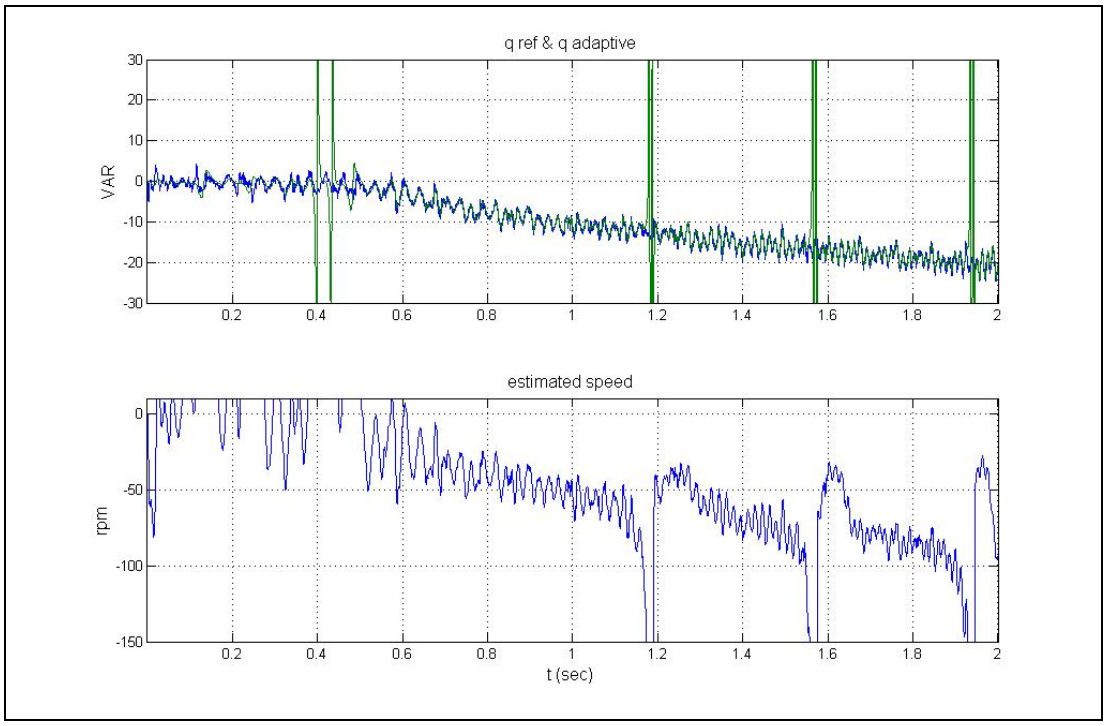


Figure 5-26 Reactive power outputs of reference and adaptive models and estimated rotor speed

## 5.3. Discussions

Simulations show that, speed estimator based on reactive power MRAS scheme and closed-loop rotor flux observer have very high tracking capability. For all conditions adaptive model follows the output of reference model without losing stability. No-load performance of the speed observer is very high, even at high slip region. The speed does not change very fast due to the lack of a mechanical loading, speed outputs obtained in the simulation are very smooth with negligible speed errors. We expect that a heavy loading causes higher transient speed errors due to fast speed changes. Under all circumstances transient speed tracking at starting and at steady-state, the speed estimation performances are quite high. It is seen that there usually exists a small steady-state error between the estimated and actual speed values but this seems to be at negligible levels.

The steady state accuracy of MRAS obtained in the simulations meets the expectations, and therefore the performance of MRAS may be considered as successful. Both speed and flux estimators work properly.

Same no load flux estimation performance has been obtained for all speeds during experiments. Then torque loop is closed by rotor flux position estimate of flux observer. Stability is maintained in all speed range.

Some assumptions have been done during implementation of voltage model. One of them was considering stator resistance constant. The other one is the calculations of phase voltages from a linear model assuming that terminal voltage does not change during operation and no dead time present between upper and lower switching elements. Although these assumptions may be valid at high speeds, they cause significant errors in low speeds. So, the voltage model gives completely wrong results in low speeds. Fortunately, the current model corrects these errors at low speed operations, and widens the operating speed range for flux estimators. This is not the case, however, for the speed estimator. Despite the fact that the stator resistance variation has not considerable effect, reference model reactive power output is related to phase voltage directly. As a result, although a good estimation performance was obtained at high speeds, at low speeds the stability has been lost

and the speed estimate was not accurate as expected. This problem may be solved by nonlinear modeling of driver.

Closed loop speed control could not be implemented experimentally because, selected DSP processor was not capable of solving necessary equations, together with data logging, in specified sampling time interval. Actually this problem can be solved by decreasing sampling rate of speed loop with respect to that of torque loop. It is expected that speed loop performance does not change considerably in this case, regarding that mechanical time constant of the system is big.

# CHAPTER 6

# CONCLUSION

Focus of this work has been closed loop speed control of induction machine using direct field orientation technique. For this speed and flux observers has been designed. The rotor flux position estimate of flux observer is employed in modified torque control algorithm and speed estimate of reactive power MRAS scheme is fed back to outer control loop.

First generalized dynamic model of induction motor was investigated in different reference frames. Space vector PWM and field oriented control concept was defined, theoretical backgrounds of flux and speed observers were studied. Then Model reference adaptive system based closed-loop speed and torque control of induction machines is simulated. Performances of observers were investigated from simulations. Next experiments were done to understand the validity of simulations. It was shown that proposed regulator in closed loop flux estimator scheme, errors appearing at low frequencies, due to non-linear model of driver and pure integration, can be compensated. By this compensation closed loop flux observer is capable of realize torque control for entire speed range. However speed estimator has needed to be improved by non-linear modeling of driver at low speeds.

It was seen that, at specified sampling time C2000 series processor was not capable of handling flux and speed estimators' calculations and data logging all together. Because of this drawback the speed loop could not be closed with a sampling rate at 10Kz which is the same rate with that of the torque loop. It is expected that, reducing the sample rate of speed loop can solve this problem.

For future work, flux and speed estimators can be designed by extended Kalman filter (EKF) technique, using the non-linear model of the machine. In this case it should be noted that, matrix calculations used in EKF technique will require more computational power. Due to this handicap, a C6000 series processor instead of C2000 may be selected for computational purposes. Moreover designing an interface between the user and code generation will be useful, in order to prevent the user making mistakes in introducing motor parameters into this software package.

# APPENDIX A

As with Lyapunov's method, an adaptive law designed using hyperstability theory is guaranteed to be stable. In the hyperstability approach the designer has to propose an adaptive law, and with the aid of hyperstability theory one can check whether this law gives a stable result. In general, a model reference adaptive speed estimator system can be represented by an equivalent non-linear feedback system which comprises a feed-forward time invariant linear subsystem and a feedback non-linear time varying subsystem. The first part normally contains the reference model, and its output is the error signal to be used in the adaptation. The second part contains the adaptive laws and has an output W. This division is illustrated in Figure.A-1.

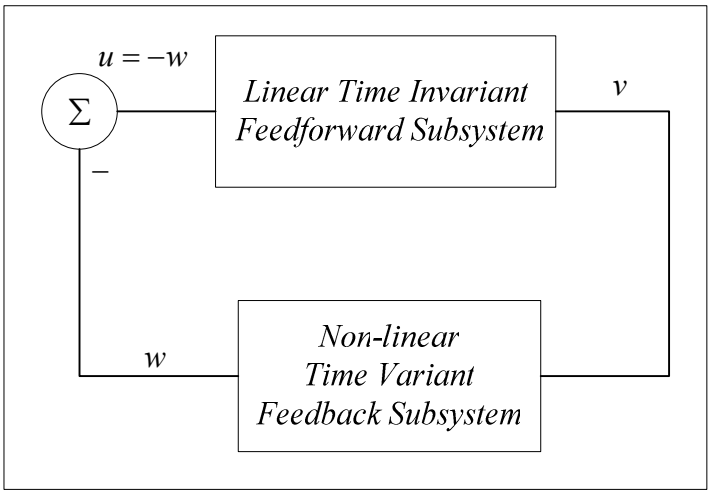


Figure A-1 Division of error equation into time invariant linear part and a time varying nonlinear part

Usually, the input -*w* of the linear block equals the multiplication of the parameter error $\theta$ and the signal vector $v$ used in the adaptation: $-w=\theta^T v$. Hyperstability theory guarantees an asymptotically stable system if both the linear and nonlinear parts satisfy a positivity condition. A controllable, linear system with input u and output y :

$$\dot{x} = Ax + Bu$$
$$y = C^T x$$

$$with\ a\ transfer\ \ function: \qquad \text{(A-1)}$$

$$H(s) = \frac{Y(s)}{U(s)} = C^T (sI - A)^{-1} B$$

is said to be positive real (PR) if *Re{H(s)}* equal or greater than zero. Hence the real part of the transfer function can never become negative as long as the real part of s is larger than or equal to zero. According to hyperstability theory the linear part H must be strictly positive real (SPR) which means that the real part of *H(jw)* is larger than zero for all $w>0$ thus Nyquist diagram of *H(jw)* must lie in the right half of the complex plane, including the imaginary axis. This implies that the number of poles and zeros in *H(s)* differs at most by 1, and the phase shift is never larger than $90^o$.

The nonlinear part must satisfy Popov's integral inequality, which states that a positive constant $\gamma_0^2$ exists such that :

$$\int_0^{t_1} v \bullet w\, dt \geq -\gamma_0^2 \quad for\ all\ \ t_1 \geq 0 \qquad \text{(A-2)}$$

This requirement is also denoted the passivity requirement. Observing nonlinear part as an electrical network, the inequality can be shown to state that the amount of energy output by the nonlinear system is never larger than the sum of the incoming energy and the energy stored in the system. The energy in the system depends on the external input of power and on the power generation in the system

$$\frac{d}{dt}[\text{stored energy}] = [\text{ext. power input}] + [\text{int. power generation}] \qquad \text{(A-3)}$$

Considering $v$, the input, as voltage and $w$ as output, current, the external power input equals $vw$. If the internal power generation is negative, the system is said to be dissipative or strictly passive. If the internal power generation is less than or equal to zero, the system is passive. Strict passivity is equivalent to SPR and asymptotic stability. The main result using positivity and passivity concepts is that any parallel combination of passive blocks is also passive. A feedback combination of two passive blocks in which at least one is strictly passive. This is of great interest in hyperstability theory, in which an SPR (and hence strictly passive) linear block is connected to a passive nonlinear block in a feed back configuration. This combination is strictly passive (and hence asymptotically stable).

# REFERENCES


[1] H. Kubota and K. Matsuse “Flux observer of induction motor with parameter adaptation for wide speed range motor drives,” in Proc. IPEC’90, Tokyo, Japan, 1990, pp. 1213-1218.

[2] R. Nilsen and M. Kazmierkowski, “New reduced-order observer with parameter adaptation for flux estimation in induction motors,” in Proc. PESC’92, 1992, pp. 245-252.

[3] R. Lorenz and D. Lawson, “A simplified approach to continuous, on-line tuning of field-oriented induction machine drives,” IEEE Trans. Ind. Applicat., vol. 26, pp.420-425, May/Jun 1990.

[4] K. T. Hung and R. D. Lorenz, “A rotor flux error-based adaptive tuning approach for feedforward field-oriented machine drives,” in Proc. 1990 IEEE-IAS, Annu. Meeting, pp. 589-594.

[5] L. Garces, “Parameter adaptation for the speed-controlled static AC drive with a squirrel cage induction motor,” IEEE Trans. Ind. Applicat., vol. 16, pp. 173-178, Mar./Apr. 1980.

[6] T. M. Rowan, R. J. Kerkman, and D. Leggate, “A simple on-line adaptation for indirect field-orientation of an induction machine,” in Proc. 1989 IEEE-IAS Annu. Meeting, pp.579-587.

[7] J. Moreira, K. Hung and T. Lipo, “A simple and robust adaptive controller for the tuning correction in field-oriented induction machines,” IEEE Trans. Ind. Applicat., vol. 28, pp. 1359-1366, Nov./Dec. 1992.

[8] P.L.Jansen and R.D.Lorenz “Transducer less position and velocity estimation in induction an salient ac machines”, IEEE Tran. IA, vol. 31, no.2, pp.240-247, Mar/April, 1995

[9] R.Gabriel, W.Leonhard and C.Nordby " Field oriented control of standard AC motor using microprocessor", IEEE Tran. IA, vol.16, no.2, pp.186.192, 1980

[10] B.Robyns, B.Frederique, "A methodology to determine gains of induction motor flux observers based on a theoretical parameter sensitivity analysis", IEEE Trans. PE, vol. 15, no.6, pp.983-995, 2000

[11] Takahashi and T. Noguchi, "A new quick-response and high-efficiency control strategy of an induction motor," IEEE Trans. Ind. Applicat., vol. 22, pp.820-827, Sep./Oct. 1986.

[12] P. L. Jansen and R. D. Lorenz, "A physically insightful approach to the design and accuracy assessment of flux observers for field-oriented induction machine drives," in Proc. IEEE-IAS Annu. Meeting, Oct.1992, pp. 570-577.

[13] P. L. Jansen, C. O. Thompson, and R. D. Lorenz, "Observer based direct field orientation for both zero and very high speed operation," in Proc. PCC, Yokohama, Japan, Apr. 1993, pp.432-437.

[14] P. L. Jansen and R. D. Lorenz, "Accuracy limitations of velocity and flux estimation in direct field-oriented induction machines," in Proc. EPE Conf., Brighton, England, Sep. 1993

[15] P.L.Jansen and R.D.Lorenz "Observer based direct field orientation: Analysis and comparison of alternative methods", IEEE Tran. IA, vol. 30, no.4, pp.945-953, Jul/Aug, 1994

[16] K Minami, M. Vélez-Reyes, D. Elten, G. C. Verghese and D. Filbert, "Multi-stage speed and parameter estimation for induction machines," IEEE Power Electronics Specialist's Conference, Boston MA, Jun. 1991.

[17] M. Vélez-Reyes and G. C. Verghese, "Decomposed algorithms for speed and parameter estimation in induction machines," IFAC Symposium on Non-linear Control System Design, Bordeaux, France, 1992.

[18] M. Vélez-Reyes, K Minami, G. C. Verghese, "Recursive speed and parameter estimation for induction machines," IEEE Ind. Applicat. Society Meeting, San Diego, 1989

[19] M. Bodson and J. Chiasson, “A comparison of sensorless speed estimation methods for induction motor control,” Proc ACC, Anchorage, AK May.2002, pp. 3076-3081

[20] I. J. Ha and S. H. Lee, “An on-line identification method for both stator and rotor resistances of induction motors without rotational transducers,” ISIE’96, Warsaw, Poland, Jun. 1996.

[21] H. S. Yoo and I. J. Ha, “A polar coordinate-oriented method of identifying rotor flux and speed of induction motors without rotational transducers,” IEEE Trans. on Control Systems Technology, vol. 4, no. 3, pp. 230-243, May. 1996.

[22] F.Z.Peng, T.Fukao “Robust Speed Identification for Speed Sensorless Vector Control of Induction Motors” IEEE Tran. IA vol. 30, no. 5, pp.1234-1239, Oct.1994

[23] C.Schauder “Adaptive Speed Identification for Vector Control of Induction Motor without Rotational Transducers” IEEE Tran. IA vol. 28, no. 5, pp. 1054-1061, Oct.1992

[24] G.Yang and T.Chin “Adaptive-Speed identification scheme for a vector controlled speed sensorless inverter induction motor drive” ,IEEE Tran. IA, vol. 29, no.4, pp.820-825, 1993

[25] M.Elbuluk, N.Langovsky and D.Kankam “Design and Implementation of a Closed Loop Observer and Adaptive Controller for Induction Motor Drives” IEEE Tran. IA vol. 34 no. 3 pp. 435-443, May/June 1998

[26] H.Tajima, Y.Hori “Speed Sensorless Field Orientation Control of the Induction Machine” IEEE Tran. IA vol. 29, no. 1, pp. 175-180, Feb.1993

[27] D.W.Novotny and T.A.Lipo, “Vector Control and Dynamics of AC Drives”, Oxford University Press Inc., Oxford, New York, 1997.

[28] C.Lascu, I.Boldea, F.Blaabjerg “A Modified Direct Torque Control for Induction Motor Sensorless Drive” IEEE Tran. IA vol. 36, no. 1, pp. 122-130, Jan 2000

[29] H.Butler "Model Reference Adaptive Systems" London: Printice Hall,(1992)

[30] L.Zhen and L. Xu “Sensorless Field Orientation Control of Induction Machines Based on Mutual MRAS Scheme” IEEE Tran. IE vol. 45 no. 5, pp. 824-831, October 1998

[31] M.Elbuluk, L.Tong and I.Husain “Neural Network Based Model ReferenceAdaptive Systems for High Performance Motor Drives and Motion Control” IEEE Tran. IA vol. 38, no. 3 pp. 879-886 May/June 2002

[32] K.K.Shyu, H.J. Shieh and S.S. Fu “Model Reference Adaptive Speed Control for Induction Motor Drive Using Neural Network ”, IEEE Tran. IE vol. 45, no. 1 pp. 180-182, Feb. 1998

[33] C.Attainese, Alfonso Damiano “Induction Motor Drive Parameters Identification” IEEE Tran. PE vol. 13, no. 6, pp. 1112-1123,Nov. 1998

[34] H.Sugimoto and S.Tamai “Secondary Resistance Identification of an Induction Motor Applied Model Reference Adaptive System and its Characteristics” IEEE Tran. IA vol. 23, no. 2 pp. 296-303 March/April 1987

[35] R.Krishnan, F.C.Doran “Study of parameter sensitivity in high performance inverter-fed induction motor drive systems”, IEEE Tran. IA, vol. 23,pp.623-635, 1987

[36] Texas Instruments, “Digital Motor Control Software Library”, Literature number: SPRU 485 August 2001